



저작자표시-비영리-변경금지 2.0 대한민국

이용자는 아래의 조건을 따르는 경우에 한하여 자유롭게

- 이 저작물을 복제, 배포, 전송, 전시, 공연 및 방송할 수 있습니다.

다음과 같은 조건을 따라야 합니다:



저작자표시. 귀하는 원저작자를 표시하여야 합니다.



비영리. 귀하는 이 저작물을 영리 목적으로 이용할 수 없습니다.



변경금지. 귀하는 이 저작물을 개작, 변형 또는 가공할 수 없습니다.

- 귀하는, 이 저작물의 재이용이나 배포의 경우, 이 저작물에 적용된 이용허락조건을 명확하게 나타내어야 합니다.
- 저작권자로부터 별도의 허가를 받으면 이러한 조건들은 적용되지 않습니다.

저작권법에 따른 이용자의 권리는 위의 내용에 의하여 영향을 받지 않습니다.

이것은 [이용허락규약\(Legal Code\)](#)을 이해하기 쉽게 요약한 것입니다.

[Disclaimer](#)

A DISSERTATION FOR THE DEGREE OF DOCTOR OF PHILOSOPHY

**Synthesis and Properties of UV Laser Debondable
Temporary Bonding and Debonding Adhesives
for 3D Multi-chip Packaging Process**

3D 멀티칩 패키징용 자외선 레이저 디본딩형
임시 고정 접착제의 합성과 물성

By

Seung-Woo Lee

PROGRAM IN ENVIRONMENTAL MATERIALS SCIENCE

GRADUATE SCHOOL

SEOUL NATIONAL UNIVERSITY

FEBRUARY, 2015

Abstract

Synthesis and Properties of UV Laser Debondable Temporary Bonding and Debonding Adhesives for 3D Multi-chip Packaging Process

Seung-Woo Lee

Program in Environmental Materials Science

Graduate School

Seoul National University

Recently, mobile devices with a focus on smartphone require both high performance and lightness at the same time, so TSV (Through Silicon Via) 3D multi-chip package technology was emerging. In order to realize this technique, temporary bonding and debonding adhesive is required to process silicon wafer and handling. However, using the existing adhesive handling a thin silicon wafer having a thickness of less than 50 μm is not easy. There are two main reasons for this. First, to maintain the high purity, it is required to have over 200 °C processing temperature during the process of bonding and debonding. Due to this thermal degradation, it generates low molecular weight substances and cause contamination to the thin silicon wafer. Second, while debonding, strong adhesive force can crack or cracking the thin silicon wafer and generate defects.

In this study, the perspective on temporary bonding for TSV (Through Silicon Via) 3D multichip packaging and the perspective on debonding afterwards are divided into each technique elements, and these elements are to be used to newly synthesize the adhesive. Plus, the mechanisms of curing and

debonding are to be analyzed through these property evaluations.

In this study, the non-solvent type urethane acrylic adhesive was designed and manufactured to improve the disadvantages such as the phenomenon on flowing adhesive out from the silicon wafer after the spinning coating which the conventional solvent-based adhesive have during temporary bonding, the phenomenon of uneven coating thickness by contaminated wafer surface from the solvent evaporation and the phenomenon on the contamination of the work area. During the urethane synthesis, isophorone diisocyanate was used as a hard segment and silicone-based diols (not conventional hydrocarbon-based diols) was used as a soft segment to improve the heat resistance of the polymer structure. Also, designing for dual curing adhesive that further introduce a photo-curing after thermal curing was made (rather than a single curable adhesive, such as the conventional light curing or thermal curing) to improve the heat resistance. A multi-functional acrylic monomer was end-capped to one end of the synthesized urethane oligomer and a monomer containing a fluorine was end-capped to the other end for to analyze the measurement of the number of functional groups of the multifunctional acrylic monomer, the density of the UV irradiation energy, hardening behavior, thermal stability and the peel strength depending on the amount of photoinitiator used. As a result, the number of functional acrylic monomer was in mono < di << tri, hexa order and increase on the indirect cure rate using the Gel-minute law was confirmed. This has initial reaction in the light-curing, which give an increase of the reaction sites and hence an increase in the crosslinking density. After tri-acrylate, it is confirmed that the gel fraction was not further increased by 60%, which can be interpreted that the reaction activity is falling by the radical trap of unreacted oligomers. The Gel fraction was confirmed to become constant at 60% when the UV irradiation energy density is at 400 mJ/cm² or more. To decrease the peel strength due to the increase density of the UV energy, the pulsed irradiation method, which

examine by dividing each into 100 mJ/cm², was introduced to derive the molecular weight distribution of the polymer in a state in which heterogeneous. (The steady irradiation method, which is used primarily during irradiation, is not used.) In the steady irradiation method, the PDI value is 5.9, but the pulsed irradiation method showed 16.1 of high PDI value. This characteristic allowed showing lower intensity levels on the peel strength measurement of pulsed irradiation method than the steady irradiation method, concluding that the pulsed irradiation method is more suitable considering both temporary bonding and debonding. Type and the reaction mechanism of the photoinitiator was found through the existing studies, and the purpose of this study was to evaluate and analyze by varying the amount of light curing initiator. As a result, the gel fraction became constant without any further increase when adding the binder contrast of 2 phr or more photoinitiators. This is considered as an important research data on the optimal composition ratio of the initial dose, given a side reaction due to unreacted initiator, which can occur when an excess of added photoinitiator. Thermal decomposition behavior results, seen by varying the amount of UV energy density and photoinitiator for the thermal stability and by using thermogravimetric analysis, was confirmed that the thermal stability is maintained at a high temperature condition over 250 °C. This can interpret that the heat resistance was improved by the introduction of dual-cure mechanism and the adhesive synthesis containing all hybrid type of silicone-based, epoxy-based, fluorine-based functional group.

On the other hand, this study used the method of edge zone debonding, using the UV laser, to consider both temporary bonding and debonding. While the conventional method requiring a bonding temperature of 200 ~ 220 °C, this study was able to proceed the bonding at a low temperature of 80 ~ 150 °C. Furthermore, this study has done debonding within two minutes using a UV laser, rather than the conventional way in which this process takes time

over 6 hours by a penetration of the solvent. For this purpose, BTHPEMA (2-[3- (2-Benzotriazol-2-yl) -4-hydroxyphenyl] ethyl methacrylate) was introduced when preparing the adhesive. When debonding, identification (BTHPEMA playing a role of being the LTHC (light to heat conversion)) for debonding progression of the polymer film formation by the heat cure adhesive was made through thermal curing mechanism of epoxy functionality by the FTIR-ATR analysis and the gel fraction measurement. Absorbency, for a UV laser of a synthesis adhesive, was determined according to wavelength using a UV-visible spectroscopy. As a result, 355 nm in wavelength bands indicate the absorption of up to 60% of the binder prepared in accordance with the increase amount of BTHPEMA comparison 0.4 phr input, and the UV laser absorbency of the adhesive synthesized was adjustable by varying the blending ratio. Moreover, it was confirmed that the joined debonding was composed in the effective energy density conditions of the UV laser irradiation with 5.65 to 6.72 J/cm².

Keywords: Adhesives, dual-curing, 3D multi-chip packaging, temporary bonding and debonding, UV laser debonding, fluorinated urethane adhesive

Student number : 2009-21204

Contents

Chapter 1

General Introduction and Objectives	1
1.1. Three-dimensional (3D) Integration	2
1.1.1. Background	2
1.1.2. Application of wafer bonding for 3D integration technology	5
1.2. Temporary Bonding and Debonding for 3D Integration and Packaging ..	11
1.2.1. Background	11
1.2.2. Temporary bonding and debonding technologies	14
1.2.2.1. Thermoplastic adhesive, slide-off debonding approach	19
1.2.2.2. Using Ultraviolet (UV) – curable adhesive and light-to heat conversion layer	21
1.2.2.3. Adhesive dissolution through perforated carrier wafer	23
1.2.2.4. Using a release layer and lift-off	25
1.2.2.5. Room temperature, low-stress debonding	27
1.2.3. Concerning for temporary bonding and debonding	29
1.2.3.1. Uniform and void-free bonding	29
1.2.3.2. Protecting wafer edge during thinning and subsequent processing	30
1.3. Objectives	32

Chapter 2

Literature Review	35
2.1. UV-curing	36

2.2. Synthesis and UV-curable Acrylate	38
2.3. Fluorinated Polyurethane Acrylate	41

Chapter 3

Adhesion Performance and Surface Morphology of UV-curable Interpenetrating Network Acrylates for 3D Multi-chip Packaging Process	42
3.1. Introduction	43
3.2. Experimental	46
3.2.1. Materials	46
3.2.2. Methods	48
3.2.2.1. Synthesis of binders	48
3.2.2.2. Formation of the acrylate film	49
3.2.2.3. Preparation of cured acrylates	50
3.2.2.4. Adhesion performance	53
3.2.2.5. Field emission-scanning electron microscopy (FE-SEM)	54
3.2.2.6. X-ray photoelectron spectroscopy (XPS)	55
3.3. Results and Discussion	56
3.3.1. Adhesion performance	56
3.3.2. Gel fraction of the acrylates with the hexafunctional monomer at different photoinitiator contents	63
3.3.3. Field emission-scanning electron microscopy (FE-SEM)	65
3.3.4. X-ray photoelectron spectroscopy (XPS)	67
3.4. Conclusion	70

Chapter 4

Adhesion Performance and Curing Behaviors of UV-curable Acrylates with 3-MPTS for 3D Multi-chip Packaging Process72

4.1. Introduction	73
4.2. Experimental	75
4.2.1. Materials	75
4.2.2. Methods	77
4.2.2.1. Synthesis of binders	77
4.2.2.2. Formation of the acrylate film	78
4.2.2.3. Preparation of cured acrylates	79
4.2.2.4. Adhesion performance	81
4.2.2.5. Fourier transform infrared (FTIR) spectroscopy	82
4.2.2.6. Gel permeation chromatography (GPC) measurement	83
4.2.2.7. Advance rheometric expansion system (ARES) analysis	84
4.2.2.8. Field emission-scanning electron microscopy (FE-SEM)	85
4.2.2.9. X-ray photoelectron spectroscopy (XPS)	86
4.3. Results and Discussion	87
4.3.1. Adhesion performance	87
4.3.2. Advance rheometric expansion system (ARES) analysis	92
4.3.3. Fourier transform infrared (FTIR) spectroscopy	96
4.3.4. Field emission-scanning electron microscopy (FE-SEM)	98
4.3.5. X-ray photoelectron spectroscopy (XPS)	100
4.4. Conclusion	103

Chapter 5

UV-curing and Thermal Stability of Dual-curable Urethane Epoxy Adhesives for Temporary Bonding and Debonding in 3D Multi-chip Packaging Process	104
5.1. Introduction	105
5.2. Experimental	109
5.2.1. Materials	109
5.2.2. Methods	111
5.2.2.1. Synthesis of silicone urethane methacrylate (SiUMA)	111
5.2.2.2. Preparation of dual-curable adhesive	113
5.2.2.3. Fourier transform infrared (FTIR) spectroscopy	115
5.2.2.4. Gel fraction	116
5.2.2.5. Photo-differential scanning calorimetry (photo-DSC)	117
5.2.2.6. Thermogravimetric analysis (TGA)	118
5.3. Results and Discussion	119
5.3.1. Photo-differential scanning calorimetry (photo-DSC)	119
5.3.2. Fourier transform infrared (FTIR) spectroscopy	121
5.3.3. Gel fraction	123
5.3.4. Thermogravimetric analysis (TGA)	125
5.4. Conclusion	128

Chapter 6

Synthesis and Properties of UV Laser Debondable Fluorinated Silicone-modified Urethane Acrylic Adhesives for Temporary Bonding and Debonding in 3D Multi-chip Packaging Process	129
---	-----

6.1. Introduction	130
6.2. Experimental	136
6.2.1. Materials	136
6.2.2. Methods	138
6.2.2.1. Synthesis of fluorinated silicone-modified urethane acrylates	138
6.2.2.2. Temporary bonding and UV laser debonding condition	143
6.2.2.3. Fourier transform infrared (FTIR) spectroscopy	151
6.2.2.4. Gel fraction and swelling ratio	152
6.2.2.5. Shrinkage	153
6.2.2.6. Thermogravimetric analysis (TGA)	154
6.2.2.7. Peel strength	154
6.2.2.8. Optical microscopy	156
6.2.2.9. Field emission-scanning electron microscopy (FE-SEM) and energy dispersive spectroscopy (EDS)	157
6.2.2.10. Atomic force microscopy (AFM)	158
6.3. Results and Discussion	159
6.3.1. Fourier transform infrared (FTIR) spectroscopy	159
6.3.2. Gel fraction and swelling ratio	161
6.3.3. Shrinkage	165
6.3.4. Thermogravimetric analysis (TGA)	167
6.3.5. Peel strength	169
6.3.6. Optical microscopy	171
6.3.7. Atomic force microscopy (AFM)	173
6.3.8. Field emission-scanning electron microscopy (FE-SEM) and energy dispersive spectroscopy (EDS)	176
6.4. Conclusion	178

Chapter 7

Concluding Remarks 179

References 184

초록 210

List of Tables

Table 3-1. Atomic concentration (%) of C _{1s} and Si _{2p} determined by XPS according to the UV does	69
Table 4-1. Atomic concentration (%) of C _{1s} and Si _{2p} determined by XPS according to the UV does	102
Table 5-1. Blend ratio of dual-curable adhesives (unit: phr)	114
Table 5-2. Characteristic thermal decomposition data of the UV-cured adhesives	127
Table 6-1. Raw materials used for synthesis of fluorinated silicon-modified urethane acrylic adhesives	137
Table 6-2. UV laser process parameters	150
Table 6-3. Different UV laser processing conditions	174

List of Figures

Figure 1-1. Schematic of TSV process flows	4
Figure 1-2. Schematic of main wafer bonding technologies for 3D integration	6
Figure 1-3. Power consumption comparison flip chip (FC) PoP versus 3D system-in-package (SiP) with TSV	8
Figure 1-4. Beyond Moore's law	9
Figure 1-5. 3D TSV platforms motivations per applications	10
Figure 1-6. Scheme of temporary bonding and debonding process	13
Figure 1-7. Schematics of via-first and via-last processes	15
Figure 1-8. Temperature requirements in process sequences	18
Figure 1-9. Process flow for slide-off debonding approach	20
Figure 1-10. Process flow for 3M wafer support system	22
Figure 1-11. Overview of single-wafer debonding process using dissolution through perforated wafer plate	24
Figure 1-12. Overall description of release using liftoff process	26
Figure 1-13. Overview of Brewer Science's low-stress, room temperature debonding process	28
Figure 1-14. Overview of edge protection methods	31
Figure 3-1. Schematic diagram of the process on thin Si-wafer manufacture applied with acrylates	45
Figure 3-2. Chemical structure of the dipentaerythritol hexacrylate (DPHA)	47
Figure 3-3. Crosslinking of carboxylated functionality with methylaziridine	51
Figure 3-4. Process of producing IPN structure in UV-cured acrylates	52
Figure 3-5. Peeling strength with the curing agents at the stainless steel (SUS) and Si-wafer	59

Figure 3-6. Peeling strength with different hexafunctional monomer contents	60
Figure 3-7. Peeling strength with different photo-initiator contents	61
Figure 3-8. Effect of the UV dose on the peeling strength at different coating thickness	62
Figure 3-9. Gel fraction with a hexafunctional monomer at different Photo-initiator contents	64
Figure 3-10. Field-emission scanning electron images of UV-cured acrylates at UV dose; (a) 0 mJ/cm ² , (b) 50 mJ/cm ² , (c) 100 mJ/cm ² , (d) 200 mJ/cm ²	66
Figure 3-11. (a) C _{1s} and (b) Si _{2p} XPS spectra of Si-wafer surface after peeling at varying UV dose	68
Figure 4-1. Chemical structures of (a) the dipentaerythritol hexaacrylate (DPHA) and (b) 3-methacryloxypropyl trimethoxysilane (3- MPTS)	76
Figure 4-2. Process of producing IPN structure in UV-cured acrylates	80
Figure 4-3. Peel strength by two types of UV irradiation	89
Figure 4-4. Probe tack by two types of UV irradiation	90
Figure 4-5. GPC measurement by two types of UV irradiation	91
Figure 4-6. Temperature dependence of storage modulus <i>G'</i> with different UV dose	94
Figure 4-7. Tan delta with different UV dose	95
Figure 4-8. Conversion of C=C bonds at 810 cm ⁻¹ as a functional of UV dose for UV-curable groups in binders blended with an additional monomer	97
Figure 4-9. Field-emission scanning electron images of UV-cured acrylates at UV dose; (a) 0 mJ/cm ² , (b) 400 mJ/cm ² , (c) 800 mJ/cm ² , (d) 1600 mJ/cm ²	99
Figure 4-10. (a) C _{1s} and (b) Si _{2p} XPS spectra of Si-wafer surface after peeling	

at varying UV dose	101
Figure 5-1. Temporary Bonding process flow	108
Figure 5-2. Structure of dipentaerythritol hexacrylate (DPHA)	110
Figure 5-3. Cleavage of hydroxydimethyl acetophenone as the photo-initiator in presence of UV light	110
Figure 5-4. Synthesis process of UV-curable silicone urethane methacrylate	112
Figure 5-5. (a) Photo-DSC thermograms and (b) exothermic area which was calculated by integration of heat flow with different contents of the photo-initiator	120
Figure 5-6. FTIR-ATR spectra of UV-curable adhesives with (a) 5 phr of Photo-initiator contents, as a function of the UV dose at 810 cm^{-1} , and (b) relative conversion vs. UV dose	122
Figure 5-7. Gel fraction of UV-curable adhesives after UV-curing	124
Figure 5-8. Thermogravimetric analysis of the UV-cured adhesives	126
Figure 6-1. Whole experimental processes	135
Figure 6-2. Synthesis process of dual-curable fluorinated silicone-modified urethane acrylic adhesives	139
Figure 6-3. Observing changes in the FT-IR peak at 2265 cm^{-1} (NCO peak), which decreased with the polyurethane reaction	140
Figure 6-4. Observing changes in the ^1H NMR peaks for threefold urethane reactions	142
Figure 6-5. Temporary bonding process flow	144
Figure 6-6. Procedures and dual curing mechanism in temporary bonding	146
Figure 6-7. UV laser debonding process flow	146
Figure 6-8. FTIR-ATR during dual curing and UV laser debonding	147
Figure 6-9. UV-curing profiles of UV-curable adhesives with different Photo-initiator contents by FTIR-ATR spectra	160

Figure 6-10. Gel fraction of UV-curing adhesives with different photo-initiator contents after UV-curing	162
Figure 6-11. Swelling ratio of UV-curable adhesives with different Photo-initiator contents after UV-curing	163
Figure 6-12. Correlation between swelling ratio and gel fraction of UV-curable adhesives	164
Figure 6-13. Linear shrinkage of UV-curable adhesives during UV irradiation	166
Figure 6-14. Thermogravimetric analysis of UV-cured adhesives with different UV doses	168
Figure 6-15. The peel strength (N/mm) vs. out-focusing length (mm) on (a) the line spacing from 20 μm to 40 μm , and (b) the scan speed from 900 mm/s to 1100 mm/s	170
Figure 6-16. Microscopy observations of specimen (a) – (f). The laser beam was irradiated from top to bottom	172
Figure 6-17. AFM images and depth profiles after UV laser irradiation with different processing conditions (process condition (a) ~ (c)) ...	175
Figure 6-18. SEM image and atomic fraction (%) of damaged area (spot A) and undamaged area (spot B) on Si wafer after cleaning, sample (a)	177

Chapter 1

General Introduction and Objectives

1.1. Three-Dimensional Integration

1.1.1. Background

Three-dimensional (3D) integration is commonly defined as bonding of stacked device substrates with vertical electrical interconnects between the device layers (Garrou *et al.*, 2008). A device layer may consist of one particular integrated circuitry or one set of functional devices. Besides wafer thinning and through-silicon via (TSV) formation, wafer bonding is the key unit process of 3D integration technologies. The choice of wafer bonding technologies has to be made by considering the full process conditions such as temperature limitations and the sequence of the technology modules, which may vary for different applications. The large spectrum of corresponding application-specific 3D integration technologies can be reasonably classified in the following main categories:

- Stacking of packaged devices (or substrates);
- Stacking of embedded bare devices (without TSVs);
- 3D TSV technology

Most of the applications discussed here are based on TSV technologies showing the capability for volume production of high-performance products (Ramm *et al.*, 2012).

The large variety of existing TSV processing flows is categorized, according to ITRS (Semiconductor Industry Association, 2009), explicitly corresponding to the order of TSV processing, wafer thinning, and wafer bonding. The order of TSV process with respect to device fabrication is one of the main criteria and today commonly characterized by fabrication of TSVs

(Figure 1-1):

- Prior silicon front-end-of-line (FEOL) – “*via first*”
- Post silicon back-end-of-line (BEOL) – “*via last*”
- Post FEOL but prior BEOL – “*via middle*” (Ramm *et al.*, 2012)

Via First, Middle and Last Process Flows

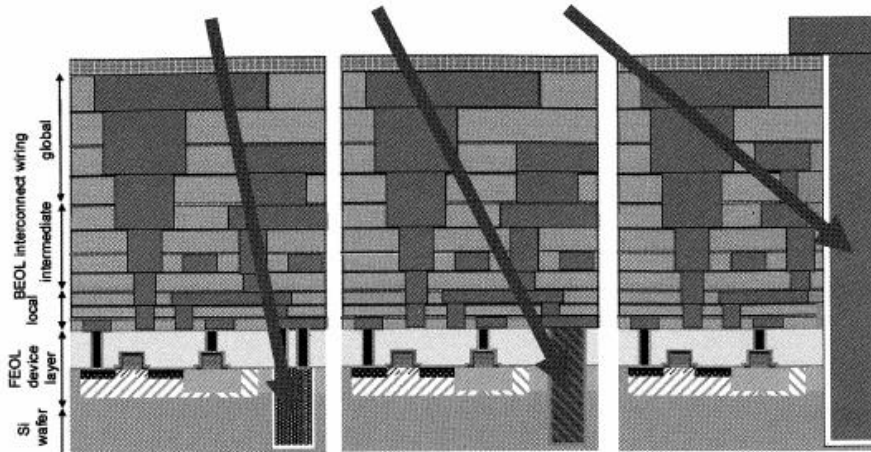


Figure 1-1. Schematic of TSV process flows (SEMATECH, 2009).

1.1.2. Application of wafer bonding for 3D integration technology

Figure 1-2 shows the most commonly applied techniques of oxide fusion, and metal bonding for 3D TSV integration. “*via last*” 3D integration technologies can be used to form the vertical electrical interconnects at the bonding interface during the bonding process, while TSVs can be made at any stage of the processing flow, depending upon the applications and processing constraints. The performance and economic motivations for moving to 3D integration technology have been clear for several years. By stacking a thinned die, or circuit, on top of another it was achieved the shortest interconnect distances which results in less power required to drive a signal, because the signal has less distance to travel. In addition entire layers can be re-used, either through customization on a separate layer or by connection to other functions through an interposer. This is summarized as follows:

Performance

- Shorter nets;
- Lower capacitance interconnect;
- Wide I/O bandwidth.

Volumetric efficiency (size/density)

- Stacking separated functions.

Reduced power

- Lower cap and shorter nets;
- Fewer buffers.

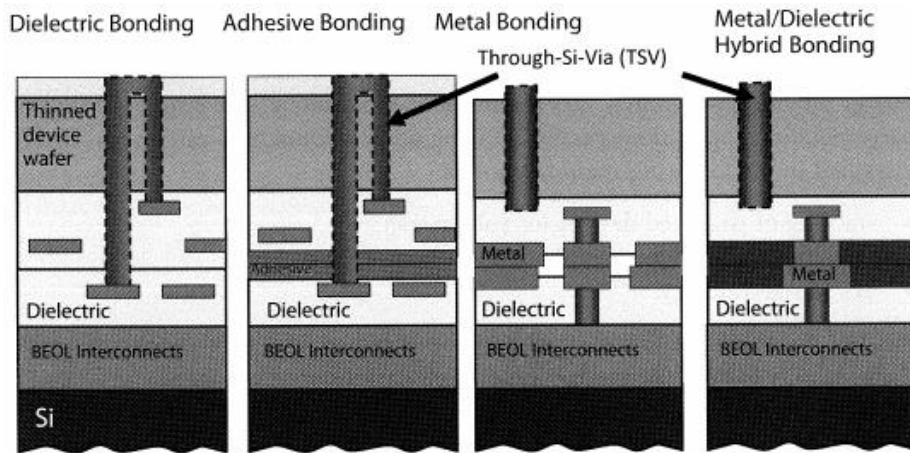


Figure 1-2. Schematic of main wafer bonding technologies for 3D integration (Ramm *et al.*, 2012)

Modularity

- IP reuse;
- Lower design cost (Ramm *et al.*, 2012)

A comparison between an equivalent package-on-package (PoP) solution and a 3D TSV solution showed that 3D TSV solution has significant advantages (Figure 1-3) (Kwon, 2011). Once the infrastructure is in place, it is hoped that 3D IC technology will reduce both risk and cost. The 3D IC approach should create economic benefits such as: reducing the time it takes to design and verify chips at the most advanced nodes; allowing the use older analog IP blocks rather than having to develop new IP blocks at the most advanced process nodes; and allowing the mixing of normally incompatible technologies (heterogeneous integration – more than Moore; Figure 1-4) (Ramm *et al.*, 2012).

Three-dimensional integration is recognized as a key technology for heterogeneous product, demanding for smart system integration rather than extremely high interconnect densities. According to surveys on revenue forecast by Yole Development such “more than Moore” products, for example heterogeneous microelectromechanical system (MEMS)/IC systems, may even be the main driving markets for 3D TSV integration (Zinck, 2010). Many R&D activities worldwide are focusing on heterogeneous integration for novel functionalities (Fernandez-Bolanos *et al.*, 2010). Also, 3D TSV platforms motivations per application are introduced (Figure 1-5) (SUSS Microtec, 2012).

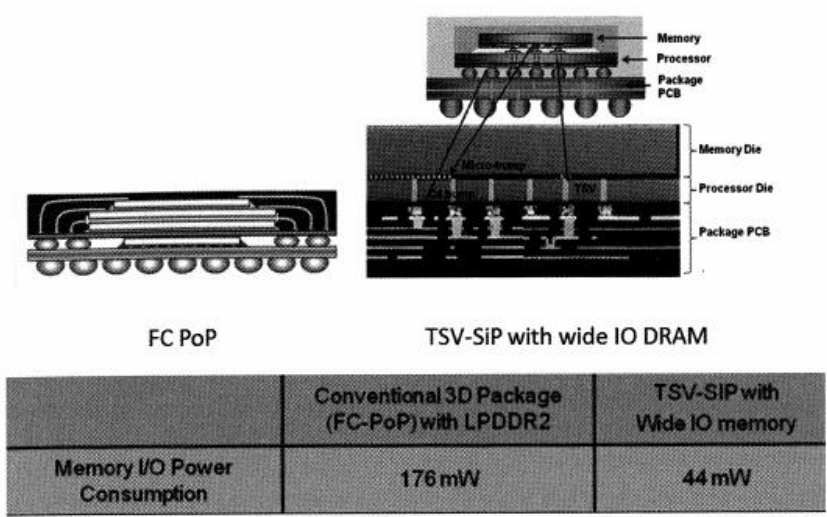


Figure 1-3. Power consumption comparison flip chip (FC) PoP versus 3D system-in-package (SiP) with TSV (Kwon, 2011).

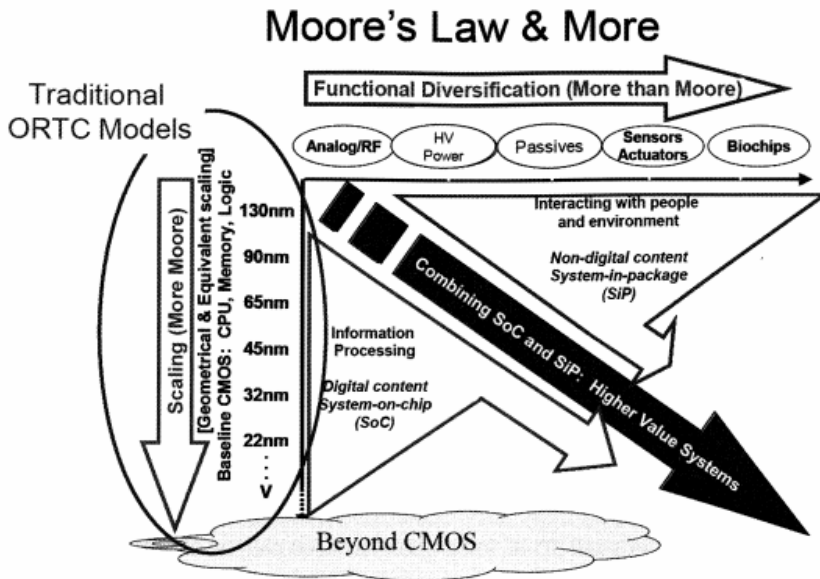


Figure 1-4. Beyond Moore's law (SEMATECH, 2009).

	3D WLP Encapsulation	3D TSV Stack	3D TSV interposer Module	3D TSV "ground" via
	★ Smaller and highly reliable module for harsh environments		★ High heat conductivity module for higher performances	
	★ Thin package. Defect-free & low cost cavity. Access to backside electrical contacts	★ Stacking of DSP and memories at the backside of the sensor		
	★ Inertial, RF-MEMS, MOEMS: smaller cavity package at lower cost. Possibility to stack the ASIC		★ Low cost and small form factor MEMS + ASIC integration	
	★ PA Modules: small package and high RF performance		★ Passives + transceiver + MEMS + antennas + ...heterogeneous integration	★ Higher RF performance (MMIC, LTE chipsets ...)
		★ DRAM: shortest connection path (bandwidth) + density challenge ★ Flash: density / form factor	★ SSD interposer for memory stack applications	
		★ 3D-SOCs: Lower cost through segregation of Analog / IOs / Embedded memories ★ Multi-core CPU: staking of huge cache memory capacities	★ → 'Companion' chip to bridge CMOS to PCB substrate gap ★ → Thermal management substrate	★ Lower Power consumption for high performance computers
			★ Possibility for passive IPD integration with other analog functions (e.g. DC-DC converters)	★ → All electrical interconnects on backside for vertical comp. ★ → Simplify routing of embedded die PCB laminates

Figure 1-5. 3D TSV platforms motivations per applications (SUSS Microtec, 2012).

1.2. Temporary Bonding and Debonding for 3D Integration and Packaging

1.2.1. Background

The end of device scaling based on Moore's law or the possibility of prolonging this legendary law by the next generation of lithography technology has been the subject of debate for nearly a decade. Building three-dimensional (3D) devices has recently emerged as a plausible solution to the ever-increasing challenge to make smaller and faster devices with higher functionality. Three-dimensional integration and packaging require new ways to process and handle wafers. Most commonly, making 3D structures by means of through-silicon vias (TSVs) is considered to be 3D integration, while making stacked packages and other stacked structures by means of external connections is termed 3D packaging (Garrou *et al.*, 2008).

Numerous ways of stacking devices exist, but they all have wafer-thinning processes in common and some approaches require thin-wafer handling. Wafers thinned to a thickness of 150 μm or more have been shown to survive handling without significant damage, but these wafers need highly sophisticated and often expensive equipment to avoid chipping and breakage. However, TSV formation and filling at thickness greater than 100 μm can be challenging and costly. Additionally, interconnect delay and heat dissipation issues can be better addressed with thinner substrates. To make TSV technology viable, wafers must be thinned to thicknesses of 100 μm or less. Thinned silicon wafers are extremely fragile and tend to warp and fold, the risk escalating with increasing wafer size. It is already highly desired for most 3D integrated circuit (IC) manufacturers to thin wafers to a thickness of 50 μm or less to realize the full benefit of 3D integration. Handling such thin

wafers demands that each wafer be temporarily bonded to a carrier or handle wafer using a temporary bonding material. Alternatively, the device wafer can be bonded permanently or mounted directly onto another device wafer face-to-face, followed by thinning and processing (Ramm *et al.*, 2012).

Once a device wafer is attached to a carrier wafer, the wafer pair can be processed like a standard full-thickness wafer without additional modification of the processing equipment or the process flow (Puligadda, 2007; Hosali, 2008; Hermanowski, 2009; Pargfrieder, 2009; Wolf, 2008). When the backside processing is complete, the thinned wafer can be separated (released or debonded) from the carrier and attached to a dicing frame, where it is diced to create dies for the pick-and place process. Alternatively in a wafer-to-wafer scheme, the entire device wafer can be bonded permanently to another device wafer before being released from the carrier wafer (Ramm *et al.*, 2012). A scheme of temporary bonding and debonding process is introduced (Figure 1-6) (SUSS Microtec, 2012).

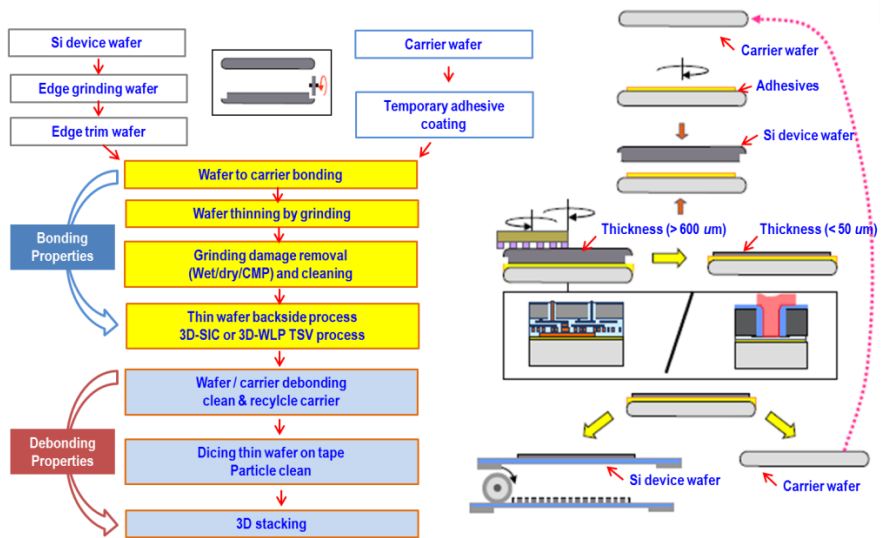


Figure 1-6. Scheme of temporary bonding and debonding process (SUSS Microtec, 2012).

1.2.2. Temporary bonding and debonding technologies

Temporary bonding a device wafer to a carrier and effectively releasing the device wafer are considered to be among the most critical and enabling technologies for achieving 3D integration of devices. The requirements of the temporary bonding materials heavily depend not only on the backside processes, but also on the condition of the device wafer and the processes it has been through prior to bonding (Ramm *et al.*, 2012). A “via-first” (Garrou *et al.*, 2008) device wafer presents different challenges from a device wafer in a “via-last” process. In a via-first process, the TSVs are fabricated in the device wafer prior to bonding. The higher coefficient of thermal expansion of copper, tungsten, or polysilicon used to fill the TSVs compared to that of silicon causes stress in the wafer, which becomes important when the wafer is thinned to 100 μm or less. In a via-last process, the TSVs are fabricated after the device wafer is thinned and bonded to a carrier wafer. The temporary bonding agent in this case must go through many processing steps including deep via etching, electroplating, etc. Schematics of the via-first and via-last processes are shown in Figure 1-7. In addition to the backside process, requirements of the adhesives depend on the condition of the device wafer. For instance, bumps on the device side impart greater challenges than a device wafer with low topography. Additionally, bumping on the backside of the thinned wafer requires special chucking for release and further handling. Several different technology options are available today for bonding and debonding or demounting after processing. While tapes and waxes are commercially available and used industry-wide for a limited number of applications today, they typically do not survive high-temperature processes and harsh chemical environments. Additional limitations include high total thickness variation (TTV) and the presence of residues after release (Ramm *et al.*, 2012).

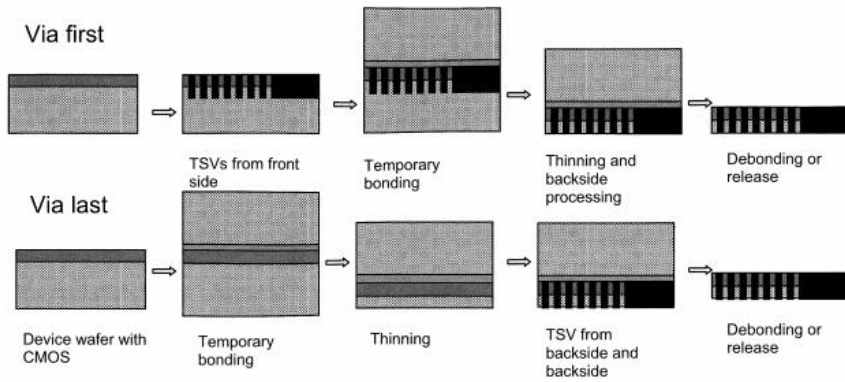


Figure 1-7. Schematics of via-first and via-last processes (Ramm *et al.*, 2012).

The key requirements for temporary bonding agents or adhesives and the related bonding and debonding processes include the following (Ramm *et al.*, 2012).

- **Ease of application** - the process flow for application of the temporary bonding agent should enable high throughput and preferably use industry-known and accepted unit processes.
- **Low TTV** – the TTV of the adhesive is transferred to the thinned wafer during the thinning process. For a thermoplastic type of adhesive, reflow during the bonding process allows greater uniformity in the bond line.
- **Good adhesion to a wide variety of surfaces** – a typical device wafer has several different surfaces in contact with the adhesive. Poor wetting to any of these surfaces may lead to delamination or voiding in the bondline.
- **Bonding and debonding at appropriate temperature** – low bonding and debonding temperatures are advantageous for conserving thermal budgets of the device wafer. For obvious reasons, these processes should be performed below temperatures limited by device stability.
- **High thermal stability** – the adhesive layer must remain stable through the high-temperature backside process including debonding to avoid breakage failure and equipment contamination. Examples of high-temperature processes include dielectric deposition, annealing, metal deposition, permanent bonding, and solder reflow.

Furthermore, outgassing from the adhesive layer is an important consideration. Also, certain processes between temporary bonding and debonding are conducted at higher temperature atmosphere. Accordingly, the adhesive must maintain high thermal stability (Figure 1-8) (SUSS Microtec, 2012).

- **High chemical resistance to process chemicals** – the adhesive material must be resistant to process chemicals such as etchants and corrosive electroplating solutions yet remain soluble in the removal solutions after debonding.
- **Good mechanical strength to keep device wafer in place** – the mechanical stability of the adhesive become important during high-temperature processes where it must hold down the thinned, often highly stressed device wafer to prevent buckling or curling.
- **No damage to wafer during thinning, debonding, or handling** – Damage to device wafers during thinning can be mitigated to a large extent using one of the several edge protection schemes. In addition to damage that the grinding process can cause, significant damage can occur during handling after debonding if the wafer is not fully supported. Flattening or smearing of backside bumps is an additional concern and therefore requires special debonding and handling chucks.
- **No residue** – it is imperative that the bonding agents or adhesives must be completely removed from the surface of the wafer to avoid difficulties in downstream processing and to prevent negatively affecting the reliability of the device package.

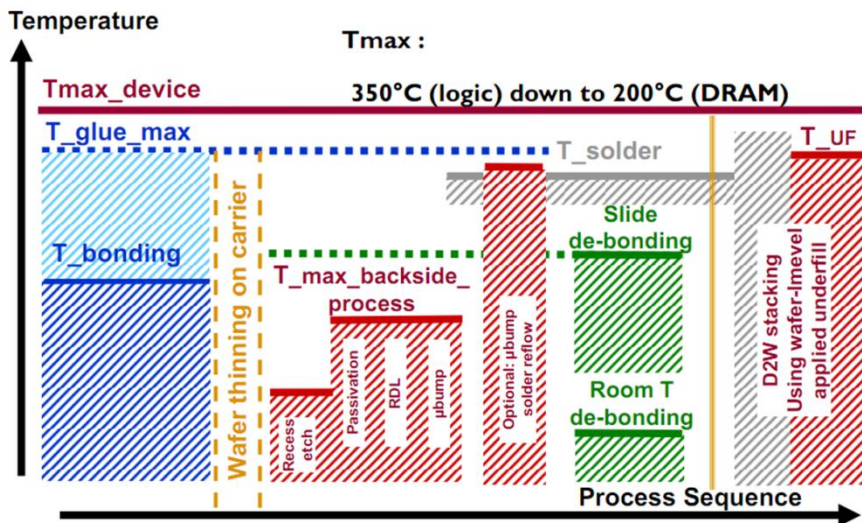


Figure 1-8. Temperature requirements in process sequences (SUSS Microtec, 2012). To maintain the high purity, it is required to have over 200 °C processing temperature during the process of bonding and debonding

1.2.2.1. Thermoplastic adhesive, slide-off debonding approach

The materials used in this approach are primarily developed by Brewer Science Inc., and were originally designed to be compatible with equipment manufactured by EV Group (EVG) (Mathias, 2007). The adhesive solution is applied to either the carrier or the device wafer by spin-coating. An important consideration for the coating process is that the adhesive thickness must exceed the height of device features to ensure complete planarization. The remaining solvent in the film is then eliminated using a baking process. The device wafer and carrier are bonded in a vacuum chamber at a temperature above the softening point of the adhesive and at pressures ranging from 5 to 20 psi. This technology can be used with silicon, glass, or sapphire carriers of the same size as the device wafer. As a result, this approach requires no modification to the lithography, etch, or deposition tools. After backside thinning and other processes on the device wafer, the wafer pair is heated to a temperature above the softening point of the adhesive, and the device wafer is separated from the carrier by sliding off the carrier wafer. The thin device wafer is completely supported on a vacuum chuck in the debonding equipment. The device wafer and carrier are then cleaned on a specially designed chuck using an appropriate remover, which is typically supplied with the adhesive. The thin device wafer is then transferred to a dicing frame or a coin stack. Other output formats such as individual carriers have also been investigated. The wafers are processed in a single-wafer-processing mode in each of these processing steps. The slide-off approach is shown in Figure 1-9. When automated, this approach requires an equipment set consisting of a bonder unit where the device wafer is coated and bonded and a debonder unit where the wafers are separated and cleaned (Ramm *et al.*, 2012).

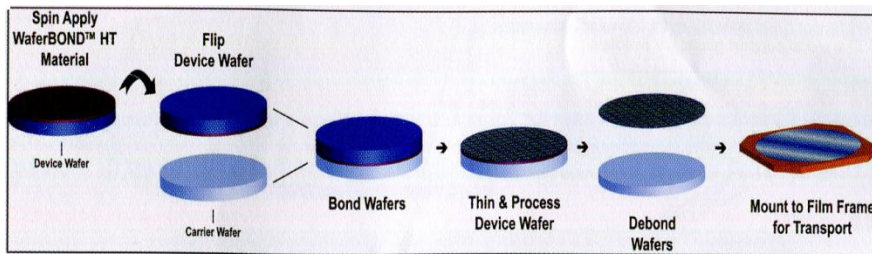


Figure 1-9. Process flow for slide-off debonding approach (Ramm *et al.*, 2012).

1.2.2.2. Using Ultraviolet-curable adhesive and light-to-heat conversion layer

This approach has been developed by 3M to be used in conjunction with specially designed equipment (Kessel, 2007; Sukengwu, 2008). A liquid adhesive is applied using a spin-coating process, and the adhesive planarizes the topography on the device wafer. The device wafer is then mounted onto a glass carrier. The glass carrier is coated with a material called a light-to-heat conversion (LTHC) layer before the carrier is laminated to the wafer. The adhesive is cured using ultraviolet (UV) light to create a bond. The LTHC layer can absorb certain wavelengths of light such that irradiating this layer with a focused laser beam can generate enough heat to decompose it. As a result, the wafer detaches from the glass carrier. The backside of the device wafer is first attached to supporting tape before rastering the laser through the glass side. The cured adhesive film is peeled from the device wafer after separation of the glass carrier. An overview of 3M's process is shown in Figure 1-10. This approach also requires an equipment set with two members, a "mounter" and a "demounter". Additional equipment may be required for preparing the glass carrier with the LTHC layer (Ramm *et al.*, 2012).

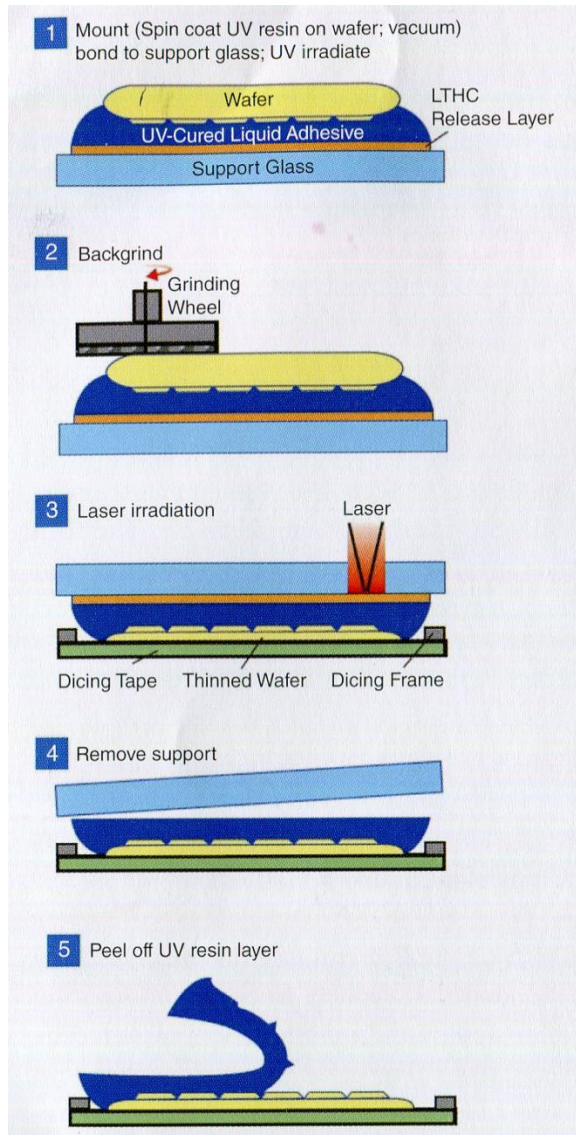


Figure 1-10. Process flow for 3M wafer support system (Ramm *et al.*, 2012).

1.2.2.3. Adhesive dissolution through perforated carrier wafer

The equipment and materials needed for this approach are being developed by Tokyo Ohka Kogyo, Japan. The adhesive is spin-coated onto the device wafer, and the adhesive's solvent is removed by baking. Following the coating process, the device wafer is bonded to a perforated support carrier. The device wafer goes through subsequent backside processing such as grinding, etching, dielectric deposition, etc. Upon completion of backside processing, the wafer is separated by dissolution of the adhesive. Solvents or removal solutions penetrate through the perforations in the carrier wafer and dissolve or etch the adhesive layer. The thin wafer is supported on a film frame through the demounting process. The thin wafer is further cleaned to remove any residue. Dedicated equipment units for mounting and demounting of the support plate are also needed for this approach. Figure 1-11 shows an overall description of the process and equipment used in this approach (Ramm *et al.*, 2012).

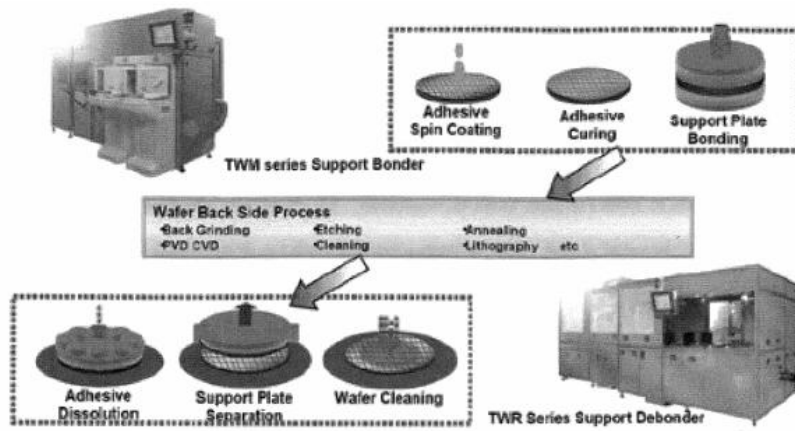


Figure 1-11. Overview (Garrou, 2009) of single-wafer debonding process using dissolution through perforated wafer plate (Ramm *et al.*, 2012).

1.2.2.4. Using a release layer and lift-off

This technology, developed by Thin Materials AG, Germany, involves separating the thinned wafer from the carrier by a lift-off process. The device wafer in this approach (Garrou, 2009) is coated with a very thin (a few hundred nanometers thick) release layer. The release layer is deposited in a two-step process. First, a precursor material is spin- or spray-coated onto the wafer and it is then subjected to a plasma treatment to give it nonstick characteristics. This step is followed by spin-coating a silicon-based elastomeric material and curing at temperatures near 200°C. Following thinning and backside processing, the backside of the device wafer is attached to a film frame, and the carrier wafer is lifted off the wafer. Figure 1-12 shows a schematic of the overall process (Ramm *et al.*, 2012).

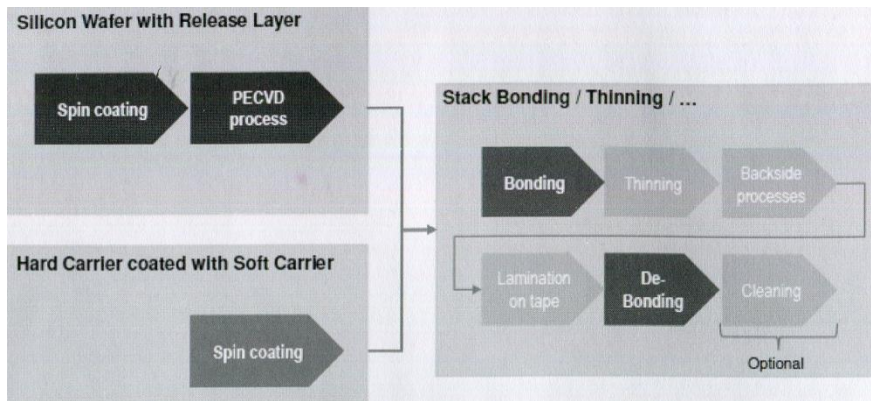


Figure 1-12. Overall (Boudaden *et al.*, 2008) description of release using liftoff process (Ramm *et al.*, 2012).

1.2.2.5. Room temperature, low-stress debonding

Developed recently by Brewer Science, this approach utilizes two zones to bond the device wafer to the carrier wafer. It uses a material in the center (one of the zones) to fill in the gap while not adhesively bonding them together. The outer edge is adhesively bonded to ensure the wafers remain together during subsequent processing and to prevent corrosive process chemicals from penetrating the bond line between the wafer stack. The two zones are achieved by treating the carrier wafer to give it a nonstick quality except at the periphery. This technique allows the adhesive coated on the device wafer to adhere only to the edge zone of the carrier. Figure 1-13 shows a schematic of the process used to achieve selective adhesion at the edges. Unlike the approach described previously, the carrier wafer is peeled away after thinning and backside processing while the device wafer is supported on a vacuum chuck (Ramm *et al.*, 2012).

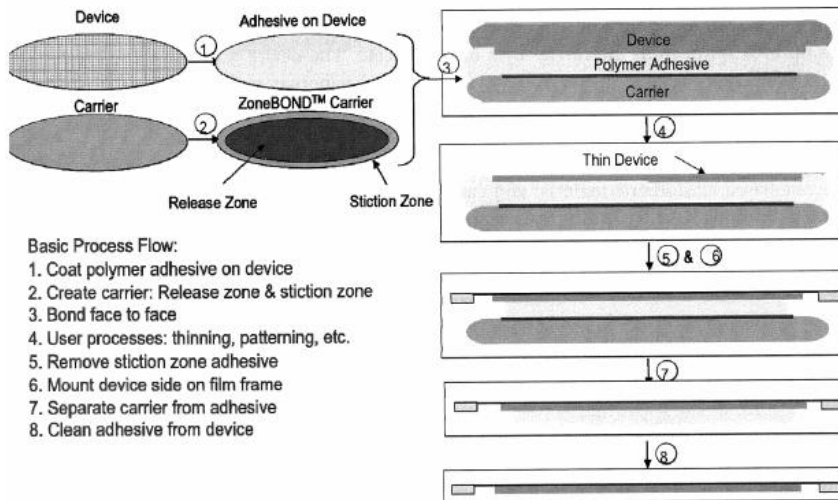


Figure 1-13. Overview of Brewer Science’s low-stress, room temperature debonding process (Ramm *et al.*, 2012).

1.2.3. Concerning for temporary bonding and debonding

1.2.3.1. Uniform and void-free bonding

Uniformity of the bond is one of the factors that affect the TTV of the thinned wafer. Contribution of temporary bonding layer uniformity to TTV can be minimized by utilizing a spin coating process to deposit the temporary bonding layer and ensuring that chucks on the bonder are flat and leveled. A drop micrometer is frequently used to measure total stack thickness at several points on the wafer to ensure low variation. A void in the bond line is a more severe problem. Scanning acoustic microscopy is an effective method to detect voids in the bonding layer. A large void trapped between the two wafers can expand in a subsequent high-temperature, low-vacuum process and cause delamination of the device wafer from the carrier. In extreme cases, it can cause breakage of the thinned wafer. Additionally, small voids can agglomerate during the high-temperature processes to make larger voids. Voids caused by air trapped during the bond process can be avoided by drawing a vacuum in the bonding chamber before bringing the two wafers into contact. Another common source of voids in the adhesive is the outgassing from the device wafer surface. This can be alleviated by treatment of the device wafers at high temperature for a limited time before coating with adhesive (Ramm *et al.*, 2012).

1.2.3.2. Protecting wafer edges during thinning and subsequent processing

Edge chipping and breakage is one of most common failure modes for thinning processes. Grinding a device wafer from the backside creates a very sharp edge that is prone to chipping and cracking. A study conducted by Brewer Science (Bai, 2009) compared the efficacy of the most common edge protection schemes. Control wafer pairs were simply bonded and thinned. Figure 1-14 shows each of the four schemes. All four of the protection schemes showed improvement with regard to edge chipping. The size and number of chips were markedly less than those of the control pairs (Ramm *et al.*, 2012).

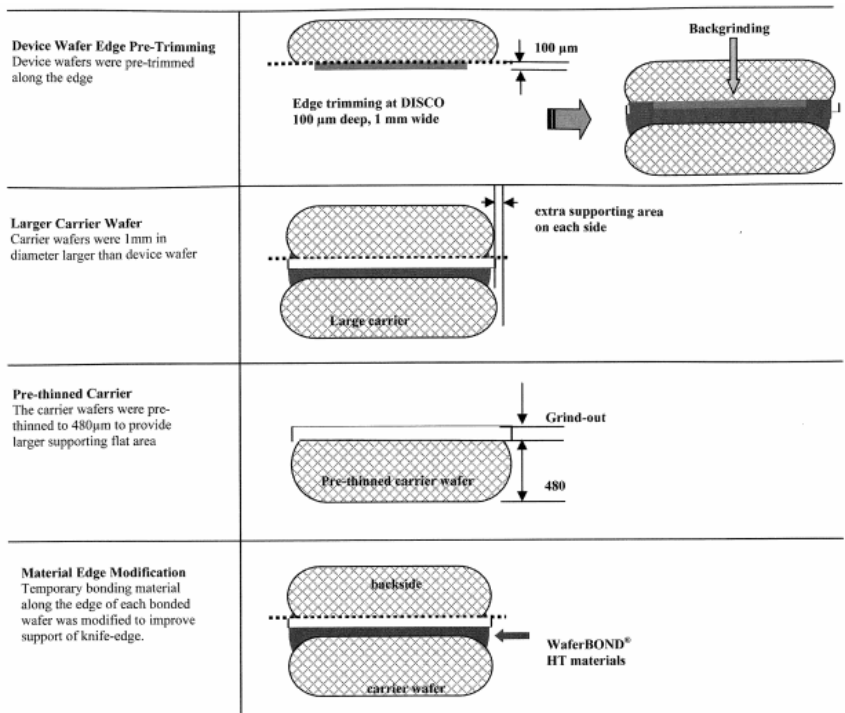


Figure 1-14. Overview of edge protection methods (Ramm *et al.*, 2012).

1.3. Objectives

Almost all of ultrathin wafers of less than 50 μm of thickness should be controlled by using the process on a temporary carrier wafer. Those carrier wafers need to be perfectly compatible with common semiconductor processes which are used during backside processing. For this, there are several technologies that the bond can be released after thinning of the device wafer. In one technique, a thermoplastic layer is used for bonding. The adhesion force of this layer is weakened on heating to elevated temperatures which allows separation of the wafers. In another method, the carrier is released by exposing the adhesive to intense laser irradiation. In a third method, the adhesion layer can be dissolved by chemicals applied through holes in a special, perforated carrier wafer. Unfortunately, the temperature range for subsequent processing may be too low for the first method, and the other approaches require expensive carrier wafer (Ramm *et al.*, 2012).

Conventional processing temperature between temporary bonding process and debonding process is raised to more than 200 $^{\circ}\text{C}$ for high purity. So, surface contamination of thin silicon wafer is generated by low molecular substances which are induced by thermal degradation of conventional adhesives. Also, cracking or broken thin silicon wafer is presented because of bonding strength after debonding process.

In this study, an alternative newly method for temporary bonding and debonding has been developed and proposed which not only obtains advantages but also avoids drawbacks of mentioned some technologies. It is based on a released layer treated glass carrier wafer, dual curable adhesives and UV laser debonding. This means as followings;

- To synthesize dual curable adhesive for UV laser debonding

- To investigate UV and thermal curing behaviors
- To optimize and evaluate UV laser debonding

Studies were proceeded as dividing to two aspects, bonding and temporary bonding and debonding.

For bonding properties, three experimentals were conducted as following objectives;

- **First experimental**
 - To employ a hexafunctional acrylic monomer for interpenetrating network structure (IPNs) for enhancing thermal stability.
 - Increasing a photo-initiator control and UV dose to control adhesion properties
- **Second experimental**
 - To synthesize an adhesive with a silicon containing acrylic monomer (as a solvent polymerization, not a blending for UV-curing) for enhancing thermal stability and decreasing adhesive manufacture steps
 - To control adhesion properties by using different UV curing methods (steady irradiation and pulsed irradiation) as an UV curing process
 - To investigate thermal stability and adhesion properties by using different concentration of a photo-initiator and UV dose
- **Third experimental**
 - To employ certain types of a silicon containing monomer and

acrylic monomers using twofold urethane reactions for 100% solid polymerization because of enhancing thermal stability and a reasonable spin coating

- To investigate dual curing (UV and thermal) for enhancing thermal stability
- To investigate thermal stability and adhesion properties by using different concentration of a photo-initiator and UV dose in this system

For temporary bonding and debonding properties, fourth experimental was conducted as following objectives;

- **Fourth experimental**

- To employ certain types of a fluorine containing monomer, silicon containing monomer and acrylic monomers using threefold urethane reactions for 100 % solid polymerization because of enhancing thermal stability and a reasonable spin coating
- To synthesize using an UV absorbing material, which absorbs UV energy, especially approximately 40 % of absorbance in the wavelength at 355 nm
- To investigate surface morphologies, properties and debonding mechanism

Chapter 2

Literature Review

2.1. UV-curing

The use of radiation curing provides an opportunity to develop products that are highly competitive. Since often they are virtually 100 % solid, generally they have less shrinkage than traditional solvent-based or water-based adhesives, and since they are cross-linked, they usually have better thermal and flow resistance than the majority of hot-melt adhesives available. They may also be used with heat-sensitive substrates since they need to be exposed to less heat than the their types, and when one considers the total economics of the system including, besides the raw-material costs, the costs of energy, pollution control and speed of throughput, they are seen to be cost competitive. Improvements in technology, performance attributes, curing characteristics and toxicity hazards have all contributed to the growth of the radiation-curable laminating adhesives (Ellerstein *et al.*, 1993).

Adhesives that cure by exposure to a UV or light radiation have become essential to many assembly operations where high throughput or delicate components are prevalent. These adhesives require the presence of the correct wavelengths of light at sufficient intensity to form durable structural bonds. UV and light cure adhesives use photo-initiators to activate the free radical curing mechanism (Petrie, 2000).

UV-curing technology can be divided into UV-polymerization and UV-crosslinking methods. UV-polymerization are formulated with relatively low molecular weight (M_w ; 400~5,000) monomers or prepolymers and photo-initiators; however, UV-crosslinkable PSAs are composed with high molecular weight (M_w ; 1,000,000~20,000,000) PSA polymer containing UV-crosslinkable site in side chain. For example, hot-melt pressure-sensitive

adhesives, when heated, assume a low viscosity suitable for a homogeneous thin layer application. These polymers achieve their adhesive strength during subsequent cooling on the base material. The absence of a thinner gives this group of adhesives its high economic and ecological significantly lower space requirement, lower energy costs and emission free processing (Do *et al.*, 2005).

UV exposition the intermolecular benzophenone derivatives H-abstractors structures are excited and react with the neighboring C-H positions of polymer side-chains (Czech, 2004).

2.2. Synthesis and UV-curable acrylate

Prepared photo-curable aliphatic epoxy acrylate with acrylic acid and 1,4-butanediol diglycidyl ether that was obtained by reacting 1,4-butanediol with epichlorohydrin. They investigated the properties of photo-curable aliphatic epoxy acrylate after the dilution with three kinds of reactive monomers: 2-hydroxyethyl acrylate, tri(propylene glycol) diacrylate, trimethylpropane triacrylate. Their viscosities decreased with the increased amount of reactive monomers, but increased when higher functionality of monomers were used. Also, glass transition temperature of UV-cured film shifted to higher temperatures as the functionality of monomer was increased, and thermal stability exhibited similar behavior. In addition other physical properties such as hardness, abrasion resistance, and tensile strength of UV-cured film, increased with increased functionality of monomer, but elongation was reduced with the higher monomer functionality (Lim *et al.*, 2003).

Three types of epoxy acrylate were synthesized One is liquid crystalline epoxy acrylate containing the mesogenic core *a*-methylstilbene, the other was synthesized with 4,4'-dihydroxy-*a*-methylstilbene and epichlorohydrin, another epoxy acrylate oligomer was synthesized from epoxy oligomer and acrylic acid in the presence of a reaction medium and a phase transfer catalyst for 12 h. The synthesized epoxy acrylate oligomer showed smectic liquid crystalline phase from room temperature to near 50°C compared with the nematic epoxy oligomer. The synthesized epoxy acrylate showed high photo-reactivity (Kim *et al.*, 2002).

Epoxy urethane acrylates were prepared from epoxy resins, acrylic acid and 4,4'-diphenylmethane diisocyanate using two-stage polymerization.

Synthesized epoxy acrylate is more flexible and have lower viscosity. The low molecular weight of the oligomers results in low viscosity, making it possible to use these materials as solvent less coatings (Oprea *et al.*, 2000).

It was prepared UV-curable polyurethane acrylates from urethane-acrylate prepolymer, three types of reactive diluents, and 1-hydroxycyclohexyl phenyl ketone (Irgacure 184) as a photo-initiator. They investigated the effects of the chemical structure and the reactive diluent composition on mechanical and dynamic thermal mechanical properties of UV-cured polyurethane acrylates. Also, they investigated that the structure and properties of the film obtained from the UV photo-polymerization of urethane-acrylate prepolymer using FT-IR spectroscopy, dynamic mechanical measurement, and tensile testing (Lee *et al.*, 1999).

It was synthesized UV-curable polydimethylsiloxane epoxy acrylate by hydrosilylation of allyl glycidyl ether with H-containing polydimethylsiloxane to give polydimethylsiloxane-type epoxy resin which modified with acrylic acid. They reported that the curing speed and the double bond conversion in the UV-cured film were influenced by the purity of PSEA using FT-IR. Also, he was characterized the substrates of this resin using ¹H-NMR and FT-IR spectra (Wang, 2003).

It was prepared epoxy acrylates such as bisphenol type, propylene glycol type, and phthalic acid ester type from addition reaction between each epoxy resin and acrylic acid in the absence of solvent and in the presence of quaternary ammonium salt. They reported that the rates of photo-crosslinking of epoxy acrylates using by IR spectrophotometry. When epoxy acrylates with benzoin ethyl ether were irradiated by UV, the photo-crosslinking rates of epoxy acrylates decrease (Sun *et al.*, 2005).

It was investigated that UV-curing behavior of an epoxy acrylate resin system comprising an epoxy acrylate oligomer, a reactive diluent, and a photo-initiator using FTIR spectroscopy. They reported that the conversion of the resin system increased rapidly at the initial stage of the UV-curing process but increased very slowly after that. The final conversion of the resin system was mainly affected by total UV dosage (Hong *et al.*, 2005).

It was reported that a series of multiethylene glycol dimethacrylate (MEGDMA) was characterized with respect to the polymerization behavior, kinetics, and mechanism. They reported that the influence of the monomer structure was determined by studying a series of MEGDMA's with the number of ethylene glycol units ranging from 2 to 14. For each monomer, the propagation and termination kinetic constants were quantified as a function of conversion to provide insight surrounding the controlling polymerization mechanisms. The influence of the double bond concentration diethylene glycol dimethacrylate in the presence of an inert solvent. Finally, in addition to characterizing the general reaction behavior, the influence of volume relaxation on the polymerization behavior and kinetics was studied (Anseth *et al.*, 1995).

It was investigated the radiation curing behavior of poly(ethylene glycol 400) dimethacrylate and ethylene glycoldimethacrylate using photo-DSC as a function of temperature and photo-initiator concentration. They reported that the reaction speed of PDG400DMA and EGDMA increased as the number of ethylene glycol unit, the concentration of photo-initiator, and the reaction temperature increased (Do *et al.*, 2003).

2.3. Fluorinated polyurethane acrylate

It was synthesized a novel fluorinated polyurethane from fluorinated polyether glycol (PTMG-g-HFP), 1,6-hexamethylene diisocyanate (HDI) or toluene diisocyanate (TDI) and 1,4-butanediol (BDO), and the structure was characterized by FT-IR and NMR. The incorporation of fluorinated polyether glycol in the polyurethane backbone showed a significant effect on the thermal stability of PU. XPS analysis results showed that there was an obvious mobility of fluorinated groups to the fluorinated polyurethane had outstanding chemical resistance and strain-hardening property compared with the conventional PU (Ge *et al.*, 2009).

It was reported that a telechelic polyurethane end-capped with perfluoropolyether segments was prepared from polyether glycol as a soft segment, 4,4'-methylene-bis-(phenylisocyanate), and mono-functional perfluorinated oligomer. XPS results indicated that surface of the fluorine containing polyurethane was enriched with fluorine component. It exhibited a hydrophobic property with a water contact angle of 113°. The polyurethane terminated with perfluoropolyether segments shows a better. A mechanism was proposed to explain thermal decomposition of polyurethanes (Zhu *et al.*, 2010).

Chapter 3

Adhesion Performance and
Surface Morphology of UV-curable
Interpenetrating Network Acrylates
for 3D Multi-chip Packaging Process

3.1. Introduction

Photo-induced polymerization includes polymerization by UV light, visible light electron beam, or by laser. Photo-curing refers to polymerization that includes unsaturated inks, coatings and pressure-sensitive adhesives (PSAs) (Dufour, 1993; Joo *et al.*, 2007). UV-curing systems involving photo-curing are used widely because of their rapid production rate in a small working place and solvent-free curing at ambient temperatures (Joo *et al.*, 2007).

Adhesive tape is commonly adopted to tightly hold silicon wafers during the fabrication of semiconductor chips. Such adhesive tapes are called dicing tape. With the rapid development of integrated semiconductor technology, a higher reliability is needed for the manufacture of electronic devices (Ebe *et al.*, 2003). An excessive degree of cross-linking in pressure-sensitive adhesives (PSAs) prepared from unsaturated polyester resins by electron beam irradiation results in poor adhesive strength (Ebe *et al.*, 2003). This observation led us to establish a novel dicing process, as shown in Figure 3-1. A piece of silicon wafer was tightly held using dicing tape with strong adhesion strength, which enabled rapid and smooth dicing of the wafer. Subsequently, the adhesive layer was irradiated with UV light through the reverse side of the substrate. After UV irradiation, the adhesion strength decreased to a certain level, where it easily picked up the diced chips for a further die-bonding process. Dicing tapes developed using this process has been reported and similar suggestions have been made (Ebe *et al.*, 2003).

On the other hand, acrylic monomers and oligomers are used widely on account of their superior properties, such as transparency, colorlessness, resistance to yellowing under sunlight and resistance to oxidation due to their saturated structures. However, they have poor thermo-mechanical stability because of their linear structure. Therefore, the cross-linking of

multifunctional acrylates is needed to increase their thermo-mechanical stability. It was reported that an adhesive shows fluid-like behavior when it is widely cross-linked. However, the creep resistance increases greatly for a more cross-linked adhesive (Joo *et al.*, 2007; Sosson *et al.*, 2005). Cross-linked Multifunctional acrylates produce semi-interpenetrating polymer networks (IPNs). Semi-IPN structured adhesives have advantages, such as improved heat and creep resistance (Joo *et al.*, 2007; Sosson *et al.*, 2005; Joo *et al.*, 2006). In addition, it was reported that photo-polymerization was effective in obtaining networks with a high degree of interpenetration (Athawale *et al.*, 2003).

In the fabrication of semiconductors, adhesives are used for processes other than dicing, wherein the required adhesion strength is different. Accordingly, control of the peel strength by UV-curing has the potential to facilitate the procedure and/or broaden the applications. An acrylic copolymer itself would not change its adhesion strength with UV irradiation due to the absence of a reactive site to UV irradiation (Ebe *et al.*, 2003; Amagai *et al.*, 1995; Ozawa *et al.*, 2000).

In this study, IPN acrylic adhesives in a wafer manufacture process, were prepared using a hexafunctional acrylate monomer with a UV-curing system. Emphasis was placed on curing behaviors according with the curing agent contents, hexafunctional acrylate monomer contents, photo-initiator contents and coating thickness, which were examined using the 180° peel strength. The analysis by FE-SEM and XPS showed that there was little residue on the wafer after the release of adhesive layer by UV irradiation (Lee *et al.*, 2012).

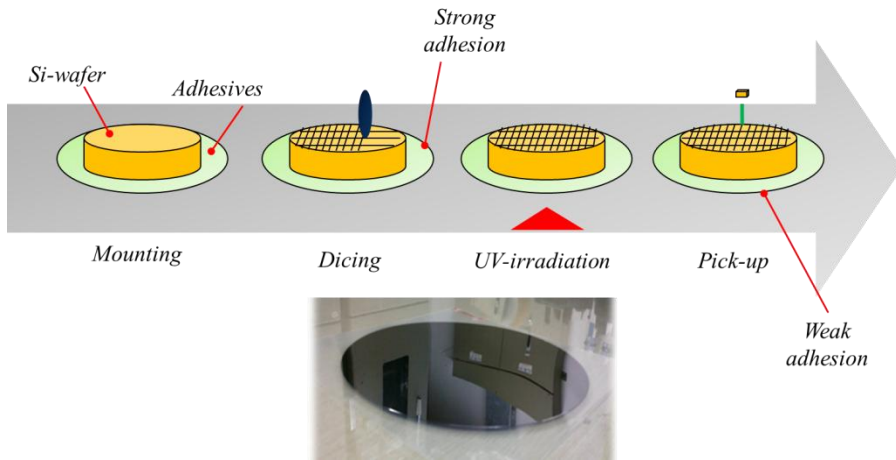


Figure 3-1. Schematic diagram of the process on thin Si-wafer manufacture applied with acrylates (Lee *et al.*, 2010)

3.2. Experimental

3.2.1. Materials

The 2-ethylhexylacrylate (2-EHA, 99.0% purity, Samchun Pure Chemical Co., Ltd, Republic of Korea) and acrylic acid (AA, 99% purity, Samchun Pure Chemical Co., Ltd, Republic of Korea) were commercially available and used without purification. The ethyl acetate (EAc, Samchun Pure Chemical Co., Ltd, Republic of Korea) and methanol (MeOH, Samchun Pure Chemical Co., Ltd, Republic of Korea) were used as solvents. The chemical 2,2'-azobisisobutyronitrile (AIBN, Junsei Chemical, Japan) was used as a thermal initiator, a methylaziridine derivative (MAZ, DSM Neoresins, USA) was used as the cross-linking agent and dipentaerythritol hexacrylate (DPHA, Miwon Specialty Chemical, Republic of Korea) was used as the diluent monomer. Figure 3-2 shows the chemical structure of hexafunctional acrylate, which has six C=C double bonds. The compound, 2-hydroxy-2-methyl-1-phenylpropane-1-one (Miwon Specialty Chemical, Republic of Korea) was used as the photo-initiator (Lee *et al.*, 2012).

3.2.2. Methods

3.2.2.1. Synthesis of binders

Acrylic monomers (2-EHA, AA) were synthesized as 95 and 5 wt% by solution polymerization. The amount of AIBN in the binders was 0.3 phr. The mixture was placed into a 500 ml four-neck flask equipped with a stirrer, condenser and thermometer, and heated to 75°C with constant stirring. At the end of the exothermic reaction, the temperature was maintained for 30 m, and a blend of ethyl acetate and AIBN was added. The reaction was allowed to proceed for 0.5 and 2.5 h. Finally, polymerization was terminated by cooling the mixture to room temperature (Lee *et al.*, 2012).

3.2.2.2. Formation of the acrylate film

All acrylic binders were coated onto the corona treated polyethylene terephthalate (PET, SK Chemical, Republic of Korea) film using coating bars, kept at room temperature for 1 h and then dried in an oven at 80 °C for 20 m. The dried film was kept at 22±2 °C and 60±5% RH for 24 h before performing the tests (Lee *et al.*, 2012).

3.2.2.3. Preparation of cured acrylates

The acrylates were cured using two methods: the addition of a curing agent followed by UV-curing. The curing agent was the multifunctional methylaziridine. The cross-linking of the acrylates with multifunctional methylaziridine is based mainly on the carboxyl groups of the vinyl carbonic acids within the polymeric chain. The oxygen of the nucleophilic carboxyl group causes ring opening of the tense aziridine rings, whereas the hydrogen atoms accompanying the carboxyl groups protonate the nitrogen atoms (Figure 3-3) (Czech, 2007). UV-curable acrylates were prepared by blending the polymerized binders with a photo-initiator and hexafunctional acrylic monomer. The UV-curable acrylates were coated onto polyester (PET) films and cured using conveyor belt type apparatus fitted with a 100 mJ/s high pressure mercury lamp (main wavelength : 365 nm). The UV doses were measured using an IL 390C Light Bug UV radiometer (International Light, USA). Despite low molecular weights, the hexafunctional monomers in the acrylates can be photo-polymerized after a UV dose to form IPN structures (Figure 3-4). The cured samples were weighted and immersed in toluene for 24 h at 50°C, and then screened and dried at 80°C to a constant weight. The gel fraction of the samples was calculated using the following equation: (Lee *et al.*, 2012).

$$\text{Gel fraction (\%)} = W_t / W_0 \times 100, \quad (1)$$

Where W_0 and W_t are weight of samples before and after immersion, respectively. The gel content provides information on the degree of cross-linking (Wu *et al.*, 2010; Yang *et al.*, 2008).

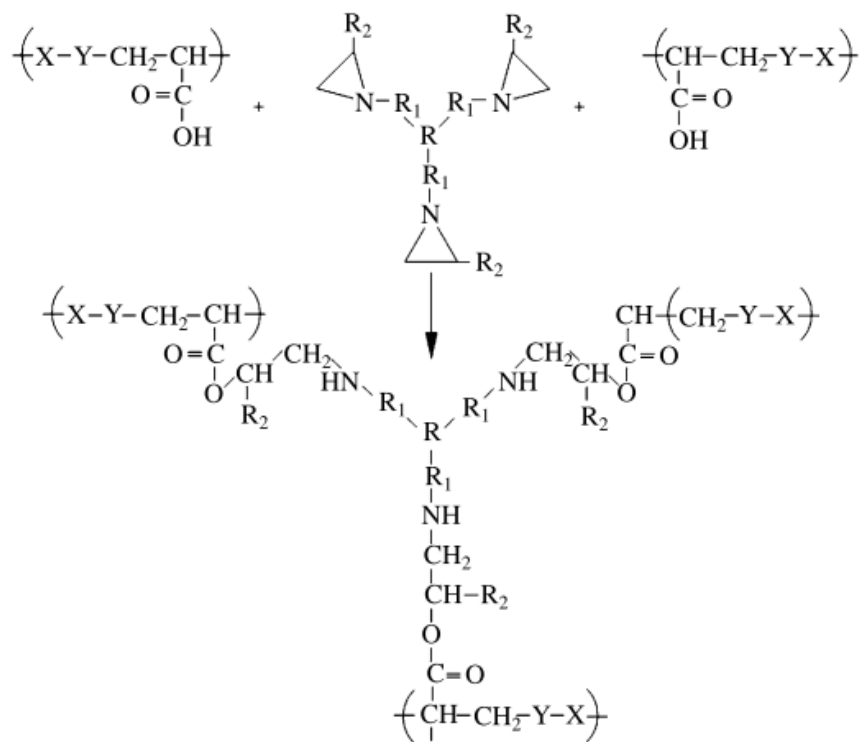
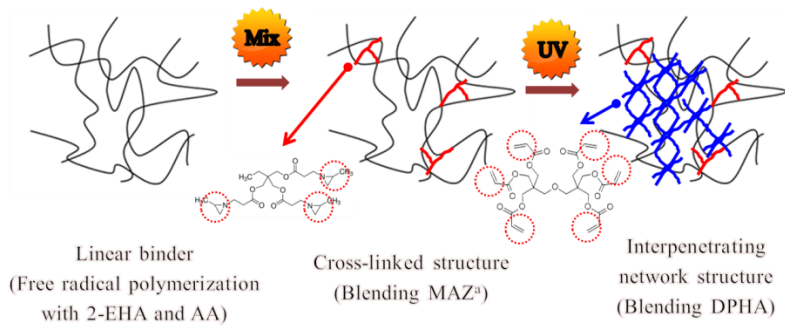


Figure 3-3. Crosslinking of carboxylated functionality with methylaziridine (Czech, 2007).



*MAZ reacts with carboxylated functionality of acrylic acid in binder (Czech, 2007)

Figure 3-4. Process of producing IPN structure in UV-cured acrylates.

3.2.2.4. Adhesion performance

The peel strength was measured using a texture analyzer (Micro Stable Systems, TA-XT2i). The specimens were 25 mm in width. The specimens were pressed onto the Si-wafer substrate by 2 passes of a 2 kg rubber roller and stored at room temperature for more than 12 h. The peel strength was determined at a 180° angle with a crosshead speed of 300 mm/m at 20°C based on the ASTM D3330. The peel strength was the average force on the debonding process. The force was recorded in g unit for 10 different runs and the average force was reported as gf / 25 mm.

3.2.2.5. Field emission-scanning electron microscopy (FE-SEM)

The surface morphology of each sample after the peel strength test was measured by field-emission scanning microscopy (SUPRA55VP, NICEM at Seoul National University, Republic of Korea). The fractured samples were coated with a thin layer of gold (purity 99.99 %) prior to the FE-SEM examination to prevent electron charging.

3.2.2.6. X-ray photoelectron spectroscopy (XPS)

X-ray photoelectron spectroscopy (XPS, PHI 5000 Versa Probe, Ulvac-PHI) was performed using Al Ka radiation (1486.6 eV, Anode (25W, 15kV)). The bonding energies were calibrated with reference to the C (1s) peak at 284.6 eV. For the measurement, the samples were placed into an ultra-high vacuum chamber and data analysis of the sensitivity factors of each element present, was performed (Wu *et al.*, 2010; Song *et al.*, 2006; Asahara *et al.*, 2004).

3.3. Results and Discussion

3.3.1. Adhesion performance

The adhesion performance of the acrylates was determined by measuring the 180°C peel strength. The peel strength decreased sharply to approximately 150 gf / 25 mm through the use of 1 phr (in binder) of aziridine, as shown in Figure 3-5. Interfacial failure, which means that there was no residue, was observed on all samples. This was attributed to networking formation of the acrylates due to the aziridine derivative. Furthermore, the cross-linked structure indicated increased cohesion force within the acrylates. Using cross-linking agents, the increase in cohesion might be accomplished during drying step. Logically, the tackifying properties of the coating and peel adhesion should decrease (Lee *et al.*, 2010; Czech, 2007; Czech, 2004). Two different types of substrates were used to measure the 180° peel strength. The peel strength on a Si-wafer was lower than that on SUS when less than 2 phr (in binder) of aziridine was used because the surface free energy of a Si-wafer is considered to be lower than one of stainless steel substrates, SUS (Chibowski, 2005). However, the peel strength was similar on both substrates (30~50 gf / 25 mm) when more than 2 phr (in binder) of aziridine was used. At more than 2 phr (in binder) of aziridine, all cross-linked samples affected the peel strength to a greater extent regardless of the substrate. In the debonding process of Si-wafer manufacture, the initial adhesion strength is an important factor because of the loss the fitted thin Si-wafers (Lee *et al.*, 2010). The optimum peel strength value was attained at approximately 0.5 phr (in binder) of aziridine, as shown in Figure 3-6 (Lee *et al.*, 2012).

Figure 3-7 shows the effect of the UV dose on the peel strength at different hexafunctional acrylate monomer contents. Soluble linear binders turned into

UV-cured insoluble IPN structured polymers by blending the hexafunctional acrylic monomer with photo-initiator (Joo *et al.*, 2006). The hexafunctional acrylic monomer contents were 10, 15, 20 and 30 wt.% (in binder). The photo-initiator content was 2 phr (in the hexafunctional monomer) in all samples. The peel strength decreased with increasing hexafunctional monomer formed a tightly cross-linked IPN structure in the acrylates because of its short chain length. In addition, the molecular mobility could be decreased because of the over-cured hexafunctional monomer, which overly increased the cohesion of the acrylates and decreased the peel strength (Joo *et al.*, 2006). The peel strength of the blends with monomer contents of 20 and 30 phr (in binder) decreased sharply to approximately 50 gf / 25 mm using an approximately 100 mJ/cm² of UV dose and almost leveled off. However, the peel strength of the blend with a hexafunctional monomer content of 30 phr (in binder) was lower than that with a content of 20 phr (in binder). The optimum peel strength was attained using a hexafunctional monomer content of approximately 30 phr (in binder) (Lee *et al.*, 2012).

The influence of the photo-initiator contents on the peel strength of acrylic adhesives after UV irradiation was examined. UV light is absorbed mainly by the photo-initiator and is attenuated progressively as it passes through the sample. The penetration of the incident photons is related directly to the photo-initiator content. Therefore, photo-initiated radical polymerization is an effective process for readily cross-linking functionalized polymers (Decker *et al.*, 2001). Figure 3-8 shows the effect of the amount of the photo-initiator on the peel strength of the samples with different UV doses. A low peel strength was obtained at a photo-initiator content > 2 phr (in the hexafunctional monomer) regardless of UV doses. The optimum peel strength was obtained with a photo-initiator content and UV doses of approximately 2 phr (in the hexafunctional monomer) and 200 mJ/cm², respectively (Lee *et al.*, 2012).

The coating thickness of the samples is a very important factor affecting the

performance, including the peel strength. As the Si-wafers become thinner, the adhesives thickness is different from 10~20 μm can be considered (Lee *et al.*, 2010). Figure 3-8 shows that the increase in UV dose from 0 to 200 mJ/cm^2 decreased the peel strength from approximately 450 to 20 $\text{gf} / 25 \text{ mm}$ at a coating thickness of 20 μm . A low peel strength was obtained at approximately < 20 μm despite the UV dose being more than 200 mJ/cm^2 (Lee *et al.*, 2012).

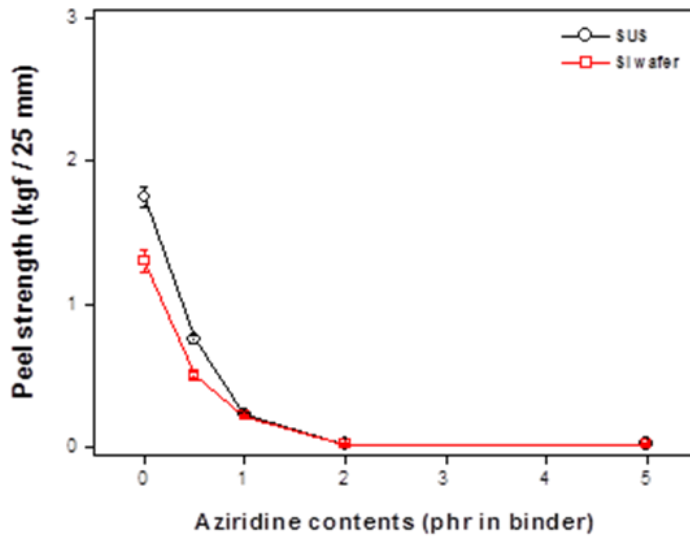


Figure 3-5. Peeling strength with the curing agents at the stainless steel (SUS) and Si-wafer (Lee *et al.*, 2012).

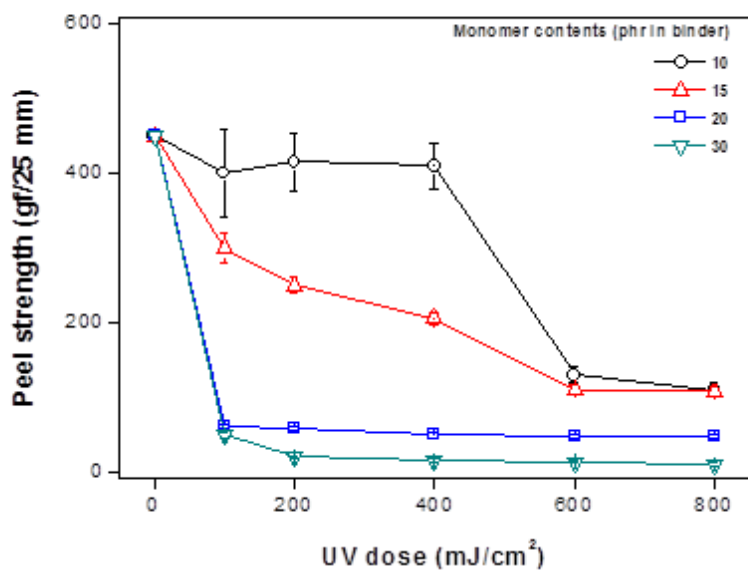


Figure 3-6. Peeling strength with different hexafunctional monomer contents (Lee *et al.*, 2012).

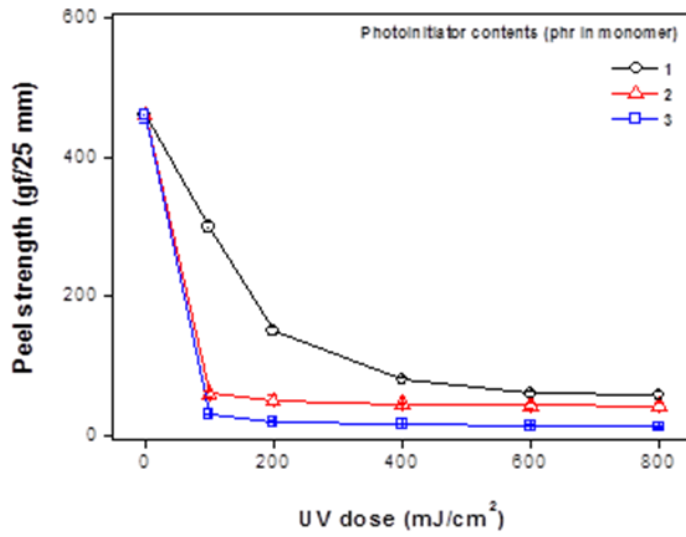


Figure 3-7. Peeling strength with different photo-initiator contents (Lee *et al.*, 2012).

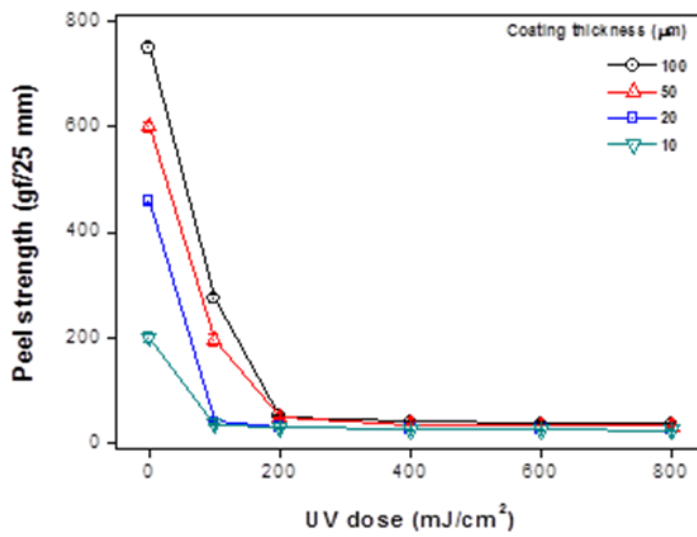


Figure 3-8. Effect of the UV dose on the peeling strength at different coating thickness (Lee *et al.*, 2012).

3.3.2. Gel fraction of the acrylates with the hexafunctional monomer at different photo-initiator contents

The photo-initiator plays a key role in controlling both the rate of initiation and the penetration of incident light (Wu *et al.*, 2010; Decker *et al.*, 2000). An increase in photo-initiator concentration will accelerate the cross-linking reaction, but a small excess of organic photo-initiator can be poisonous and harmful cleavage products can form during the application (Wu *et al.*, 2010). Figure 3-9 shows the gel fraction of the acrylates with a hexafunctional monomers at different photo-initiator contents (1/2/5 phr in binder). The gel content provides information on the degree of cross-linking. The gel fraction was calculated using equation (1). The gel fraction of cross-linked the acrylates increased with increasing UV doses and photo-initiator content. However, the gel fraction of the acrylates was similar when more than 2 phr of the photo-initiator was used. This shows that the cross-linking reaction accelerates more than 2 phr of the photo-initiator contents (Lee *et al.*, 2012). This means that the gel fraction can be controlled facilely by the UV dose and photo-initiator content (Kloosterboer, 1988).

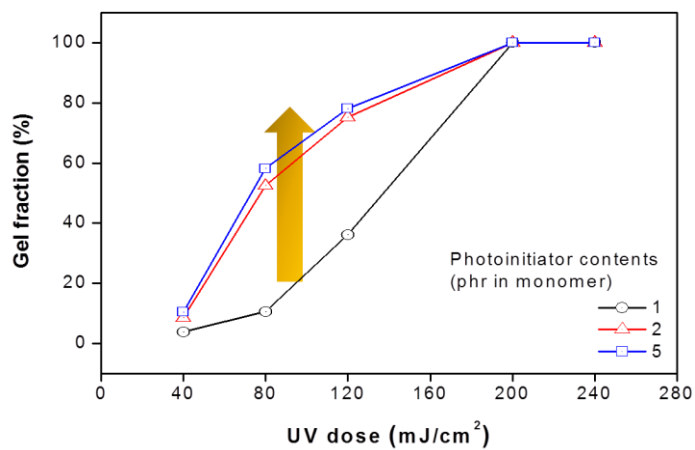


Figure 3-9. Gel fraction with a hexafunctional monomer at different photoinitiator contents (Lee *et al.*, 2012).

3.3.3. Field emission-scanning electron microscopy (FE-SEM)

The second aim of this study was to observe the morphology using FE-SEM (Figure 3-10) and to characterize contaminations of the polymers on the surface of the Si-wafers by XPS (Figure 3-11). The acrylates might remain on the Si-wafers after peeling after the UV dose during the process. Figure 3-10 shows the effect of the UV dose on the acrylates remaining after peeling. In the Si-wafer manufacturing process, it is important to check whether there is any acrylates remaining as the Si-wafer becomes thinner. The increase in UV irradiation indicates more cross-linking reactions (Lee *et al.*, 2010; Decker *et al.*, 2001). The proper UV dose in this study was found to be $\sim 200 \text{ mJ/cm}^2$ (Lee *et al.*, 2012).

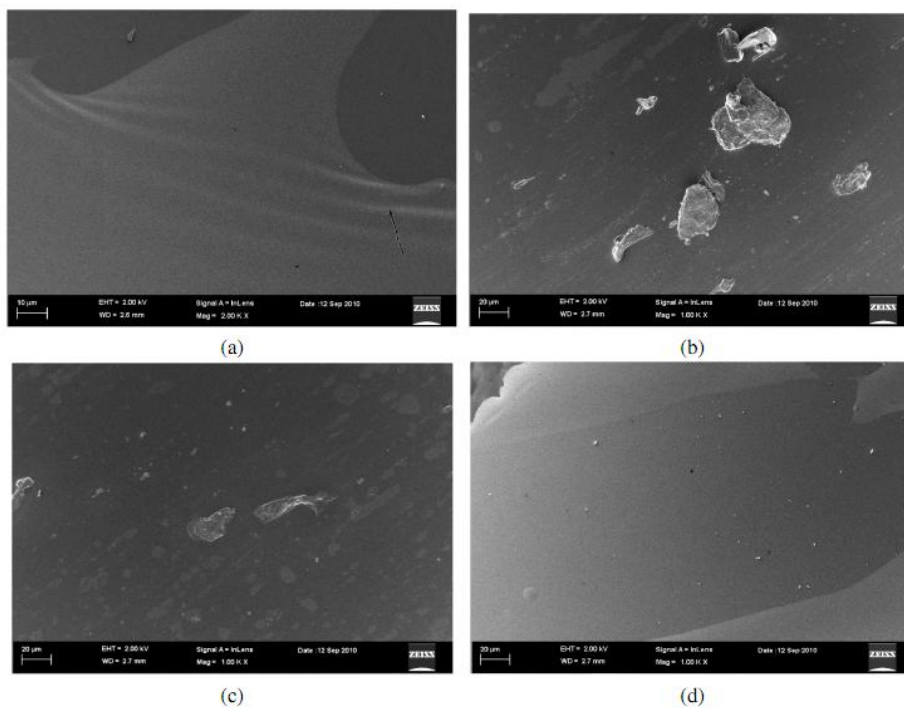
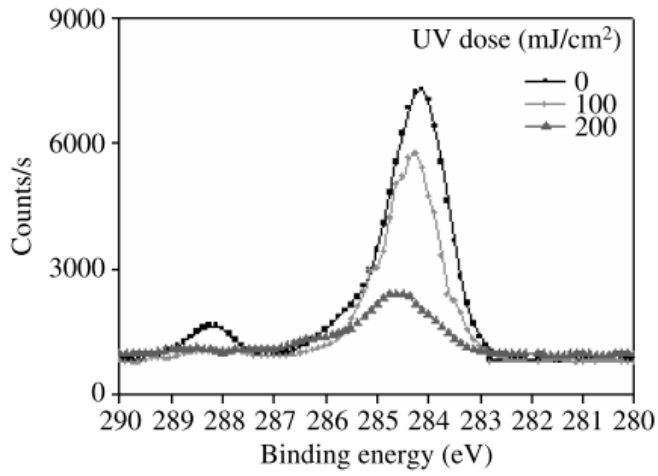


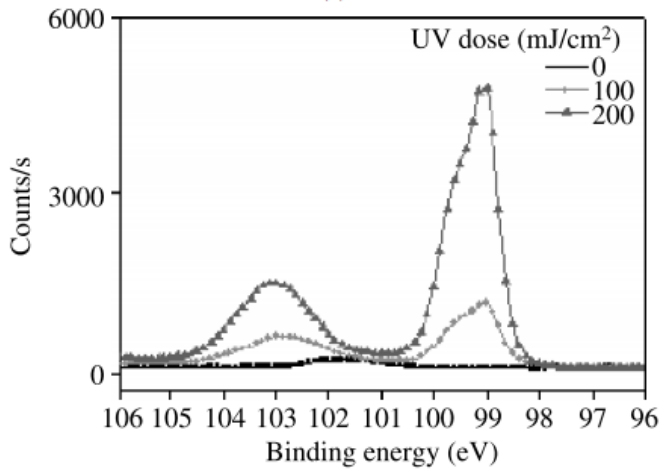
Figure 3-10. Field-emission scanning electron images of UV-cured acrylates at UV dose; (a) 0 mJ/cm², (b) 50 mJ/cm², (c) 100 mJ/cm², (d) 200 mJ/cm² (Lee *et al.*, 2012).

3.3.4. X-ray photoelectron spectroscopy (XPS)

XPS was used to determine the surface compositions of the Si-wafer after peeling at different UV doses. According to XPS, the C_{1s} core-level spectrum was curve-fitted with two peak components with binding energies at 284.6 and 288.5 eV, corresponding to the C-C/C-H and O-C=O functional groups, respectively (Song *et al.*, 2006; Zhang *et al.*, 2001; Severini *et al.*, 2001; Uchida *et al.*, 1990). In addition, a peak was observed at 283.9 eV in the C₁ spectra, which was assigned to inhomogeneous charging effect on the polymer surface due to its insulating nature (Massey *et al.*, 2003). The above C atoms were derived from the acrylic base polymer (Asahara *et al.*, 2004). As shown Figure 3-11, the peak at 284.6 eV, which was related directly to the characteristic of the polymer (C-C and C-H), decreased with increasing UV dose. On the other hand, the Si_{2p} peaks at approximately 100 eV and 103 eV (SiO₂) and increased with increasing UV dose. These results are in agreement with the reference values (Jin *et al.*, 1987; Weng *et al.*, 1995; Rimmer *et al.*, 1991). As listed in Table 3-1, the amount of carbon on the Si-wafer surface decreased with increasing UV dose a concomitant increase in the amount of the silicon, as a result of the cross-linking of the acrylates (Lee *et al.*, 2012).



(a)



(b)

Figure 3-11. (a) C_{1s} and (b) Si_{2p} XPS spectra of Si-wafer surface after peeling at varying UV dose (Lee *et al.*, 2012).

Table 3-1. Atomic concentration (%) of C_{1s} and Si_{2p} determined by XPS according to the UV does (Lee *et al.*, 2012).

UV dose (mJ/cm ²)	C _{1s} (%)	Si _{2p} (%)
0	81.55	1.18
100	67.32	11.72
200	19.49	39.07

3.4. Conclusion

In general, “multi-chip packaging” or MCP means a packaging configuration containing at most five chips, connected *via* wire bonds to a multilayer circuit board. It is as if all the chips were integrated into one single die and packaged as such, since the same form factor and footprint are kept to facilitate subsequent board assembly operations. For MCP, UV-curable acrylates can be used in the Si-wafer handling including both dicing and pick-up. The coating thickness has been about 40 μm so far. But as Si-wafers become ultrathin (under 50 μm), the acrylates have to satisfy the requirements such as coating thickness below about under 20 μm because of difficult Si-wafer handling (Lee *et al.*, 2012).

This study examined the adhesion performance of polymers formed on Si-wafers from a hexafunctional acrylate monomer and photo-initiator using a UV-curing system. The IPN structured acrylates were prepared using different UV doses. The residue on the Si-wafer was also observed by FE-SEM and XPS surface analysis after peeling, according to the UV dose. In UV-curing system of acrylates, the cross-linking reaction is influenced by: the UV dose; the diluent monomers; photo-initiators; and the coating thicknesses of the acrylates. In this work, the effects of the curing agent, hexafunctional monomer and photo-initiator at a constant binder concentration, were examined. The effect of the coating thickness was assessed. Proper peel strength is needed in the process of Si-wafer manufacture whereas lower peel strength is required after UV irradiation to prevent damaging the Si-wafers. Therefore, UV-curable IPN acrylates for MCP need to show two opposite adhesion properties before and after UV irradiation. The following conclusions were made:

- The reasonable peel strength was attained at approximately 0.5 phr (binder) aziridine (curing agent) and 30 phr (binder) hexafunctional monomer content and obtained at photo-initiator contents > 2 phr (additional monomer).
- The coating thickness to achieve proper adhesion and then weak adhesion after UV-irradiation was approximately 20 μm .
- SEM and XPS presented selective UV doses for minimal residue after UV irradiation.

Chapter 4

Adhesion Performance and Curing Behaviors of UV-curable Acrylates with 3-MPTS for 3D Multi-chip Packaging Process

4.1. Introduction

Increasing market demand has driven the semiconductor industry to miniaturize all the materials used in semiconductor packaging. The adhesives that bond integrated circuit (IC) chips to substrates have also followed the market trend towards miniaturization. Film adhesives are able to satisfy this demand, and are now widely used, having replaced conventional liquid adhesives (Saiki *et al.*, 2010). Film adhesives are generally provided as an adhesive tape composed of an adhesive layer and a base material. The film is laminated on a wafer during the semiconductor manufacturing process. The wafer is then divided into IC chips using a rotary blade. The IC chip and the attached film adhesive are peeled away from the base material using protruding needles in a process called 'pick-up'. An excessive degree of cross-linking prepared from unsaturated polyester resins by electron beam irradiation, results in poor adhesive strength (Ebe *et al.*, 2003). This observation led us to establish a dicing process, as shown in previous study (Lee *et al.*, 2012). A piece of silicon wafer was tightly held using a dicing film with strong adhesion strength, which enables rapid and smooth dicing of the wafer. Subsequently, the adhesive layer was irradiated with UV light through the reverse side of the substrate. After UV irradiation, the adhesion strength decreased to a certain level, making it easy to pick up the diced chips for further die-bonding processes. Dicing tapes developed using this process has been reported (Ebe *et al.*, 2003).

Acrylic monomers and oligomers are used widely on account of their superior properties of transparency, colorlessness, resistance to yellowing under sunlight and resistance to oxidation due to their saturated structures. However, they have poor thermo-mechanical stability because of their linear structure. Therefore, crosslinking of multifunctional acrylates is needed to

increase their thermo-mechanical stability. It was reported that an adhesive shows fluid-like behavior when it is widely cross-linked (Joo *et al.*, 2007). However, the more cross-linked is the adhesive, the greater is the creep resistance (Joo *et al.*, 2007; Sosson *et al.*, 2005). Multifunctional acrylates cross-link rapidly by radical and cationic polymerization; the kinetics and properties of these polymers have been investigated (Joo *et al.*, 2007; Auchter *et al.*, 1999). Cross-linked acrylates produce interpenetrating polymer networks (IPNs). These IPNs are a combination of two cross-linked polymers (each made *via* independent reaction processes) held together by permanent entanglements and are prepared using special methods (Sperling, 1977). The absence of cross-reactions between the two networks is an important condition to ensure morphology control (Dubuisson *et al.*, 1980; Tan *et al.*, 1996; Dubuisson *et al.*, 1980; Hua *et al.*, 2000).

In this study, the IPN structured acrylates used in the Si-wafer 'pick-up' process were prepared using a dipentaerythritol hexacrylate, 3-methacryloxypropyl trimethoxysilane with a UV-curing system using two different types of UV irradiations. The effect of the UV-curing on the behavior, viscoelastic properties and molecular distribution were investigated using Fourier transform infrared (FTIR), gel permeation chromatography (GPC) and an advanced rheometric expansion system (ARES). Finally, field emission scanning electron microscopy (FE-SEM) and X-ray photoelectron spectroscopy (XPS) revealed little residue on the wafer on releasing the film after UV irradiation (Lee *et al.*, 2012).

4.2. Experimental

4.2.1. Materials

The compounds 2-ethylhexyl acrylate (2-EHA, 99.0% purity, Samchun Pure Chemical Co., Ltd, Republic of Korea) and acrylic acid (AA, 99.0% purity, Samchun Pure Chemical Co., Ltd, Republic of Korea) were commercially available and used without purification. Ethyl acetate (EAc, Samchun Pure Chemical Co., Ltd, Republic of Korea) and methanol (MeOH, Samchun Pure Chemical Co., Ltd, Republic of Korea) were used as solvents and 2,2'-azobisisobutyronitrile (AIBN, Junsei Chmeical, Japan) was used as a thermal initiator. Methylaziridine derivative (MAZ, DSM Neoresins, USA) was used as the cross-linking agent. Dipentaerythritol hexacrylate (DPHA, Miwon Specialty Chemical, Republic of Korea) and 3-methacryloxypropyl trimethoxysilane (3-MPTS, Dow Corning Toray Co., Ltd, USA) were used as the diluent monomer. Figure 4-1 shows the chemical structure of hexafunctional acrylate which has six C=C double bonds and silicon-modified acrylate. The compound 2-hydroxy-2-methyl-1-phenyl-propane-1-one (Miwon Specialty Chemical, Republic of Korea) was used as the photo-initiator (Lee *et al.*, 2012).

4.2.2. Methods

4.2.2.1. Synthesis of binders

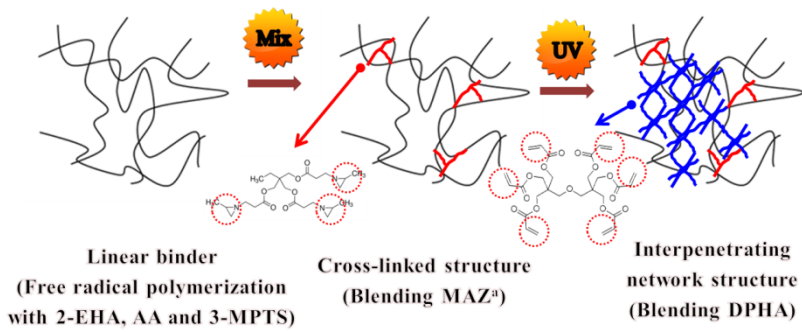
Acrylic monomers (2-EHA, AA, 3-MTPS) were synthesized as 95, 4.5 and 0.5 wt.% by solution polymerization. The amount of AIBN in the binders was 0.3 phr and the solid content was 40 %. The mixture was placed into a 500 *ml* four-neck flask equipped with a stirrer, condenser and thermometer, and heated to 75 °C with constant stirring. At the end of the exothermic reaction, the temperature was maintained for 30 m, and a blend of ethyl acetate and AIBN was added. The reaction was allowed to proceed for 0.5 and 2.5 h. Finally, polymerization was terminated by cooling the mixture to room temperature (Joo *et al.*, 2006; Lee *et al.*, 2012).

4.2.2.2. Formation of the acrylate film

All the acrylates were coated onto the corona treated polyethylene terephthalate (PET, SK Chemical, Republic of Korea) film using coating bars, kept at room temperature for 1 h and then dried in an oven at 80 °C for 20 m. These dried films were kept at 22±2 °C and 60±5 RH for 24 h before used in the experiments (Do *et al.*, 2008) Lee *et al.*, 2012).

4.2.2.3. Preparation of cured acrylates

The acrylates were cured with the addition of a curing agent followed by UV-curing. The curing agent was a multifunctional methylaziridine. The cross-linking involves mainly the carboxyl groups of the vinyl carbonic acids within the polymeric chain. The oxygen of the nucleophilic carboxyl group causes ring opening of the aziridine rings, whereas the hydrogen atoms of the carboxyl groups protonate the nitrogen atoms (Czech, 2007). The UV-curable acrylates were prepared by blending polymerized binders with a photoinitiator and a hexafunctional acrylic monomer. The UV-curable acrylates were coated onto polyethylene terephthalate (PET or polyester) films and cured using conveyor belt type UV-curing equipment with a 100 J/s high pressure mercury lamp (main wavelength: 365 nm). The UV doses were measured using an IL390C Light Bug UV radiometer (International Light, USA). Despite low molecular weights, the hexafunctional monomers in the acrylates can be photo-polymerized after a UV dose to form the IPN structures (Figure 4-2) (Lee *et al.*, 2012).



*MAZ reacts with carboxylated functionality of acrylic acid in binder (Czech, 2007)

Figure 4-2. Process of producing IPN structure in UV-cured acrylates

4.2.2.4. Adhesion performance

The prepared acrylates were attached to a silicon wafer substrate and a 2 kg rubber roller was passed over them twice. The 180° peel strength was measured using a Texture Analyzer (TA-XT2i, Micro Stable Systems, UK) after the sample was left to stand at room temperature for 24 h. The peeling speed was 300 mm/m, and the average strength of peeling period was measured five times. The probe tack was measured with a 5 mm diameter stainless steel cylindrical probe using the Texture Analyzer. The approaching speed of the probe was 0.5 mm/s and was in contact with the surface of samples for 1 s at a constant pressure of 100 g/cm². The debonding speed was 0.5 mm/s and the probe tack was measured as the maximum, debonding force (ASTM D3330) (Joo *et al.*, 2006; Lee *et al.*, 2012).

4.2.2.5. Fourier transform infrared (FTIR) spectroscopy

The FTIR spectra were obtained using an FTIR-6100 (JASCO, Japan) installed with an attenuated total reference (ATR) accessory composed of a zinc selenium (ZnSe) crystal with a 45° angle of incidence. The spectra were recorded for 30 scans with a 4 cm⁻¹ resolution over the wavelength range 650-4000 cm⁻¹. The curing behavior of the samples were characterized by monitoring the changes in the C=C bond and carboxylic group at 810 cm⁻¹ and at 1730 cm⁻¹. All the results were confirmed by determining the level of CO₂ reduction, H₂O reduction, noise elimination, smoothing and baseline correction. The curing behavior of crosslinking with the UV dose was obtained using the FTIR-ATR (Lee *et al.*, 2012).

4.2.2.6. Gel permeation chromatography (GPC) measurement

The samples were eluted using tetrahydrofuran (THF) at room temperature and filtered through a 0.2 μm polytetrafluoroethylene (PTFE) syringe filter. Molecular weights were measured by GPC at 35 $^{\circ}\text{C}$ using a YL-CLARITY system (Young-Lin Instrument Co., Ltd) equipped with a refractive index (RI) detector and a Polymer Labs PL-gel 10 μm column (two mixed-B). THF was used as an eluent solvent at a flow rate of 1 ml/m . The number-average (M_n) and weight-average (M_w) molecular weights were calculated using a calibration curve from polystyrene standards (Lee *et al.*, 2012).

4.2.2.7. Advance rheometric expansion system (ARES) analysis

The viscoelastic properties of the acrylates were determined using an advanced rheometric expansion system (ARES, Rheometric Scientific, UK, in NICEM at Seoul National University) equipped with an 8 mm parallel plate mode. The typical temperature scan range was from 60 to 200°C, and the heating rate was 5°C/m. The frequency was 1 Hz and the gap between the plates was 1 mm. Also the tan delta curves from the temperature sweep tests suggest a glass transition temperature (T_g) (Lee *et al.*, 2012).

4.2.2.8. Field emission-scanning electron microscopy (FE-SEM)

The morphology of each sample after the peel strength test was measured by field emission scanning electron microscopy (FE-SEM) (SUPRA 55VP, NICEM at Seoul National University). The fractured samples were coated with a thin layer of gold (purity 99.99%) prior to the FE-SEM examination to prevent electron charging (Kim *et al.*, 2008).

4.2.2.9. X-ray photoelectron spectroscopy (XPS)

X-ray photoelectron spectroscopy (XPS, PHI 5000 Versa Probe, Ulvac-PHI) was performed using Al Ka radiation (1486.6 eV, Anode (25W, 15kV)). The bonding energies were calibrated with reference to the C (1s) peak at 284.6 eV. For the measurement, the samples were placed into an ultra-high vacuum chamber and data analysis of the sensitivity factors of each element present, was performed (Wu *et al.*, 2010; Song *et al.*, 2006; Asahara *et al.*, 2004).

4.3. Results and discussion

4.3.1. Adhesion performance

The most important factors of the UV dose cross-linked acrylates, peel strength and tack properties, can be handled by the UV dose. In a production plant the UV dose can be controlled by adjusting the power of the lamps and/or the speed at which the Si substrate is passed under lamps. The solvent borne UV-cross-linkable acrylates by UV-irradiation and in a transfer process, depending on the carrier material, to produce the adhesive properties as required (Czech *et al.*, 2007). In this study, one of our aims was to examine the influence of the UV dose on the 180° peel strength and tack property of the samples using two types of irradiation systems. These were the steady irradiation and the pulsed irradiation of 100 mJ/cm². The results of the trials are presented in Figure 4-3 and 4-4. Cohesive failure, which means that there was little residue, was only observed on the initial peel strength and tack property test which did not involve a UV dose. The interfacial failures showed that there was no residue on the other samples. With the increase of UV dose, the peel strength and the tack property of the acrylates decreased slightly. This was still at an acceptable level because the peel strength is the sum of the energies required to break the bond deform the backing and the acrylates (Lim, 2007). UV-cross-linking promotes modulus property of the acrylates, and as a result the elongation on the acrylates was reduced after UV irradiation is attributed to the fact that the cross-link increased the stiffness of the acrylates (Wu *et al.*, 2010). Similar results have been reported in the literature (Kim *et al.*, 2002). The peel strength and the tack property of the pulsed UV irradiation (at 100 mJ/cm²) were lower than those of the steady irradiation as shown in Figure 4-2 and 4-3. That is, the pulsed irradiation (at 100 mJ/cm²)

indicates poorer adhesion strength which is attributed to inhomogeneous cross-linked network structures. This was confirmed by the GPC measurements shown Figure 4-5. A higher PDI (polydispersity index) was produced using the pulsed irradiation at 100 mJ/cm². Both the higher and lower molecular weight areas appear remarkable after pulsed irradiation at 100 mJ/cm². Results from this study, thus, show that the pulsed UV-irradiation method is successful and efficient (Lee *et al.*, 2012).

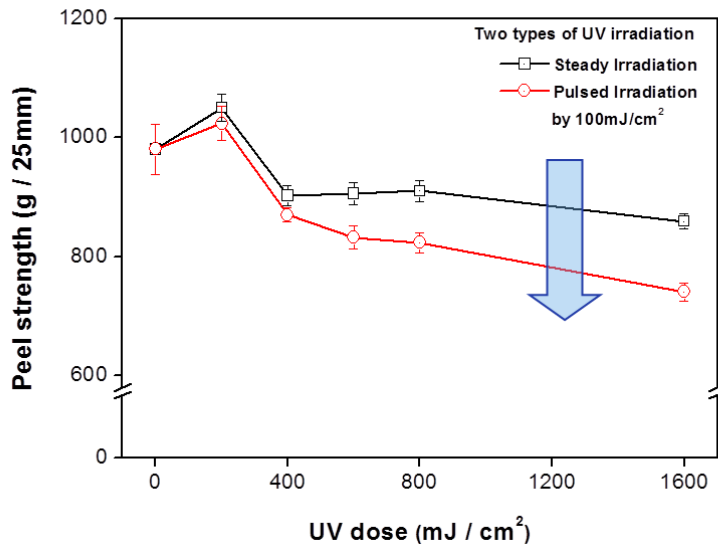


Figure 4-3. Peel strength by two types of UV irradiation (Lee *et al.*, 2012).

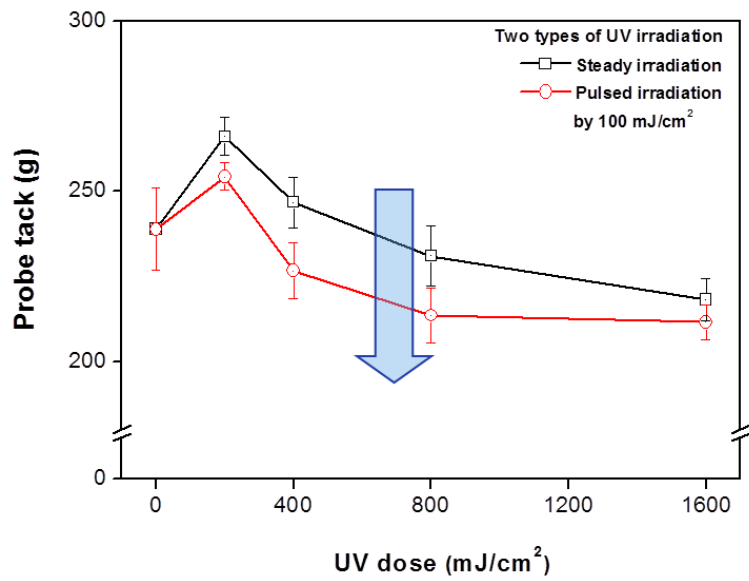
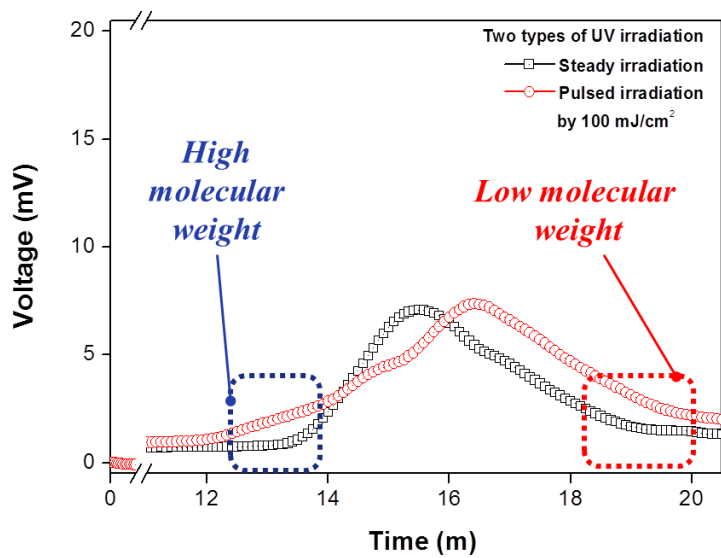


Figure 4-4. Probe tack by two types of UV irradiation (Lee *et al.*, 2012).



	M_w (g/mol)	M_n (g/mol)	PDI (M_w/M_n)
Steady	201000	33000	5.9
Pulsed	267000	16000	16.1

Figure 4-5. GPC measurement by two types of UV irradiation (Lee *et al.*, 2012).

4.3.2. Advance rheometric expansion system (ARES) analysis

The viscoelastic characteristics are important in the adhesion performance of the acrylates. In this work, the effect of the different UV doses was tested using ARES measurement. The storage modulus (G') is linked with the hardness of the adhesive, and the loss modulus (G'') is related to energy absorption. The values indicate the balance of the viscoelastic behavior. After UV irradiation, the adhesive strength of the acrylates composition including DPHA and 3-MTPS decreased drastically compared with other compositions. Because of the network formation due to the UV irradiation, this composition had a greater volume contraction. This could lead to micro-voids at the interface between the adhesive and the silicon wafer, resulting in a loss of adhesion. A higher storage modulus was expected to be more suitable for supporting the silicon wafer during the dicing and picking up of the diced chips, together with the adhesive layer from the face material (Ebe *et al.*, 2003).

Figure 4-6 shows that the storage modulus of acrylates is different, particularly at high temperatures. The storage modulus of the acrylates with UV dose was higher than the acrylates without UV dose over about 25°C. It can be showed that the acrylates' cohesion gets higher with increasing UV dose. Furthermore, the plateau area of the storage modulus in the high temperature region indicates that the acrylates formed an entanglement structure. The storage modulus at high temperatures is directly related to the thermal resistance of the acrylates. Therefore, the acrylates become more elastic at high temperatures with increasing UV dose. Figure 4-7, shows the tan delta curve of acrylates as a function of the UV dose. The T_g of the trials (temperature at tan delta peak) was similar. Moreover, the tan delta of the acrylates decreased with increasing UV dose. This suggests that the storage

modulus of the acrylates is strongly associated with the UV dose in the room temperature region. Hence, tan delta also decreased with increasing UV dose (Lee *et al.*, 2012).

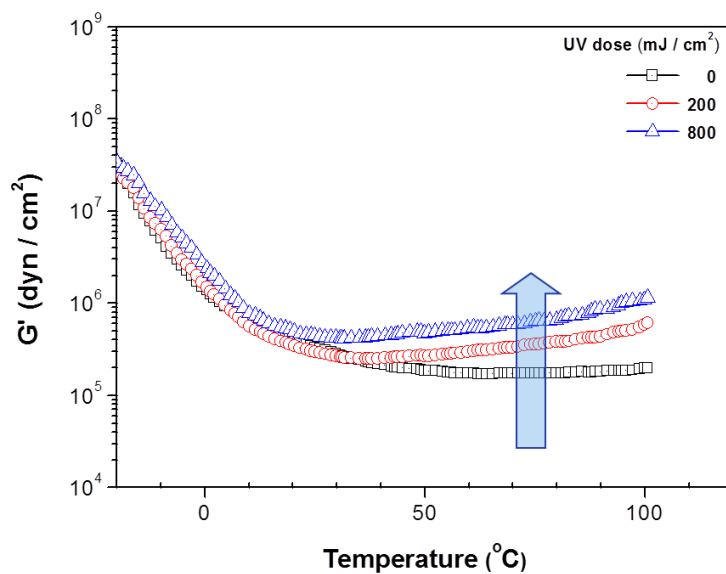


Figure 4-6. Temperature dependence of storage modulus G' with different UV dose (Lee *et al.*, 2012).

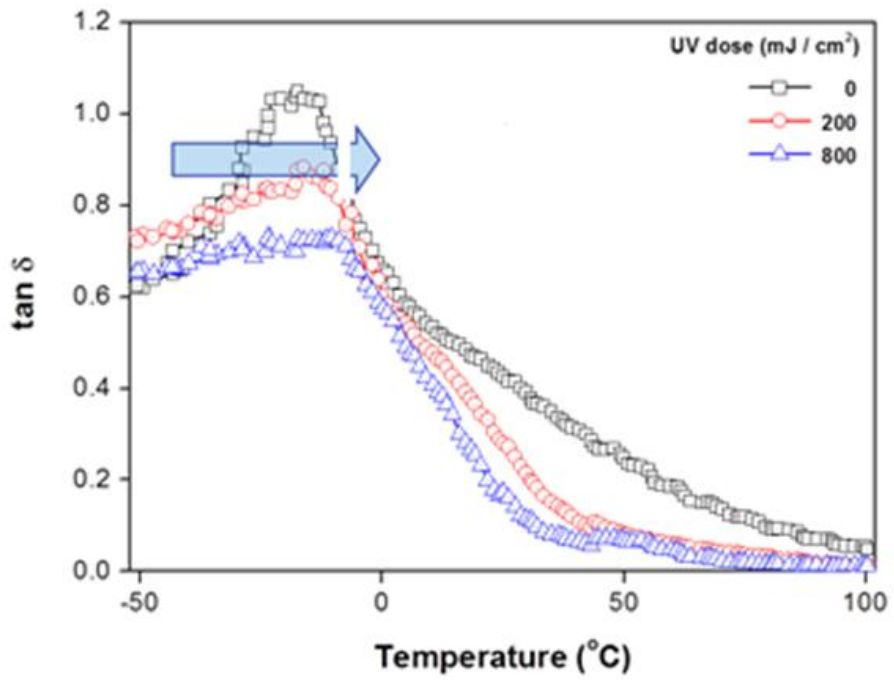


Figure 4-7. Tan delta with different UV dose (Lee *et al.*, 2012).

4.3.3. Fourier transform infrared (FTIR) spectroscopy

The kinetics of the photo-induced cross-linking was investigated using FTIR-ATR. After photo-initiation by UV dose at a certain wavelength, multifunctional monomers proceeded to polymerize. These monomers formed a cross-linked IPN structure. The curing behavior of functional monomers can be monitored using FTIR-ATR because the C=C twisting vibration in functional monomers participates in the cross-linking reaction (Scherzer, 2004). The FTIR spectra of UV-curable mixture composed of 2-EHA/AA/3-MTPS copolymer (2-EHA/AA/3-MTPS = 95/4.5/0.5) and DPHA and 3-MPTS (20/20 phr in binder) was determined. The conversion of C=C bond, as a function of UV dose was calculated according to the following equation: (Tasic, *et al.*, 2004).

$$\text{Conversion (\%)} = [(A_{810}/A_{1730})_0 - (A_{810}/A_{1730})_t] / (A_{810}/A_{1730})_0 \times 100 \quad (1)$$

where $(A_{810}/A_{1730})_0$ and $(A_{810}/A_{1730})_t$ denote the relative absorbance of the C=C bonds before curing and at a given curing time t , respectively. The conversion of C=C bonds in the blend increased sharply as the UV dose was increased to 200 mJ/cm² (Figure 4-8). This is because the entanglement and/or orientation of multifunctional monomer around the acrylic copolymer induced a rapid radical chain reaction, resulting in increased reactivity (Ebe *et al.*, 2003). The conversion of C=C bonds were not 100%. The remaining C=C bonds might have remained unreacted after the action of the photo-initiator because it was possible that they were trapped in the cross-linked polymer network (Lee *et al.*, 2012).

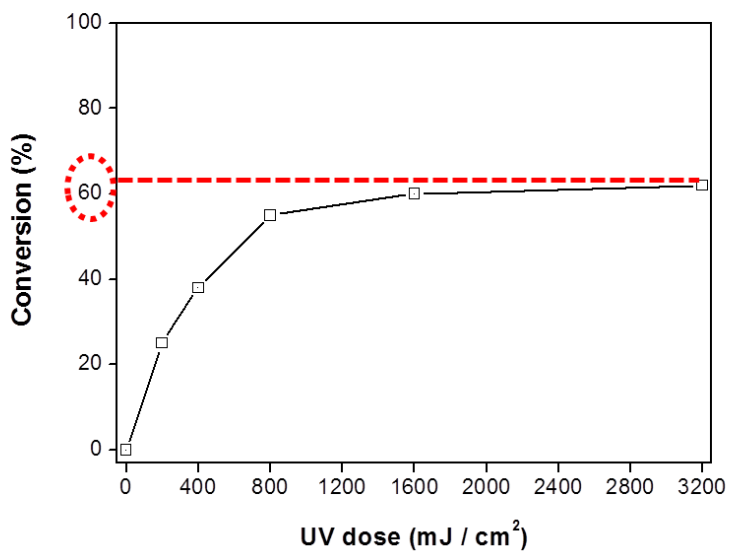


Figure 4-8. Conversion of C=C bonds at 810 cm⁻¹ as a functional of UV dose for UV-curable groups in binders blended with an additional monomer (Lee *et al.*, 2012).

4.3.4. Field emission-scanning electron microscopy (FE-SEM)

Another aim of this study was to observe the morphology using FE-SEM and to investigate the contaminants of the polymers on the surface of the Si-wafers by XPS. Some adhesives might remain on the Si-wafers after the releasing of the films. Figure 4-9 indicates the influence of the UV dose. In the 'pick-up' process, it is very important to consider whether there is the adhesives remaining, as the Si-wafer becomes thinner (Kim *et al.*, 2008). The increase of UV dose suggests more cross-linking reactions (Decker *et al.*, 2001). The efficient UV dose was found to be greater than 1600 mJ/cm² for all the specimen (Lee *et al.*, 2012).

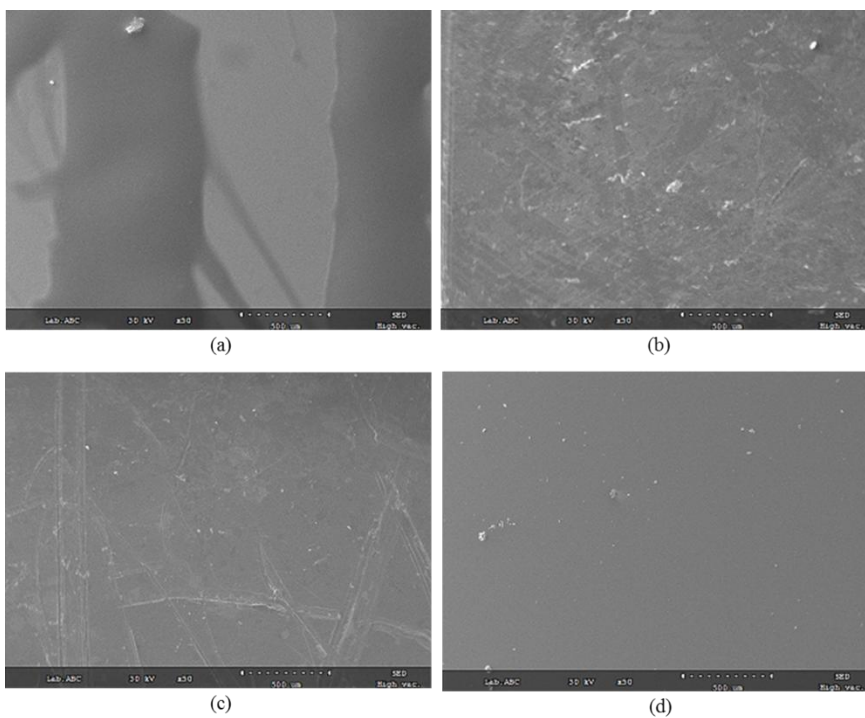


Figure 4-9. Field-emission scanning electron images of UV-cured acrylates at UV dose; (a) 0 mJ/cm², (b) 400 mJ/cm², (c) 800 mJ/cm², (d) 1600 mJ/cm² (Lee *et al.*, 2012).

4.3.5. X-ray photoelectron spectroscopy (XPS)

Analysis by XPS was used to obtain the surface compositions of the residue on the Si-wafer after peeling at different UV doses. Figure 4-10 shows the C_{1s} curve-fitted core-level spectrum with one major peak of binding energy of 284.6 eV corresponding to the C-C/C-H functional groups (Song *et al.*, 2006; Zhang *et al.*, 2001; Uchida *et al.*, 1990). In addition, a peak was observed as 283.9 eV in the C1 spectra, which was assigned to an inhomogeneous charging effect on the polymer surface due to its insulating nature (Massey *et al.*, 2003). The above C atoms were derived from the acrylic base polymer (Asahara *et al.*, 2004). The peak at 284.6 eV, which was linked directly to the properties of the polymer (C-C and C-H), was decreased with increasing UV dose. On the other hand, the Si_{2p} peaks around 100 and 103 eV (SiO₂) increased with increasing UV dose. These results are in agreement with reference values (Jin *et al.*, 1987; Weng *et al.*, 1995; Bou *et al.*, 1991). As listed in Table 4-1, the amount of carbon decreased with increasing UV dose while the amount of silicon increased on the surface of the silicon wafer, as a result of the cross-linking of the acrylates (Lee *et al.*, 2012).

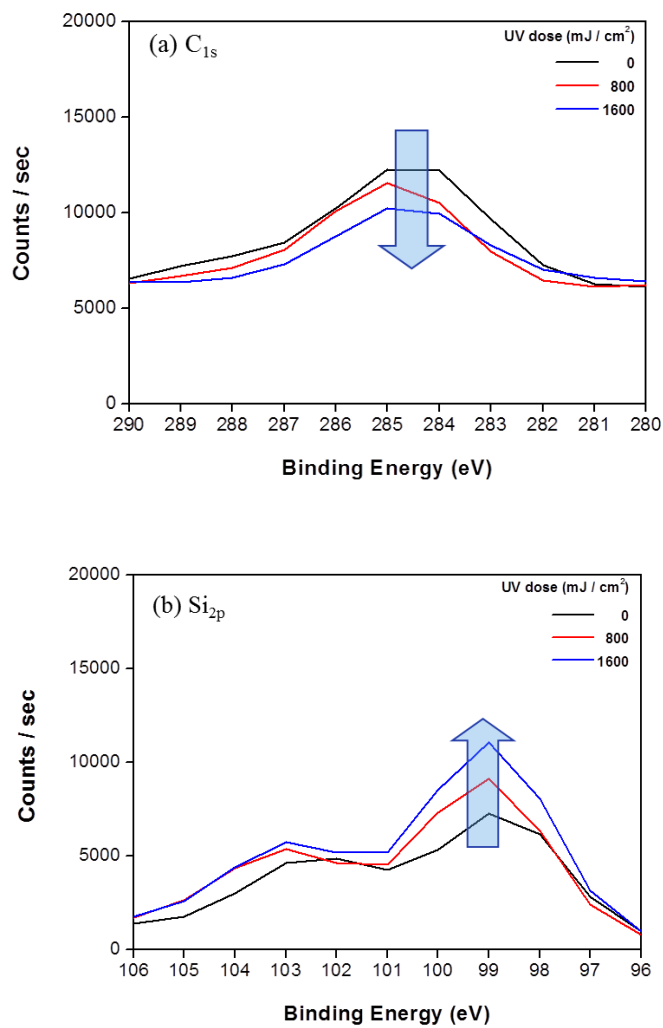


Figure 4-10. (a) C_{1s} and (b) Si_{2p} XPS spectra of Si-wafer surface after peeling at varying UV dose (Lee *et al.*, 2012).

Table 4-1. Atomic concentration (%) of C_{1s} and Si_{2p} determined by XPS according to the UV does (Lee *et al.*, 2012).

UV dose (mJ/cm ²)	C _{1s} (%)	Si _{2p} (%)
0	31.81	30.01
800	24.46	34.96
1600	17.26	42.06

4.4. Conclusion

When working with the silicon wafer process, it is important to consider the conditions that apply when using the adhesives. Besides the UV-curing of the acrylates it is necessary to pay attention to the whole process as the silicon wafers get thinner. This study investigated the suitable condition of handling the acrylates using an interpenetrated network structure (Lee *et al.*, 2012).

In this work the effect of UV-curing on the behavior and performance of the acrylates was obtained using FTIR and a 180° peel strength test. Two kinds of different UV-irradiation were considered in these experiments. One of them, the pulsed irradiation at 100 mJ/cm², makes the adhesion strength between adhesive layers and silicon substrates weaker than does the steady irradiation. The reason why it was investigated can be understood by considering the inhomogeneous polymer network structure which was highlighted by GPC. These results indicated that the adhesive property of acrylates depends not only on its modulus but also on the interfacial phenomena such as the local distribution of cross-linked acrylic monomer or polar segments at the interface between the adhesive layer and the silicon wafer (Ebe *et al.*, 2005). The results from the FE-SEM and XPS studies, indicated that the required condition was little residue on the silicon wafer after releasing the adhesive film at more than the certain level of UV dose. It was shown that under such conditions, the application of the UV-curable acrylates was reasonable and easily peeled and made suitable for further processing (Lee *et al.*, 2012).

Chapter 5

UV-curing and Thermal Stability of
Dual Curable Urethane Epoxy Adhesives
for Temporary Bonding and Debonding
in 3D Multi-chip Packaging Process

5.1. Introduction

Wafer- and chip-level bondings are crucial process steps for three-dimensional microelectromechanical system (MEMS) integration and packaging. Today a wide variety of bonding processes are available, such as direct fusion bonding, direct plasma assisted bonding, anodic bonding, solder bonding, eutectic bonding, thermocompression bonding, and low temperature melt glass bonding. These processes have different shortcomings such as the need for high temperature, high voltage, or special surface preparation. Adhesive bonding provides an inexpensive alternative to fabricate bonds at low temperatures with a high surface roughness tolerance (Bilenberg *et al.*, 2004).

Nowadays, the wafer thinning process has increased attention due to its promising application in device miniaturization and packaging. The key factors for thinned wafers are improved heat dissipation, three-dimensional stacking, reduced electrical resistance and substrate flexibility. A reduction in wafer thickness combined with an increasing wafer diameter produces to wrap and fold of wafer and hence creates a demand for new methods of wafer handling. The thinned substrates need to be supported during the backside grinding process and through the subsequent processes such as lithography, deposition, etc. Using temporary adhesives to bond the processed device wafer to a rigid carrier wafer offers an efficient solution and is becoming increasingly important in both integrated circuit board and MEMS applications, mainly due to its low cost, ease of processing, and adaptability. The process for temporary wafer bonding is shown in Figure 5-1 (Puligadda 2007). The front side of the carrier wafer is coated with the adhesive, and the wafer undergoes an initial bake to remove the solvent. The device wafer (possibly after the application of a protective layer) is brought into contact

with the adhesive-coated carrier wafer under vacuum and pressure. Adhesives for the bonding process must adhere to a variety of semiconductor substrates such as silicon, gallium arsenide, indium phosphide and different metals, insulators and dielectrics. The adhesive layer between device and carrier wafers provides the mechanical strength required for thin-wafer handling. Adhesive should possess flow properties to flow into structures on the front side of the device wafer to flow into structure on the front side of the device wafer to provide good bonding properties. In addition, the adhesives must be easy to apply; have suitable mechanical strength, thermal stability and chemical resistance; and exhibit thickness variation across large wafers. Also, temporary wafer bonding requires the adhesive to be easily removed without damaging the features on the active side of the device wafer over a short debonding time. At present, a few numbers of adhesives are available for this type of application. The adhesives currently used for temporary wafer bonding have limited thermal stability at higher temperatures and can be used only up to 170-200°C (Puligadda, 2007; Moore *et al.*, 2004; Brubaker *et al.*, 2005; Combe *et al.*, 2006; Kwon *et al.*, 2005).

UV-curing technology has been considered as an alternative to traditional solvent-borne coatings, due to its eco-compatible process and excellent properties resulting from the high crosslink density. On the other hand, acrylic monomers and oligomers are used widely. However, they have poor thermo-mechanical stability. Therefore, the cross-linking of multifunctional acrylates is needed to increase their thermo-mechanical stability (Lee *et al.*, 2012; Joo *et al.*, 2007; Sosson *et al.*, 2005).

However, the creep resistance increases greatly in more cross-linked adhesive (Joo *et al.*, 2007; Sosson *et al.*, 2005). Multifunctional acrylates cross-link rapidly by radical and cationic polymerization, their kinetics and properties have been investigated (Auchter *et al.*, 1999). Cross-linked multifunctional acrylates produce semi-interpenetrated structured polymer

networks (semi-IPNs). Semi-IPN structured the adhesives have advantages, such as improved heat resistance (Joo *et al.*, 2006; Sosson *et al.*, 2005; Joo *et al.*, 2007). It was reported that photo-polymerization was effective in obtaining networks with a high degree of interpenetration (Athawale *et al.*, 2003). The curing kinetics and peel strength of dual curable adhesive based on acrylic resins were previously reported (Park *et al.*, 2009; Kim *et al.*, 2008).

To combine the functionalities of UV and heat curing in an epoxy acrylate oligomer-based system, a thermal-curing agent should be introduced. Recently, thermal latent curing agents such as dicyandiamide, which exhibit long-term stability at ambient temperature and can be transformed into activated species at high temperature, have been studied by many researchers in an attempt to obtain epoxy based resins affording one part handling and good storage stability (Udagawa *et al.*, 1991; Chiu *et al.*, 2003; Cho *et al.*, 2004; Yin *et al.*, 2007).

In this study, IPN structured urethane epoxy adhesives as temporary bonding and debonding adhesives in wafers were introduced using a hexafunctional acrylate monomer with a UV-curing system. It was obtained by using photo-DSC, FTIR-ATR spectroscopy and gel content. Also, thermal stability was studied by TGA (Lee *et al.*, 2013).

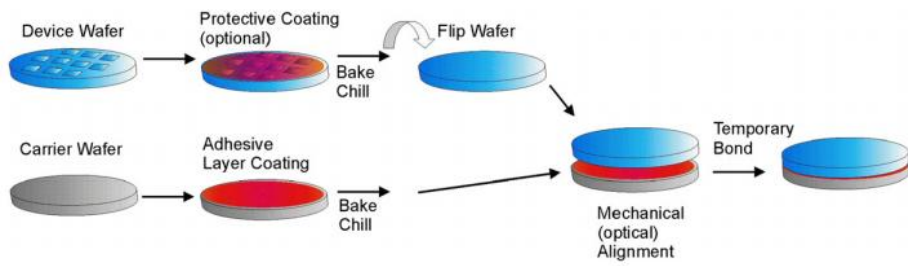


Figure 5-1. Temporary Bonding process flow (Puligadda, 2007).

5.2. Experimental

5.2.1. Materials

Polydimethylsiloxane (PDMS, Shin-Etsu Co., Ltd., Japan) and isophorone diisocyanate (IPDI, Bayer Material Science) were dried in 100°C 12 h prior use and 2-hydroxyethylmethacrylate (2-HEMA, Samchun Pure Chemical Co., Ltd., Republic of Korea) was used without pretreatment. About 0.1 wt.% of dibutyltin dilaurate is added to proceed the reaction to take place at a rapid rate as a catalyst in urethane reaction. Dipentaerythritol hexacrylate (DPHA, Miwon Specialty chemical, Republic of Korea) was used as hexafunctional monomer (Figure 5-2). Hydroxydimethyl acetophenone (Micure HP-8, Miwon Specialty chemical, Republic of Korea) was used as the photo-initiator for UV-curing in Figure 5-3 (Chattopadhyay, *et al.*, 2005). A diglycidyl ether of bisphenol A (DGEBA) (EEW: 184-190 g/eq) was supplied by Kukdo Chemical Co., Ltd., Republic of Korea) and triphenylphosphine (TPP, Fluka, Switzerland) were used as curing agents. All samples used in the synthesis were extra pure or reagent grade (Lee *et al.*, 2013).

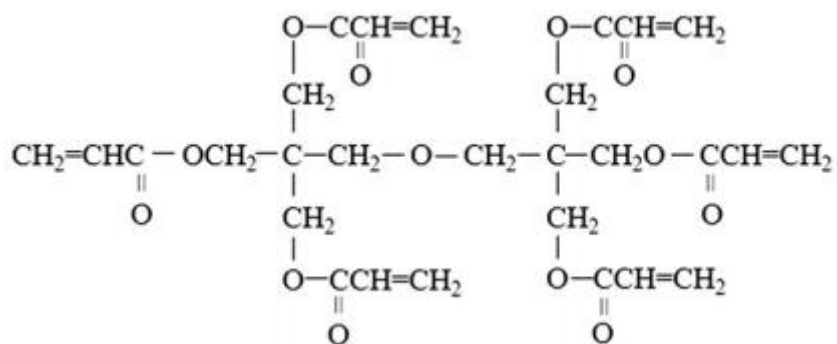


Figure 5-2. Structure of dipentaerythritol hexacrylate (DPHA).



Figure 5-3. Cleavage of hydroxydimethyl acetophenone as the photo-initiator in presence of UV light (Chattopadhyay *et al.*, 2005).

5.2.2. Methods

5.2.2.1. Synthesis of silicone urethane methacrylate

Figure 5-4 indicates a scheme of the synthesis process of UV-curable silicone urethane methacrylate. The silicone urethane methacrylate was obtained by adding an equimolar amount of PDMS with 0.1 wt.% dibutyltin dilaurate (DBTDL) dropwise to IPDI (mole ratio, NCO:OH=2:1) under a nitrogen gas. The reaction was maintained at room temperature for 3 h. An equimolar amount of HEMA with 0.5 wt.% hydroquinone as a polymerization inhibitor has been added a dropwise to the PDMS-IPDI adduct for about 5 h. Then the absorption peak of the NCO group at 2250 cm^{-1} had disappeared completely (Lee *et al.*, 2013).

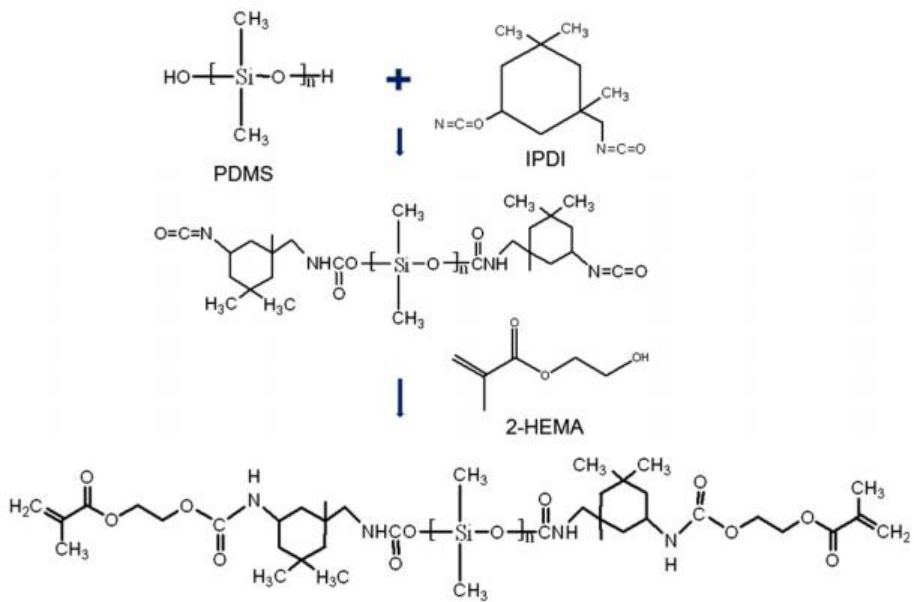


Figure 5-4. Synthesis process of UV-curable silicone urethane methacrylate (Lee *et al.*, 2013).

5.2.2.2. Preparation of dual-curable adhesive

Diglycidyl ether of bisphenol A (DGEBA), dipentaerythritol hexacrylate (DPHA) and a photo-initiator were blended first and then latent curing agent and curing acceleration agent were mixed using a paste mixer (Daewha Tech, South Korea) at room temperature. Table 5-1 shows the blend ratios of the various dual curable adhesives. The blending processes were performed in two steps to make a homogeneous mixture and to remove the air bubbles in the adhesives. In the first step, the stirring rate was 1200 rpm for 20 m and then in the second step it was 1000 rpm for 10 m (Lee *et al.*, 2013).

Table 5-1. Blend ratio of dual-curable adhesives (unit: phr).

DGEBA	100	100	100
DPHA	5	5	5
Photo-initiator (phr in DPHA)	1	2	5
Latent curing agent	10	10	10
Curing acceleration agent	10	10	10

5.2.2.3. Fourier transform infrared (FTIR) spectroscopy

The IR spectra were obtained using a JSCO FTIR-6100 (Japan) equipped with an attenuated total reflectance (ATR) accessory. In order to obtain the IR spectra of dual curable adhesives, the cured adhesive samples were cut into 0.5 x 0.5 cm² pieces. The ATR prism was diamond and its refractive index at 1000 cm⁻¹ was 2.4 with a transmission range from 4000 to 650 cm⁻¹. The resolution of the spectra recorded was 4 cm⁻¹. The curing behavior of the samples were characterized by monitoring the changes in the C=C bond and carboxylic group at 810 cm⁻¹ and at 1730 cm⁻¹. All the results were confirmed by determining the level of CO₂ reduction, H₂O reduction, noise elimination, smoothing and baseline correction (Lee *et al.*, 2012).

5.2.2.4. Gel fraction

The gel fractions of the dual-curable adhesives after UV-curing and subsequent thermal curing at different temperatures, 120 and 150°C, were determined by soaking in toluene at 50°C for 24 h. The insoluble part was removed by filtration and dried at 50°C to a constant weight. The gel fraction was calculated by applying the following equation:

$$\text{Gel fraction (\%)} = (W_t / W_0) \times 100$$

Where W_0 was the weight before filtration and W_t was the weight after filtration. The test was replicated three times (Lee *et al.*, 2013).

5.2.2.5. Photo-differential scanning calorimetry (photo-DSC)

Photo-DSC experiments were conducted using a TA Instruments Q-200 DSC equipped with a photo-calorimetric accessory (Omniscure 2000), which used light from a 100 W middle-pressure mercury lamp with a wavelength range of 300-400. Light intensity lamp with a wavelength range of 300-400. Light intensity was determined by placing an empty DSC pan on the sample cell. UV light intensity at the sample was 15 mW/cm² over a wavelength range of 300-400 nm. The weight of the sample was about 5 mg and the sample was placed in an open aluminum DSC pan. Measurements were carried out at room temperature in flowing N₂ gas at 50 ml/m (Lee *et al.*, 2013).

5.2.2.6. Thermogravimetric analysis (TGA)

The thermal stability and decomposition profiles of the dual curable adhesives were measured using a thermogravimetric analyzer (PerkinElmer Thermogravimetric Pyris 1 TGA model). The sample was loaded a ceramic pan, and heated from 30 to 600°C at a constant heating rate of 10°C/m in an inert nitrogen atmosphere (Lee *et al.*, 2013).

5.3. Results and discussion

5.3.1. Photo-differential scanning calorimetry (photo-DSC)

Photo-DSC offers a simple method of characterizing the UV-curing kinetics for the photo-polymerization of UV-cured materials. By monitoring the rate at which heat is released from the photo-polymerized sample, the reaction rate can be measured. Therefore, the profiles for the heat of reaction versus time provided by Photo-DSC can be used to characterize the photo-induced kinetics and to evaluate the polymerization rate constants (Joo *et al.*, 2006; Nelson *et al.*, 1995; Uhl *et al.*, 2006). Figure 5-5 shows the isothermal UV-curing heat enthalpy and conversion profiles of UV-curable PDMS-modified urethane epoxy adhesives. The heat flow (W/g) plotted in Figure 5-5(a) can be acquired by photo-DSC measurements. The photo-DSC experiments were performed at same temperature and light intensity, 25°C and 50 mW/cm². At the beginning of the reaction, the early onset of auto – acceleration by activation of radicals occurred as a steep increase. A difference in activity between photo-initiator contents was observed. Figure 5(a) shows that maximum is displaced to higher time by decreasing the photo-initiator contents. It means that the reactivity increased with increase in the concentration of radicals in the UV-curable adhesives. Because the broadening of the peak suggests that the curing has been proceeded more spread out. So a longer time was needed for its end. The exothermic area increased with increasing photo-initiator contents, as shown in Figure 5(b). Minor difference was shown between 1 and 2 phr of photo-initiator contents. The dual curable adhesives showed a higher exothermic area with increase in concentration of free radicals due to the increase in the reaction energy (Auchter *et al.*, 1999; Lee *et al.*, 2013).

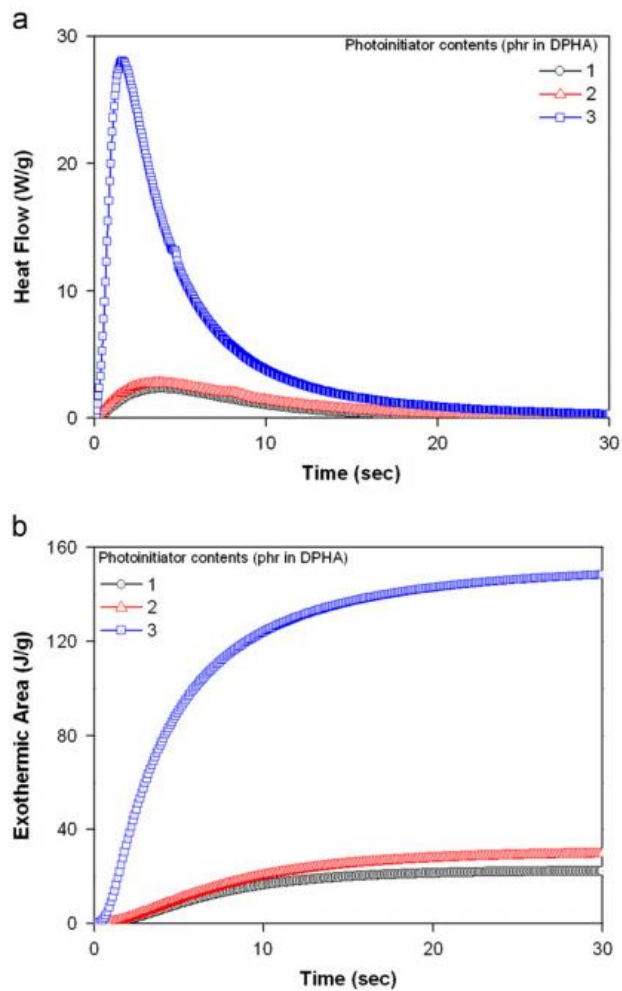


Figure 5-5. (a) Photo-DSC thermograms and (b) exothermic area which was calculated by integration of heat flow with different contents of the photo-initiator (Lee *et al.*, 2013).

5.3.2. Fourier transform infrared (FTIR) spectroscopy

The cure of the photo-induced cross-linking was measured by FTIR-ATR spectroscopy. After the photo-initiation of the adhesives by UV irradiation, the specific bands of the functional monomers and/or oligomers indicated that the polymerization was carried out. The curing reaction can be measured using FTIR-ATR spectroscopy because the C=C bonds in the functional monomers participate in the cross-linking reaction by photo-polymerization. Previous study showed that the absorption bands related to the C=C twisting vibration of the acrylate groups decrease with increase in UV exposure (Joo *et al.*, 2006; Ratnam *et al.*, 2001). These double bonds have planar conformation, but UV irradiation deforms them into an out-of-plane conformation (Park *et al.*, 2009). FTIR spectra of the UV-curable mixture, DPHA and photo-initiator (5 phr in DPHA) were investigated, as shown in Figure 5-6(a). Providing the conversions and/or absorbance data in this method makes thickness of the samples on ATR not important. (Lee *et al.*, 2012). The relative conversion of C=C bonds decreased sharply as the UV dose increases to 200 mJ/cm² regardless of the photo-initiator content, as shown in Figure 5-6(b). Entanglement and/or orientation of multifunctional monomers around the acrylic copolymer may induce a rapid radical chain reaction, resulting in fast reactivity (Zosel, 1991). As above mentioned, the photo-initiator content accelerates the cross-linking reaction. But the relative conversion of C=C bonds was not zero %. The remaining C=C bond might have remained unreacted after the action of the photo-initiator because they were trapped in the cross-linked polymer network (Joo *et al.*, 2007). The uncured polymer has an effect on thermal stability of adhesive (Lee *et al.*, 2013).

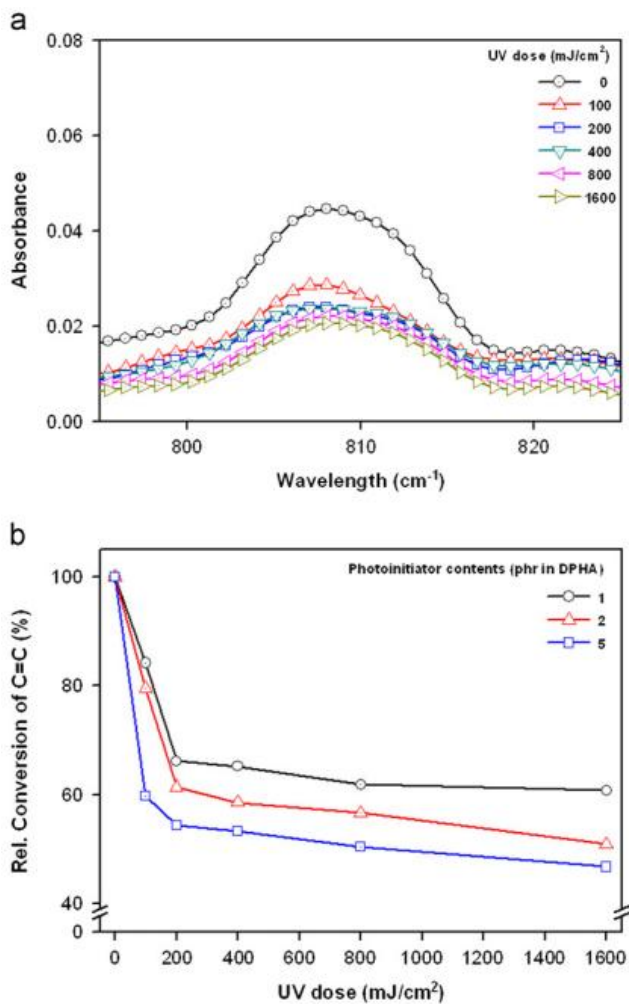


Figure 5-6. FTIR-ATR spectra of UV-curable adhesives with (a) 5 phr of photo-initiator contents, as a function of the UV dose at 810 cm^{-1} , and (b) relative conversion vs. UV dose (Lee *et al.*, 2013).

5.3.3. Gel fraction

Gel fraction determination is a convenient method of measuring the insoluble fractions, such as the fractions of cross-linked or network polymers (Park *et al.*, 2009). In this study, hexafunctional monomer in organic solvents was turned into insoluble cross-linked structures by UV-curing. The gel fraction increased with increase in photo-initiator content, due to the cross-linking reaction of the unreacted multifunctional monomers as shown in Figure 5-7. The gel fraction was relatively constant regardless of the photo-initiator contents for UV dose higher than 400 mJ/cm². And it showed that the gel fraction of adhesives with 1 phr or photo-initiator in DPHA increased with increasing UV dose up to approximately 50% of the gel fraction as a UV dose of 1600 mJ/cm². But the gel fraction increased up to around 75% in 5 phr of photo-initiator in DPHA. In other words, at a low content of photo-initiator the gel content conspicuously increased, owing to the existence of unreacted DPHA, but the rate of increase of the gel fraction decreased with increase in the UV dose, because the amount of unreacted DPHA decreased. When a photo-initiator content of 5 phr was used to the adhesives, the gel fraction did not reach 100 % irrespective of the UV dose. This indicates that the unreacted DPHA were remained in the cross-linked structure formed by UV-curing. Also, a cross-linked structure similar to an interpenetrated structured polymer network was formed by all the components (Joo *et al.*, 2007). The initial gel fraction rate sharply increased as a UV dose of 100 mJ/cm² due to rapid cross-linking which induced free radical initiation of multifunctional monomer. Furthermore, these results corresponded to the FTIR results in that more contents of photo-initiator accelerates the cross-linking reaction among DPHA (Lee *et al.*, 2013).

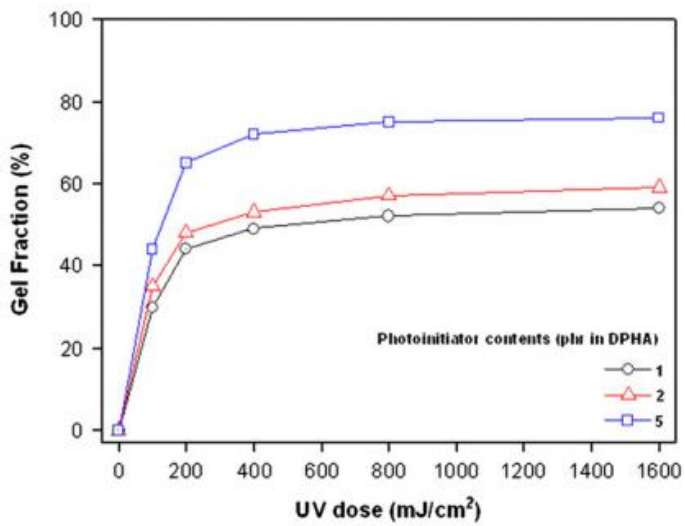


Figure 5-7. Gel fraction of UV-curable adhesives after UV-curing (Lee *et al.*, 2013).

5.3.4. Thermogravimetric analysis (TGA)

Figure 5-8 indicates the thermal stability of UV-cured adhesives at temperatures ranging from 25 to 600°C. Table 5-2 lists the characteristic thermal decomposition data of each cured adhesives. The maximum thermal degradation peak temperatures of the samples are also listed.

T_o (initial decomposition temperature); T_{max} (temperature of maximum rate of weight loss); T_f (final decomposition temperature).

The main decomposition takes place at higher than approximately 300°C corresponding to the advanced fragmentation of the macromolecules formed in reactions of dehydrogenation, thermal cracking, disproportionation and gasification processes (Sosson *et al.*, 2005). Major difference has been shown between 2 and 5 phr of photo-initiator content. This result suggests that thermal stability might have been dependent on photo-initiator content due to increased density of three-dimensional networks corresponding to FTIR analysis and gel fraction data above shown (Lee *et al.*, 2013).

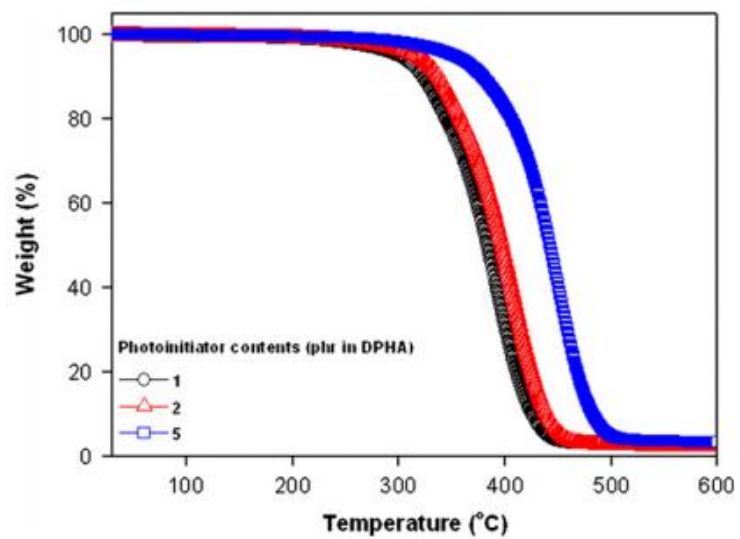


Figure 5-8. Thermogravimetric analysis of the UV-cured adhesives (Lee *et al.*, 2013).

Table 5-2. Characteristic thermal decomposition data of the UV-cured adhesives (Lee *et al.*, 2013).

Photo-initiator contents (phr in DPHA)	$T_{10\%}$ (°C)	$T_{50\%}$ (°C)	wt% at 600 °C	T_o (°C)	T_{max} (°C)	T_f (°C)
1	322	383	2	285	390	440
2	338	397	2	292	399	451
5	379	442	3	301	442	497

$T_{10\%}$, 10 wt% loss temperature; $T_{50\%}$, 50 wt% loss temperature.

5.4. Conclusion

An attempt has been made to indicate how best the points can be established in assessing the performance of UV-curing bonding process in 3D multi-chip packaging process. The practical data obtained from some of the fundamental tests based on different content of photo-initiator were discussed according to certain criteria. The results show that UV-curable acrylates with different content of the photo-initiator affects not only curing behaviors on UV doses but also thermal stability. Because UV-curing behavior is mainly affected by the photo-initiator. When UV light is irradiated on the curable adhesives, both the maximum curing and the exothermic area under the thermogram curves are also affected by a photo-initiator content (Lee *et al.*, 2013).

Chapter 6

Synthesis and Properties of
UV Laser Debondable fluorinated
Silicone-modified Urethane Acrylic
Adhesives for Temporary Bonding and
Debonding in
3D Multi-chip Packaging Process

6.1. Introduction

Bonding of two substrates or wafers has long been an important process in the fabrication of both microelectronic systems and microelectromechanical system (MEMS). Wafer bonding enables fabrication and packaging of complex three-dimensional (3D) microcomponents. Historically, some of the earliest uses of wafer bonding were in fabrication and packaging of pressure sensors (Niklaus *et al.*, 2006; Gragg *et al.*, 1984; Petersen *et al.*, 1988). The main commercial applications of wafer bonding are in the fabrication of silicon-on-insulator (SOI) substrates and the packaging of the inertia and pressure sensors for automotive and consumer products (Schmidt, 1998; Tong *et al.*, 1999; Iyer *et al.*, 2002; Alexe *et al.*, 2004). The wide variety of wafer bonding technique include direct bonding (Tong *et al.*, 1999; Iyer *et al.*, 2002; Alexe *et al.*, 2004), anodic bonding (Tong *et al.*, 1999; Iyer *et al.*, 2002; Alexe *et al.*, 2004), solder bonding (Cheng *et al.*, 2000), eutectic bonding (Mahabiz *et al.*, 1999), thermocompression bonding (Morrow *et al.*, 2004), direct metal-to-metal bonding (Kim *et al.*, 2002), ultrasonic bonding (Audet *et al.*, 1997), low-temperature melting glass bonding, and adhesive bonding (Yacobi *et al.*, 2002).

In adhesive bonding, an intermediate adhesive layer is used to create a bond between two surfaces to hold them together. Although successfully used in many industries, including the airplane, aerospace, and car manufacturing industries, to join various similar and dissimilar materials, adhesive bonding did not play a significant role during the initial research on semiconductor wafer bonding. There are many applications of adhesive bonding for micro electronic and photonic components, mainly related to relatively small bonding areas of chip-level bonding. In contrast to these applications, recent research on adhesive wafer bonding involves bonding of large-area substrates

using well-defined and defect-free intermediate adhesive layers. In some applications, precise wafer-to-wafer alignment of the bonded wafer-to-wafer alignment of the bonded wafer pairs is required. Recent developments of reliable and high-yield adhesive bonding processes have made adhesive wafer bonding a generic and in some cases enabling wafer bonding technique for a variety of applications (Niklaus *et al.*, 2006).

In the most commonly used adhesive wafer bonding processes, a polymer adhesive wafer bonding processes, a polymer adhesive is applied to one or both of the wafer surfaces to be bonded. After joining the wafer surfaces that are covered with the polymer adhesive, pressure is applied to force the wafer surfaces into intimate contact. The polymer adhesive is then converted from a liquid or viscoelastic state into a solid state, typically by exposing the polymer adhesive to heat or ultraviolet light. The main advantages of adhesive wafer bonding include relatively low bonding temperatures (between room temperature and 450°C, depending on the polymer material), insensitivity to the topology of the wafer surfaces, compatibility with standard complementary metal-oxide-semiconductor (CMOS) wafers, and the ability to join practically any wafer materials. Adhesive wafer bonding does not require special wafer surface treatments such as planarization or excessive cleaning. Structures and particles at the wafer surfaces can be tolerated and offset to some extent by the polymer adhesive. While adhesive wafer bonding is a comparably simple, robust, and low-cost process, concerns such as the limited temperature stability and limited data about the long term stability of many polymer adhesives in demanding environments need to be considered. Also, adhesive wafer bonding does not provide hermetically sealed bonds towards gasses and moisture (Niklaus *et al.*, 2006; Yacobi *et al.*, 2002).

The process for temporary wafer bonding is shown in previous study (Bilenberg *et al.*, 2004). The front side of the carrier wafer is coated with the adhesive, and the wafer undergoes an initial bake to remove the solvent. The

device wafer possibly after application of a protective layer) is brought into contact with the adhesive coated carrier wafer under vacuum and pressure. The adhesives used for the bonding process must adhere to a variety of semiconductor substrates, such as silicon, gallium arsenide, and indium phosphide, as well as different metals, insulators, and dielectrics. The adhesive layer between the device and the carrier wafer provides the mechanical strength required for handling thin wafers. Adhesives should possess flow properties to flow into structures on the front side of the device wafer to provide good bonding properties. In addition, the adhesives must be easy to apply, have suitable mechanical strength, thermal stability, and chemical resistance, and exhibit thickness variation across large wafers. Also, temporary wafer bonding requires the adhesive to be easily removed without damaging the features on the active side of the device wafer over a short debonding time. At present, only a few adhesives are available for this type of application. The tapes currently used for temporary wafers bonding have limited thermal stability at higher temperatures and can be used only up to 170 to 200°C (Bilenberg *et al.*, 2004; Puligadda, 2007; Moore *et al.*, 2004; Brubaker *et al.*, 2005; Combe *et al.*, 2006).

UV-curing technology has been considered as an alternative to traditional solvent-borne coatings, due to its ecocompatible process and excellent properties resulting from its high crosslink density. On the other hand, acrylic monomers and oligomers are used widely. However, they have poor thermomechanical stability. Therefore, crosslinking of multifunctional acrylates is needed to increase their thermomechanical stability (Lee *et al.*, 2012; Joo *et al.*, 2007; Sosson *et al.*, 2005). It was reported that photopolymerization was effective for obtaining networks with a high degree of interpenetration (Athawale *et al.*, 2003). The curing kinetics and peel strength of dual-curable adhesives based on acrylic resins have been reported (Park *et al.*, 2009; Kim *et al.*, 2008). To combine the functionalities of UV and heat

curing in an epoxy acrylate oligomer-based system, a thermal-curing agent should be introduced (Udagawa *et al.*, 1991; Chiu *et al.*, 2003; Cho *et al.*, 2004; Yin *et al.*, 2007).

Polyorganosiloxane consists of Si-O bonds, which allow flexibility of the chain as well as good chemical resistance, corrosion resistance, water resistance, and thermal and oxidative stability (Kang *et al.*, 2007). The interesting and useful properties of siloxane polymers are a result of the somewhat unusual molecular structure of the polymer chains, which consist of alternating silicone and oxygen atoms (Voronkov *et al.*, 1978). Polyurethane (PU) is the chemistry involved in isocyanate reactions with macrodiols, diisocyanate, and chain extenders (Chattopadhyay *et al.*, 2007).

Fluorinated polymers have several important properties. For instance, they are highly resistant to different thermal, chemical, and weather conditions. The presence of fluorine in the side groups of the polymer has a profound effect on nearly all the properties of these materials (Mokhtar *et al.*, 2010; Barrales - Rienda *et al.*, 1979; Matsumoto *et al.*, 1998). This effect is so striking that fluoropolymers are often treated as separate and remarkable class of polymers with properties unmatched in any other system. Fluorine confers extreme hydrophobicity and water insolubility to polymers. It raises the thermal and oxidative stability. In some instances, the element generates an interchain interaction so strong that it disables the polymer from dissolving in any solvent. It is the C-F bond that grants such properties, rather than the element itself (Allcock *et al.*, 1990). Therefore, fluorine-containing polymers have widespread applications in modern technologies ranging from the building, automotive and aerospace industries to optics and microelectronics (Sacher, 1994; Ghosh *et al.*, 2009; Pu *et al.*, 2002).

Whole experimental processes were described in Figure 6-1. Especially, UV laser irradiation was used for adhesives debonding. Laser processing is a

key technology in new developments in microelectronics. Also, the laser-lift-off process step comes into play as soon as the manufacturing strategy demands for a gentle separation of thin layer system (Delmdahl *et al.*, 2013).

In order to investigate a laser effect of temporary adhesives on debonding, the adhesives were synthesized with a silicon urethane oligomer for thermal stability and with 2-[3-(2H-Benzotriazol-2-yl)-4-hydroxyphenyl] ethyl methacrylate for UV absorbing material which mainly reacts at wavelength of 355 nm. The morphological analysis using optical microscopy was studied to select a proper combination of the laser process parameters such as out-focusing length, line spacing, and scan speed (Lee *et al.*, 2014).

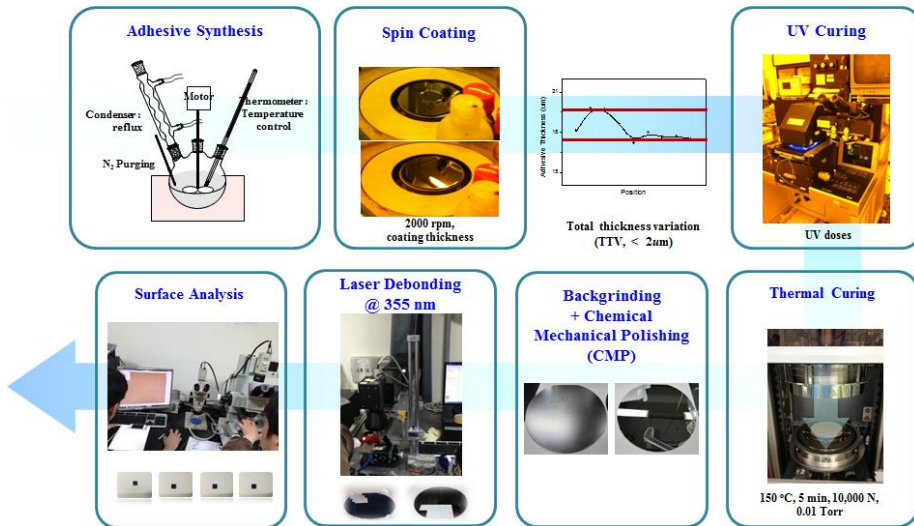


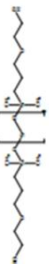
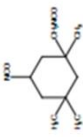
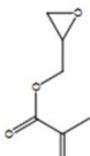
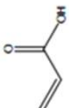
Figure 6-1. Whole experimental processes.

6.2. Experimental

6.2.1. Materials

Table 6-1 shows the chemical structures and properties of the raw materials used for the synthesis process. Hydroxy-terminated carbinol polysiloxane (Shin-Etsu Co., Ltd) and isophorone diisocyanate (IPDI, Bayer Material Science) were dried at 100°C. 1H, 1H, 7H-dodecafluoro-1-heptanol (Tokyo Chemical Industry Co., Ltd) and pentaerythritol triacrylate were used as end-capping materials without a pretreatment. Approximately 0.1 wt.% of dibutyltin dilaurate was added to cause the reaction to take place at a rapid rate as a catalyst in a urethane reaction. Hydroxydimethyl acetophenone (Micure HP-8, Miwon Specialty Chemical) was used as the photo-initiator for UV-curing. Glycidyl methacrylate (GMA, Junsei Chemicals, Japan) was used as donating epoxy functional group with the carboxyl group of acrylic acid (AA, Samchun Chemicals) in thermal curing. 2-[3-(2H-Benzotriazol-2-yl)-4-hydroxyphenyl] ethylmethacrylate (Sigma Aldrich Korea) was used as UV absorbing material (Lee *et al.*, 2014).

Table 6-1. Raw materials used for synthesis of fluorinated silicon-modified urethane acrylic adhesives (Lee *et al.*, 2014).

Function	Material	Abbreviation	Chemical structure	Molecular weight (g/mol)	Supplier
Polyl	Hydroxy-terminated carbinol polysiloxane	-		940	Shin-Etsu Co., Ltd.
Isocyanate	Isophorone diisocyanate	IPDI		228	Bayer Material Science
End-capping agent	1H,1H,7H-Dodecafluoro-1-heptanol	DFH		332	Tokyo Chemical Industry Co., Ltd.
End-capping agent	Pentaerythritol triacrylate	PETA		298	Sigma Aldrich
Acrylic monomer	Glycidyl methacrylate	GMA		142	Junsei Chemicals
Acrylic monomer	Acrylic acid	AA		72	Samchun Chemicals

6.2.2. Methods

6.2.2.1. Synthesis of fluorinated silicone-modified urethane acrylates

Figure 6-2 shows the synthesis process scheme of the dual-curable hydroxy-terminated carbinol siloxane-modified fluorinated urethane acrylic adhesives. The reaction time was determined by observing changes in the FT-IR peak at 2265 cm^{-1} (NCO peak), which decreased with the polyurethane reaction (Figure 6-3) and $^1\text{H NMR}$ (Figure 6-4). Initially, IPDI was charged into a dried 300-ml round-bottomed flask equipped with a four-necked separable flask with a mechanical stirrer, thermometer and condenser with a drying tube and an N_2 inlet. The temperature was maintained at room temperature with constant stirring. The hydroxy-terminated carbinol polysiloxane with some of the catalyst (dibutyltin dilaurate) was then added dropwise over a period of 5 h and was maintained for a further 1 h. The reaction temperature was increased to 50°C using a constant temperature heating mantle with constant stirring. A mixture of 1H, 1H, 7H-dodecafluoro-1-heptanol, and pentaerythritol triacrylate was added dropwise over a period 1 h and was reacted for 3 h until the NCO peak had almost disappeared. After cooling to ambient temperature, GMA and AA and 2-[3-(2H-Benzotriazol-2-yl)-4-hydroxyphenyl] ethylmethacrylate were mixed. Finally, a photo-initiator was blended to initiate UV-curing (Lee *et al.*, 2014).

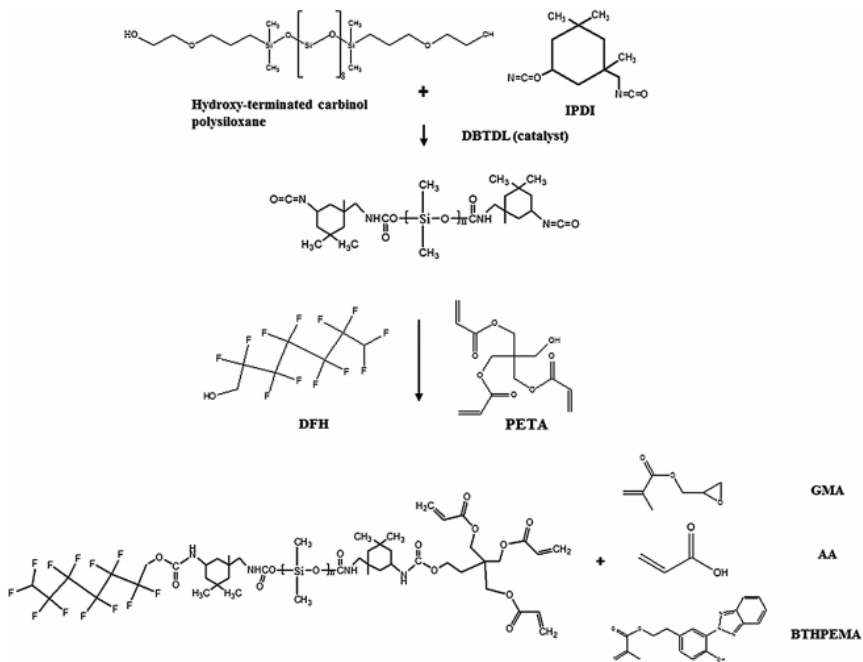


Figure 6-2. Synthesis process of dual-curable fluorinated silicone-modified urethane acrylic adhesives (Lee *et al.*, 2014).

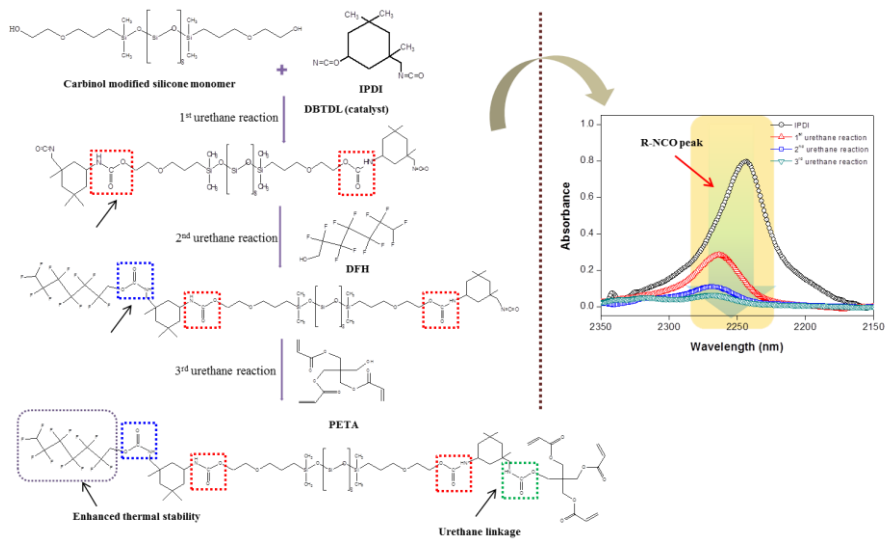
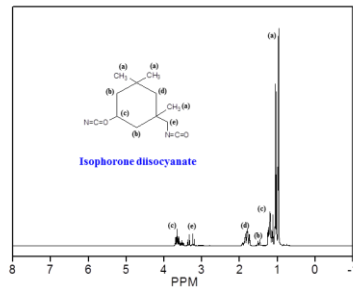
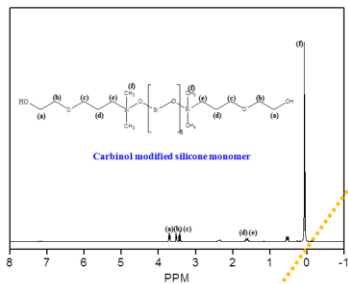
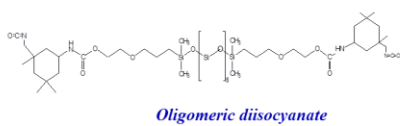
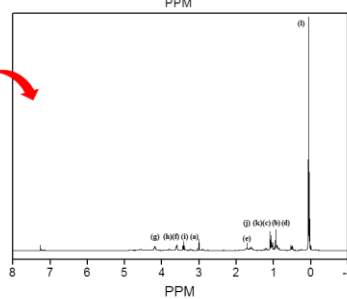
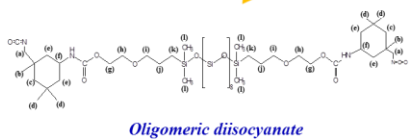


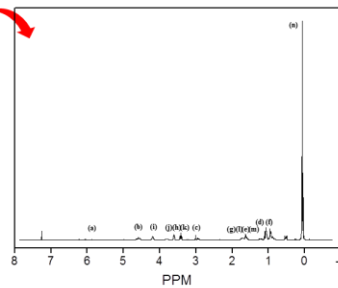
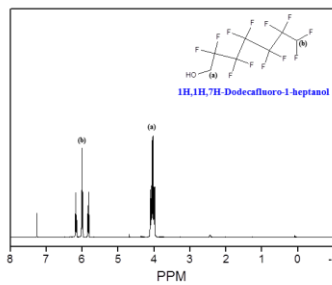
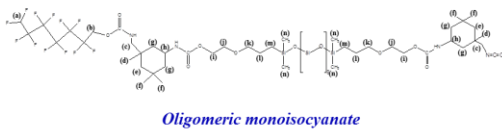
Figure 6-3. Observing changes in the FT-IR peak at 2265 cm^{-1} (NCO peak), which decreased with the polyurethane reaction.



1st urethane reaction



2nd urethane reaction



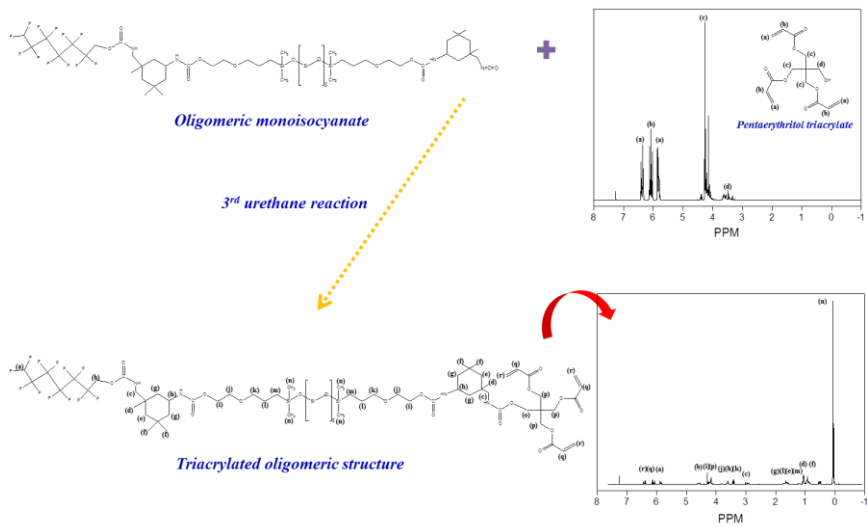


Figure 6-4. Observing changes in the ¹H NMR peaks for threefold urethane reactions.

6.2.2.2. Temporary bonding and UV laser debonding process

Temporary bonding process flow and dual curing mechanism were described and examined in Figure 6-5 (Lee *et al.*, 2013) and Figure 6-6 respectively. The bonded samples were irradiated using a UV laser of wavelength as 355 nm operated in pulsed mode (AVIA 355, Coherent) as shown in Figure 6-7. The chemical reactions were investigated using FTIR-ATR during dual curing and UV laser debonding (Figure 6-8). A projective optical system directed and defocused the laser radiation on the sample surface. The morphology of a surface after debonding depends on the laser process parameters such as, laser power, line speed and laser wavelength and so on. The parameters considered for this study are shown in Table 6-2. The experimental work was carried out at ambient temperature and in an atmospheric circumstance (Lee *et al.*, 2014).

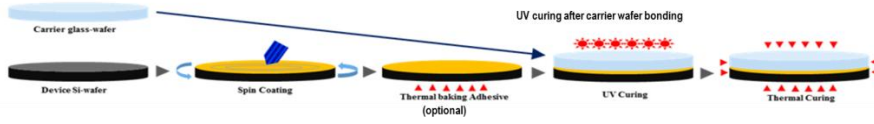


Figure 6-5. Temporary bonding process flow (Lee *et al.*, 2013).

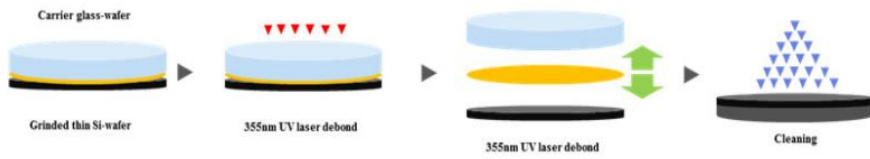
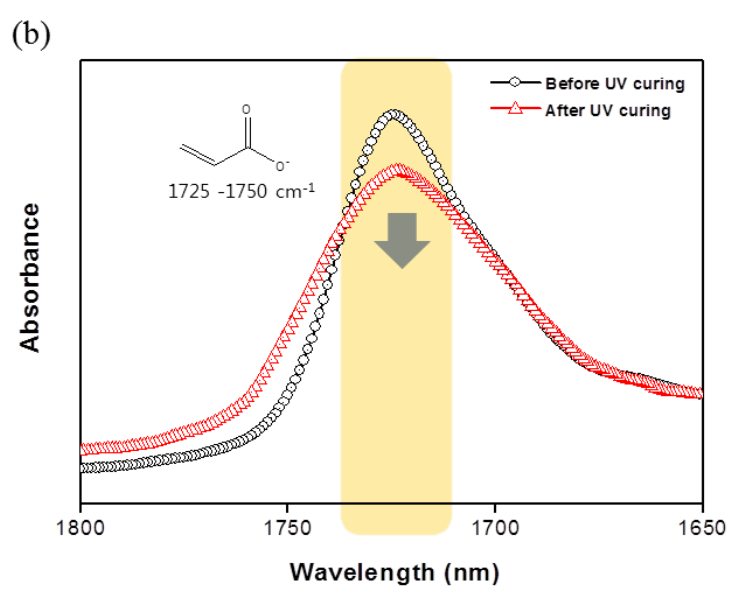
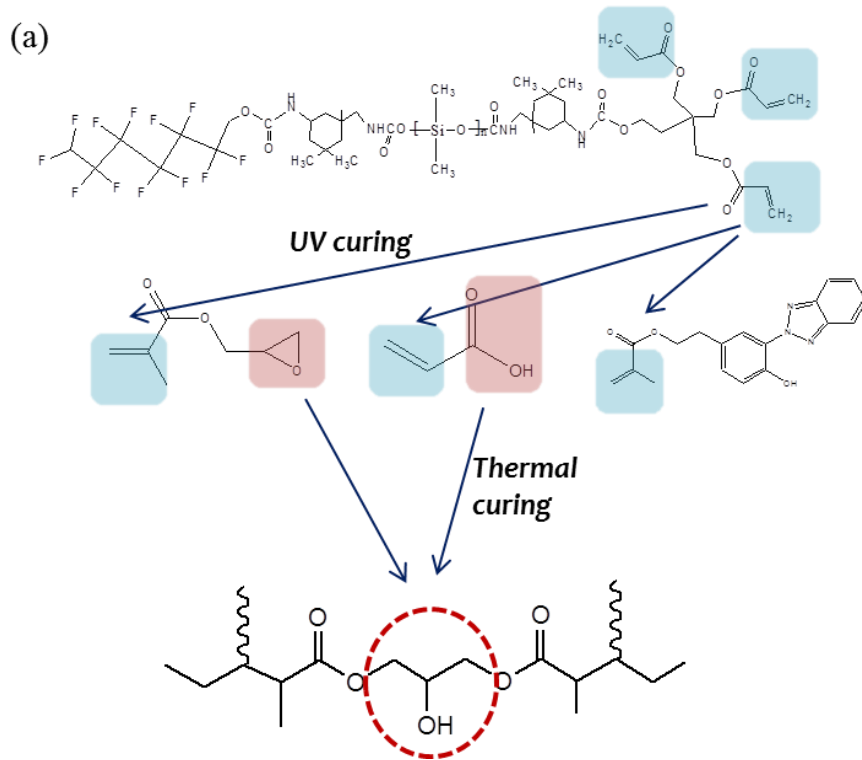
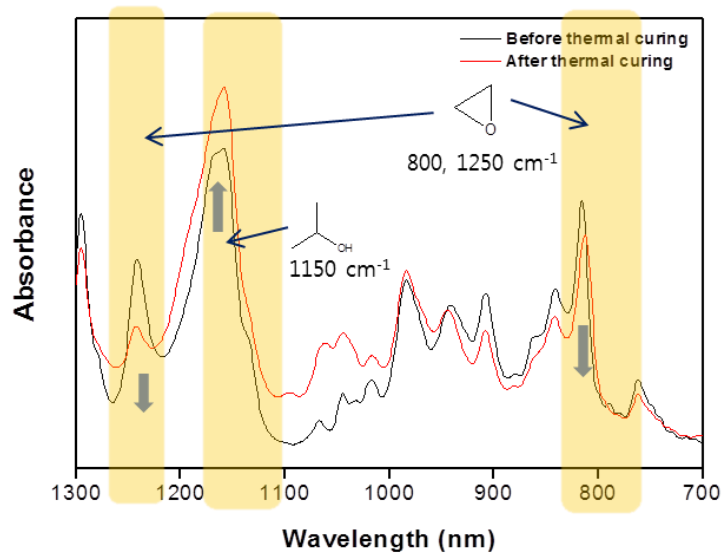


Figure 6-7. UV laser debonding process flow (Lee *et al.*, 2014).



(c)



(d)

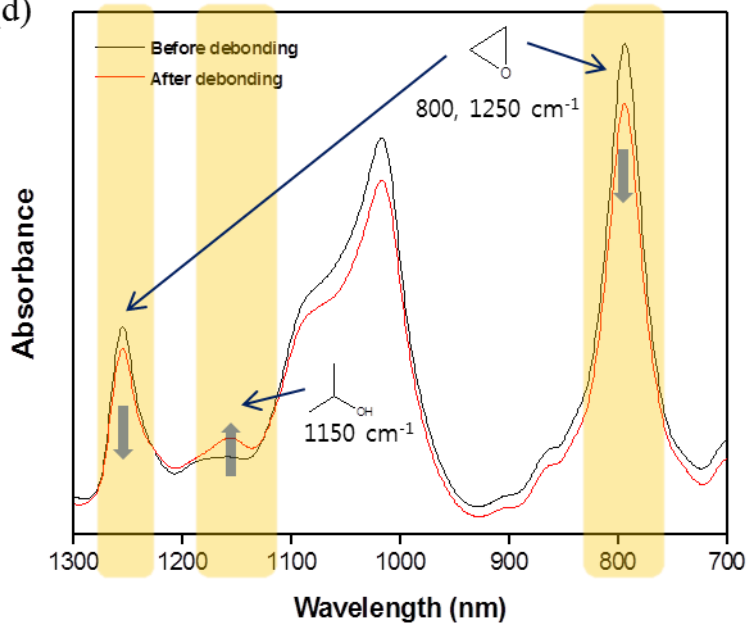


Figure 6-8. FTIR-ATR during dual curing and UV laser debonding. Chemical reactions of UV curing and thermal curing were shown. (a) The bands of the acrylic double bond at 810 and 1638 cm^{-1} are associated with UV curing in bonding properties. But the bands showed very weak intensity, so the band at 1730 cm^{-1} (C=O) stretching vibration indirectly showed the UV curing reaction. (b) The bands of the epoxy functionality at 800 and 1250 cm^{-1} are associated with thermal curing in bonding properties. (c) BTHPEMA plays an important role in both light to heat conversion (LTHC) reaction for UV laser debonding and UV curing. In LTHC reaction, the additional thermal curing between epoxy functionality of glycidyl methacrylate and carboxyl functionality of acrylic acid was generated like thermal curing in bonding process. (d)

Table 6-2. UV laser process parameters (Lee *et al.*, 2014).

Process parameters	Value
Laser wavelength, nm	355
Pulse repetition rate, kHz	100
Average power (P), W	8.3
Out-focusing length (mm)	14 – 16
Line spacing (mm)	20/30/40
Scan Speed (mm/s)	900/1100/1300

6.2.2.3. Fourier transform infrared (FTIR) spectroscopy

IR spectra were obtained using a JASCO FTIR-6100 (Japan) equipped with an attenuated total reflectance (ATR) accessory. In order to obtain the IR spectra of dual-curable adhesives, the cured adhesive samples were cut into 0.5 x 0.5 cm² pieces. The ATR prism was a diamond and its refractive index at 1000 cm⁻¹ was 2.4 with a transmission range from 4000 to 650 cm⁻¹. The resolution of the spectra recorded was 4 cm⁻¹. The curing behavior of the dual-curable adhesives was analyzed by observing the changes in the C=C bonding bands. All FTIR-ATR spectra were modified by baseline correction. The conversion (%) was calculated by the equation (Tasic, *et al.*, 2004).

$$\text{Conversion (\%)} = [(A_{810}/A_{1730})_0 - (A_{810}/A_{1730})_t] / (A_{810}/A_{1730})_0 \times 100 \quad (1)$$

where $(A_{810}/A_{1730})_0$ and $(A_{810}/A_{1730})_t$ denote the relative absorbance of the C=C bonds before curing and at a given curing time t , respectively (Lee *et al.*, 2014).

6.2.2.4. Gel fraction and swelling ratio

Gel fraction determination is a convenient method of measuring insoluble fractions, such as the fractions of cross-linked or network polymers (Park *et al.*, 2009). The gel fraction is the insoluble part while the swelling ratio is the fraction of the polymer swollen by the solvent. Both are significant factors when investigating curing behaviors. The gel fraction of the dual-curable adhesives after UV-curing was determined by soaking it in toluene at 50 °C for 24 h. The insoluble part was removed by filtration and dried at 50 °C to a constant weight. The gel fraction and swelling ratio were calculated by applying the following equations, respectively:

$$\text{Gel fraction} = (W_1/W_o) \quad (2)$$

$$\text{Swelling ratio} = 1 + [(W_s - W_1)/(W) \times \rho / \rho_o] \quad (3)$$

Here, W_o is the initial weight of the sample, W_s is the insoluble swollen part, W is the weight of the dry insoluble part, ρ is the density of the solvent, and ρ_o is the density of polymer (Seguchi *et al.*, 1985). The test was replicated three times (Lee *et al.*, 2014).

6.2.2.5. Shrinkage

To investigate the degree of linear shrinkage during the UV-curing process, 0.05 g of the dual-curable adhesives material was placed on a round stainless steel plate (ϕ 0.4 mm) and covered with a glass slide (75 x 25 x 1, mm³), after which UV light was irradiated for about 600 s using a spot-curing equipment. The average UV light intensity at the sample was approximately 10 mW/cm² over a wavelength range of 300~400 nm. The displacement of the samples during the UV-curing process was recorded by software (Lee *et al.*, 2014).

6.2.2.6. Thermogravimetric analysis (TGA)

The thermal stability and decomposition profiles of the dual-curable adhesives were measured using a thermogravimetric analyzer. The samples were loaded into a ceramic pan, and heated from 30 to 500°C at a constant heating rate of 10°C/m in an inert nitrogen atmosphere (Lee *et al.*, 2014).

6.2.2.7. Peel strength

The bonded specimen size was 8 mm x 8 mm. The 180° peel strength was measured using a Texture Analyzer, a kind of universal tensile machine, after the sample was left to stand at room temperature for 24 h. The peeling speed was 300 mm/m, and the average strength of peeling period was measured five times (Lee *et al.*, 2014).

6.2.2.8. Optical microscopy

Optical Microscopy (SV-55, Video microscope system, Sometech) was used for a qualitative analysis of the laser-irradiated samples (Lee *et al.*, 2014).

6.2.2.9. Field emission-scanning electron microscopy (FE-SEM) and energy dispersive spectroscopy (EDS)

Field emission-scanning electron microscopy (FE-SEM, JSM-7600F, JEOL, Japan) at an accelerating voltage of 10 kV was conducted to observe the surface morphology after UV laser irradiation. Prior to measurement, all samples were pre-coated with a homogeneous platinum layer (purity, 99.99 %) by ion sputtering to eliminate electron charging. Energy dispersive spectroscopy (EDS, SUPRA 55VP, Carl Zeiss, Germany) at an accelerating voltage of 15 kV was also employed to observe the samples. Prior to measurement, all samples were pre-coated with a homogeneous platinum layer (purity, 99.99 %) by ion sputtering to eliminate electron charging (Lee *et al.*, 2014).

6.2.2.10. Atomic force microscopy (AFM)

In order to observe the change of the surface morphology of the samples after UV laser irradiation, the atomic force microscopy (AFM) programmed in XE-BiO (Park Systems, USA) was used. The surface morphology was examined by recording AFM images in non-contact mode. This mode of operation is particularly advantageous on investigation of soft materials because interaction with the AFM tip does not affect the sample surface (Krok *et al.*, 2000; Khulbe *et al.*, 2000). The values of the root mean square (RMS) roughness were calculated from the height values in the AFM images (Lee *et al.*, 2014).

6.3. Results and discussion

6.3.1. Fourier transform infrared (FTIR) spectroscopy

After the photo-initiation of the adhesives by UV irradiation, the specific bands of the functional monomers and/or oligomers indicated that polymerization had occurred. The curing reaction can be measured using FTIR-ATR spectroscopy because the C=C bonds in the functional monomers participate in the cross-linking reaction by photo-polymerization (Joo *et al.*, 2006; Ratnam *et al.*, 2001). Figure 6-9 shows the conversion of acrylate bonds according to the FTIR-ATR spectra. It can be seen that as the UV dose was increased, the conversion of acrylate bonds increased rapidly then became constant regardless of the photo-initiator content. However, the photo-initiator content had an effect on the conversion rate. This occurred because the conversion of acrylate bonds is based on the functionality of the monomer, the more radical initiation, the faster the increase in the conversion of the acrylate bonds. Despite this, the conversion rate was not 100 %. The remaining C=C bonds may have remained unreacted after the action of the photo-initiator because they were trapped in the cross-linked polymer network (Joo *et al.*, 2007). Moreover, the unreacted monomers inhibit the thermal stability of adhesives (Lee *et al.*, 2014).

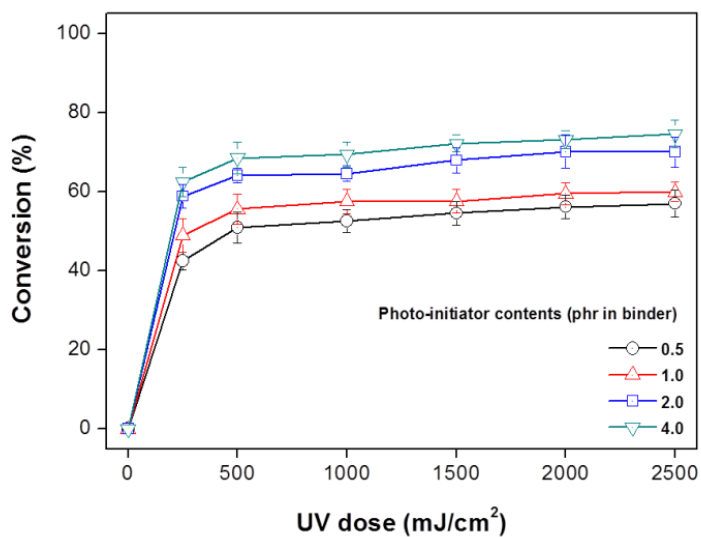


Figure 6-9. UV-curing profiles of UV-curable adhesives with different photo-initiator contents by FTIR-ATR spectra (Lee *et al.*, 2014).

6.3.2. Gel fraction and swelling ratio

Figure 6-10 shows the relationship between the UV dose and the gel fraction of UV-cured adhesives with different photo-initiator contents. As the UV dose increases, the concentration of free radicals increases, causing the crosslinking density to increase due to a three-dimensional crosslinked insoluble and infusible network. The gel fraction was constant regardless of the photo-initiator content for UV doses higher than 500 mJ/cm². The gel fraction with 0.5 phr of photo-initiator increased with an increase in the UV dose up to about 63% of the gel fraction at a UV dose of 2500 mJ/cm². However, the gel fraction increased to around 83% in 4.0 phr of photo-initiator. That is, at a low photo-initiator content, the gel content conspicuously increased, owing to the existence of unreacted monomer, but the rate of increase of the gel fraction decreased with an increase in the UV dose, because the amount of unreacted monomer decreased (Lee *et al.*, 2013).

On the other hand, the swelling ratio decreases rapidly with the dose, as shown in Figure 6-11, indicating that less space between the polymer chains is available for the swelling to occur. Figure 6-12 shows nearly linear dependence between the swelling ratio and gel fraction, suggesting that the processes of, crosslinking and chain scission occur at the same time. The variation of the two parameters with the dose may be due to oxidation-induced chain scission and the loosening of the network. In high-dose samples, the radical concentration is high and more chain scission reactions are induced, continuing for some time after UV irradiation (Elzubair *et al.*, 2003).

Considering that for higher radiation doses scission reactions are supposed to compete with crosslinking, the increase in the extent of crosslinking can be accounted for by the fact that chain scissions lead to entanglement couplings which act as crosslinks (Banik *et al.*, 1999). The main chain degradation is ultimately accompanied by crosslinking (Lee *et al.*, 2014).

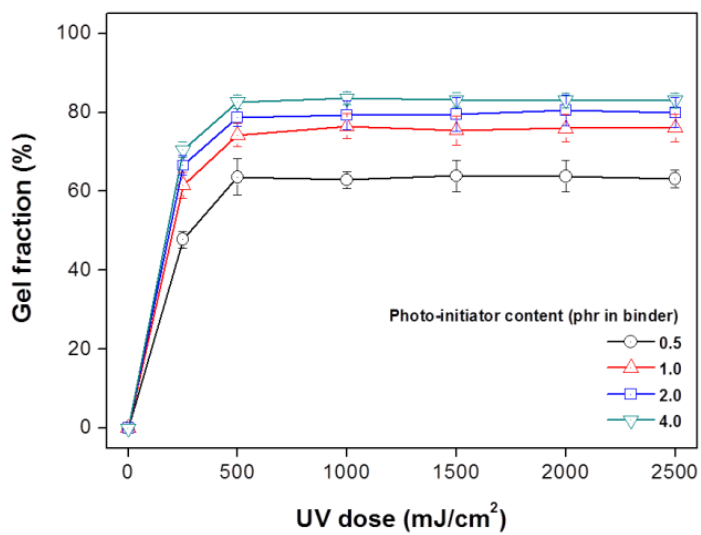


Figure 6-10. Gel fraction of UV-curing adhesives with different photo-initiator contents after UV-curing (Lee *et al.*, 2014).

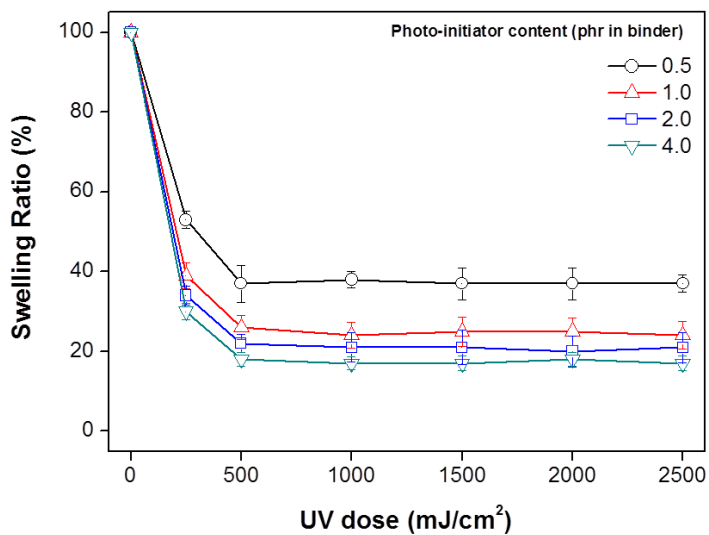


Figure 6-11. Swelling ratio of UV-curable adhesives with different photo-initiator contents after UV-curing (Lee *et al.*, 2014).

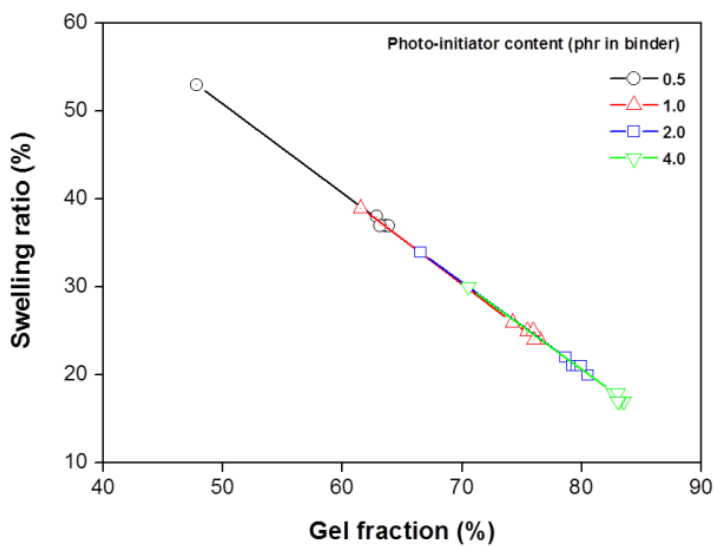


Figure 6-12. Correlation between swelling ratio and gel fraction of UV-curable adhesives (Lee *et al.*, 2014).

6.3.3. Shrinkage

Figure 6-13 depicts the typical linear shrinkage of UV-curable adhesives with reference to the irradiation time. Initially, the shrinkage of each sample increased sharply regardless of the photo-initiator contents. However, as the irradiation time elapsed, the shrinkage increased slightly and then stabilized. Also, the degree of linear shrinkage was dependent on the photo-initiator content. In general, the polymerization shrinkage of monomers and oligomers is due to the conversion of the intermolecular van-der-Waals forces to covalent single bonds during the polymerization process (Atai *et al.*, 2005). Hence, the shrinkage is the consequence of the cross-linked reaction between the multifunctional acrylic oligomer and the monomer (Lee *et al.*, 2014).

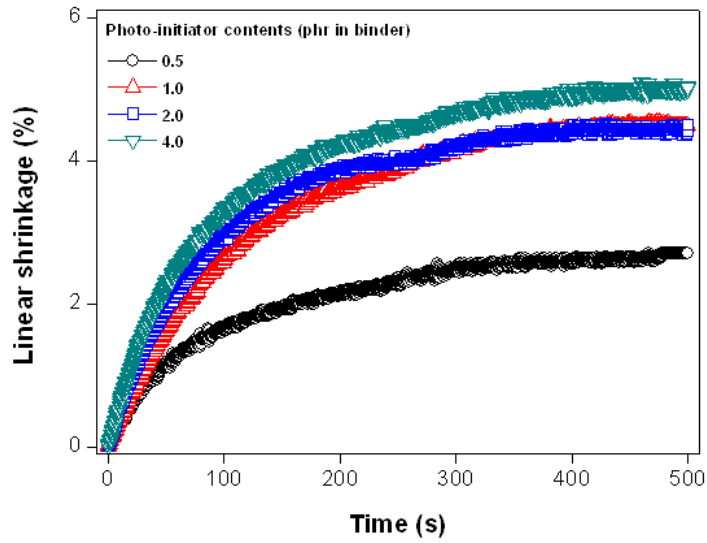


Figure 6-13. Linear shrinkage of UV-curable adhesives during UV irradiation (Lee *et al.*, 2014).

6.3.4. Thermogravimetric analysis (TGA)

Figure 6-14 shows the thermal stability of UV-cured adhesives at temperatures ranging from 30 to 500 °C. The weight loss at the temperature under 300 °C was due to the trapped volatile materials which were released (Chattopadhyay *et al.*, 2009). The thermal decomposition of the cross-linked polyurethane than started via the degradation of the polymer side chains, occurring at about 300 °C. A temperature above 450 °C led to complete decross-linking and thermal degradation of the cured adhesives (Kayaman-Apohan *et al.*, 2005). Also, thermal stability was enhanced with an increase in the UV doses due to the increased density of the cross-linked structures, corresponding to the gel fraction results shown above (Lee *et al.*, 2014).

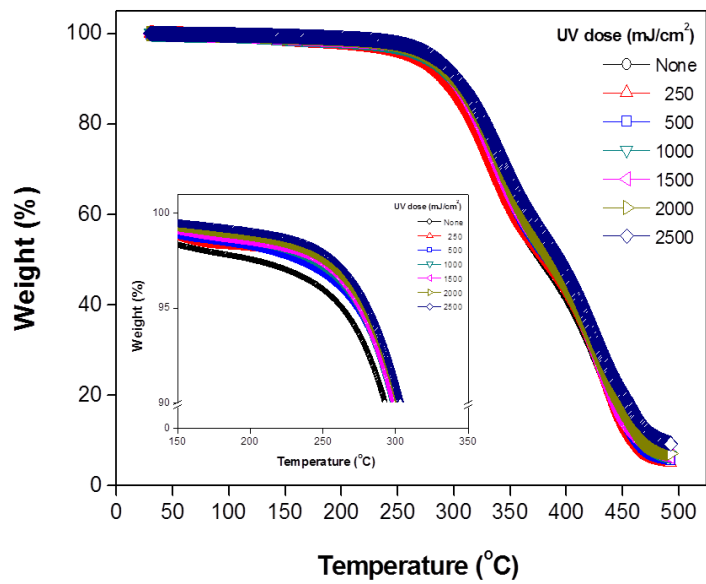


Figure 6-14. Thermogravimetric analysis of UV-cured adhesives with different UV doses (Lee *et al.*, 2014).

6.3.5. Peel strength

As shown in Figure 6-15(a), (b), the peel strength can be controlled by adjusting the out-focusing length, the line spacing, and/or the speed of the laser. The laser is absorbed mainly and attenuated progressively as it passes through the samples. With the increasing of the out-focusing length, the peel strength decreased slightly regardless of the line spacing and/or the speed in all samples. This was still at an acceptable level because the peel strength is the sum of the energies required to break the bond and deform the backing and the adhesives (Lim *et al.*, 2007; Lee *et al.*, 2014).

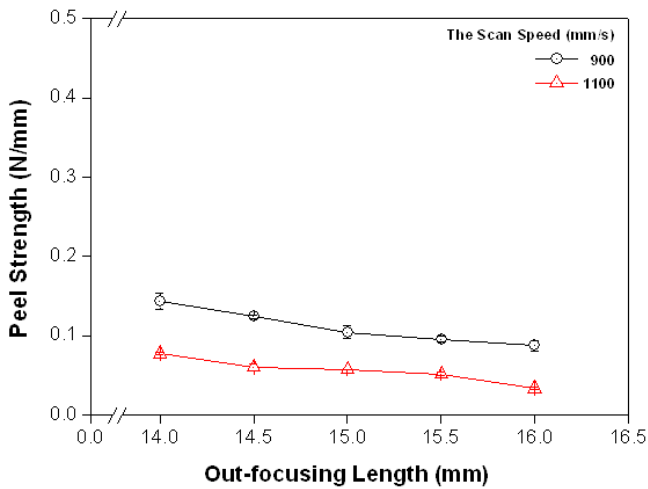
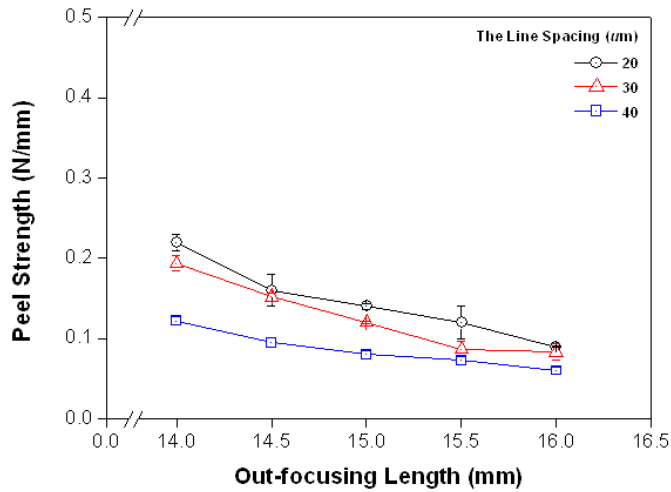


Figure 6-15. The peel strength (N/mm) vs. out-focusing length (mm) on (a) the line spacing from 20 μm to 40 μm , and (b) the scan speed from 900 mm/s to 1100 mm/s (Lee *et al.*, 2014).

6.3.6. Optical microscopy

Specimen on out-focusing lengths from 14 mm to 16 mm are reported for comparison in Figure 6-16(a)-(c). The surface of the specimen on out-focusing length at 14 mm is scratched and defected, but as increasing out-focusing length the surface of the specimen almost has been flatted. The surface roughness is clearly increased. Using laser irradiation a fraction of the laser beam energy is absorbed by the adhesives, therefore proceeding adhesives melting, surface morphological modifications. If it is compared between from Figure 6-16(c)-(e) it can be appreciated as the effect of increasing the laser spacing, on the resulting of surface morphology. For the smaller laser spacing it is not possible to distinguish the different laser scans during the process. Because the surfaces are contaminated by the remaining residue as a result of the adhesives burning. But if the spacing is increased the formation of surface patterns becomes remarkable. Finally, Figure 6-16(c) and 6-16(f) show the effect of laser speed when the spacing is held constant at 40 μm . When the speed increases from 900 to 1100 mm/s, the depth of the pattern almost decreases because the time available for the laser beam to heat substrate surface decreases (Lee *et al.*, 2014).

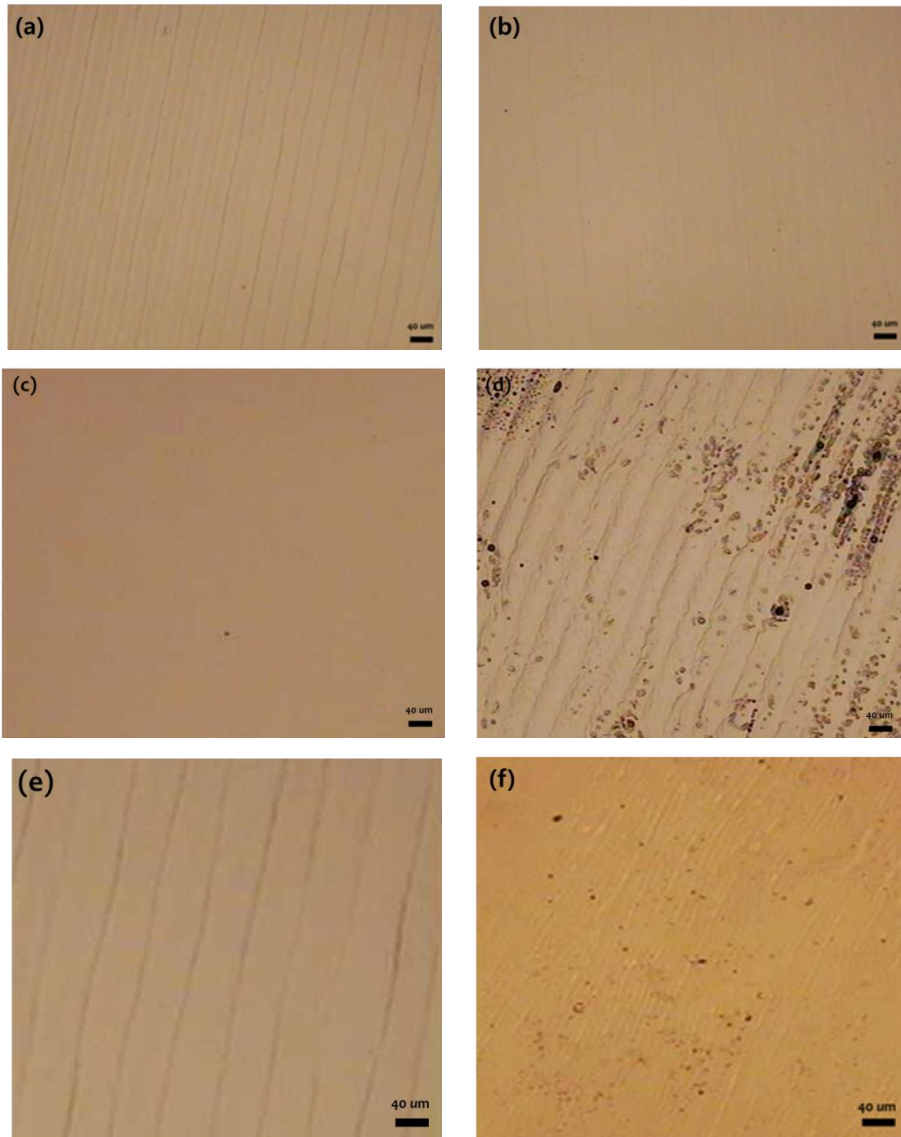


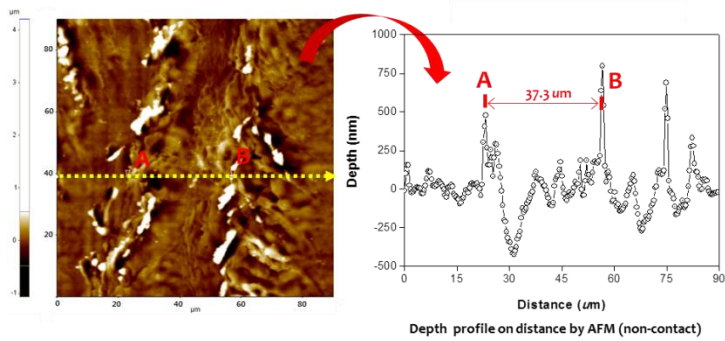
Figure 6-16. Microscopy observations of specimen (a) – (f). The laser beam was irradiated from top to bottom (Lee *et al.*, 2014).

6.3.7. Atomic force microscopy (AFM)

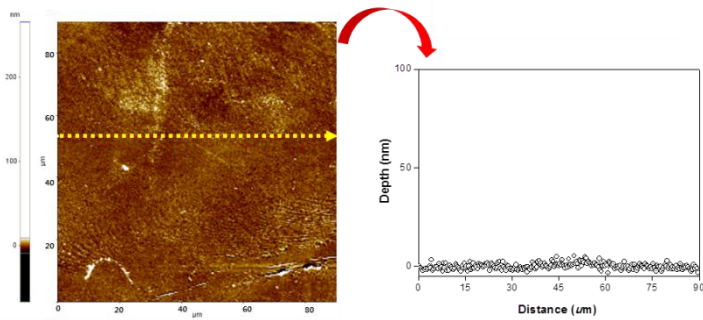
Figure 6-17 indicates that the surface morphology and depth profile after UV laser irradiation and Table 6-3 shows different UV laser processing conditions. This method provides image of the sample topology by scanning a sample with a sharp tip attached to a cantilever, which is deflected as the tip interacts with the studied surface. Because it is a non-contact mode of AFM, the tip is vibrating in a distance of about from 5 to 10 nm from the surface and it is responding to attractive van der Waals interactions. The images provide observation of the damaged and/or the undamaged Si wafer in form of uniformly consisting of distributed groove-like creator or any of particles. The irradiation energy has grown up with increasing defocusing length. So, the sample (a) is more severe damaged than any other sample, (b) and (c). The depth profiles of the samples with from the bottom to the top are also calculated by through AFM images. The depth of the sample (a) is the largest in all samples. This means that the surface morphology of Si wafer after UV laser irradiation has strongly depended on UV laser process conditions (Lee *et al.*, 2014).

Table 6-3. Different UV laser processing conditions (Lee *et al.*, 2014)

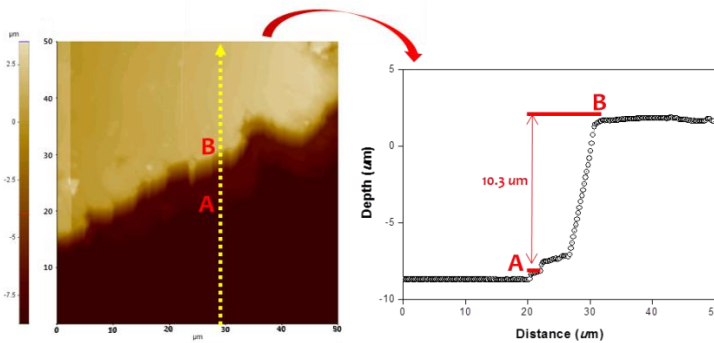
Samples	(a)	(b)	(c)
Power (W/%)	10 / 88.5	10 / 88.5	10 / 88.5
Pulse rate (kHz)	100	100	100
Wavelength (nm)	355	355	355
Scan speed (mm/s)	1500	1500	1500
Scan pitch (μm)	40	40	40
Defocusing length (μm)	11.75~15.75	16.75~17.75	18.75~19.75



(a)



(b)

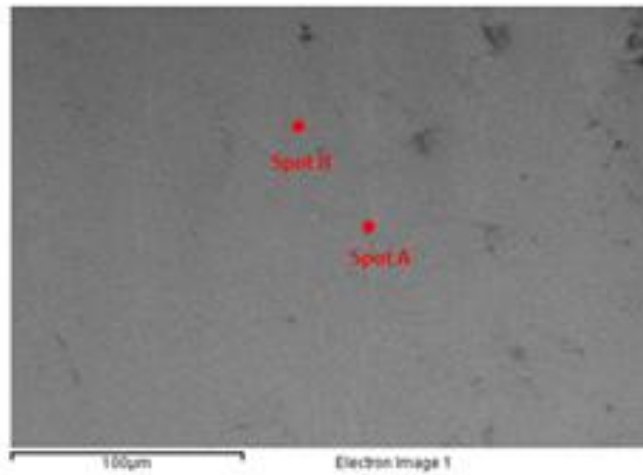


(c)

Figure 6-17. AFM images and depth profiles after UV laser irradiation with different processing conditions (process condition (a) ~ (c)) (Lee *et al.*, 2014).

6.3.8. Field emission-scanning electron microscopy (FE-SEM) and Energy dispersive spectroscopy (EDS)

Figure 6-18 indicates that SEM image and atomic fraction (%) of damaged area (spot A) and undamaged area (spot B) on Si wafer after cleaning, sample (a). As mentioned before, it is important thing to clean Si wafer after UV laser irradiation. Because if either any residue or scratches remains after cleaning, not only it was related with damages of Si wafers but also the yield rate will be dropped apparently. So, it is necessary to analysis whether it is any damage or not if it was presented as “line” on Si wafer after cleaning process. Atomic fraction (%) on Si at both damaged area (spot A) and undamaged area (spot B) in sample (a) shows almost same result. It means the “line” might have been estimated as damaged area of the Si wafer. Hence, it always should be intended to conduct surface morphologies after cleaning by FE-SEM and/or EDS (Lee *et al.*, 2014)



SEM image on Si wafer after cleaning

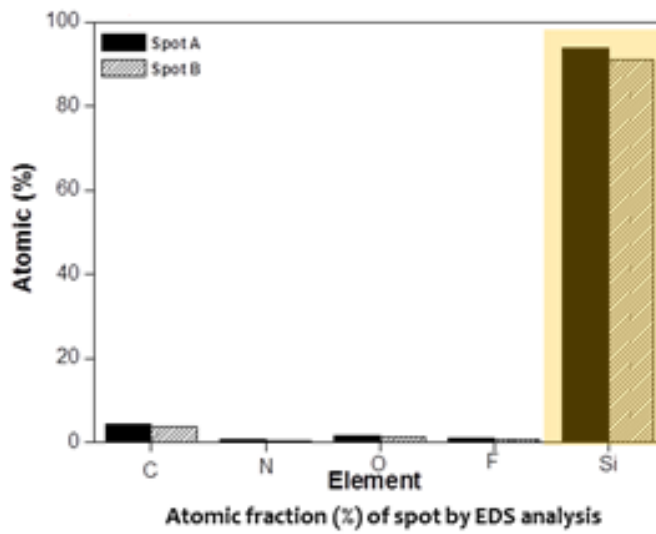


Figure 6-18. SEM image and atomic fraction (%) of damaged area (spot A) and undamaged area (spot B) on Si wafer after cleaning, sample (a) (Lee *et al.*, 2014).

6.4. Conclusion

Handling thin wafers through packaging assembly processes are not easy since the wafers may lose the supporting strength. So, UV laser debonding has been shown to be a promising technology for the temporary adhesives bonding and debonding process because of its very fast debonding time about few seconds and irradiation stability than thermal or chemical debonding. To investigate laser debonding, the surface morphology, for various sets of the out-focusing length, the line spacing, and the scan speed, was studied by means of the optical microscopy, and peel strength. The thermal curable adhesives containing UV absorbing material were fast cured by the laser irradiation. The results showed that the laser process ensures the adhesives removal thereby removing any weak layer. Among them, the suitable conditions are 12 mm of out-focusing length, 40 mm of line spacing, and 1100 mm/s of scan speed.

Chapter 7

Concluding Remarks

Temporary bonding and debonding adhesives for three-dimensional (3D) multichip package process have been synthesized. To enhance the thermal stability, the adhesives used a fluorinated silicon urethane acrylic binder and ultraviolet (UV) curing for crosslinked network structures. Also, UV absorbing material was employed in dual curable adhesives for UV laser debonding. Focusing on different photo-initiator contents, UV doses and the functional monomer types and contents, the UV-curing behaviors and thermal stability were investigated using FTIR-ATR, gel fraction, swelling ratio, shrinkage and TGA. Furthermore, optical spectroscopy, FE-SEM, AFM and XPS were conducted to analyze Si surface morphologies after UV laser debonding.

1. Adhesion performance and surface morphology of UV-curable interpenetrating network acrylates for 3D multi-chip packaging process three-dimensional integration

UV-curable acrylates have many applications in industries. As the Si wafers become thinner, the acrylics for MCP need to show proper adhesion and leave little residue on the Si wafer after UV irradiation when released from the process. Strong adhesion is required in the process to hold the Si wafer before UV irradiation. On the other hand, weak adhesion strength is required after UV irradiation to prevent damage to the Si wafers during the “pick-up” process. This study employed interpenetrating polymer network structured acrylates in the Si wafer manufacture process. The binder contained 2-ethylhexyl acrylate (2-EHA) and acrylic acid (AA). The adhesion performance of the peel strength on a Si wafer was examined as a function of the UV dose. The results showed that the above mentioned two requirements were achieved using IPN structured acrylates using a hexafunctional acrylic

monomer and a UV-curing system. FE-SEM and XPS revealed little residue on the wafer after removing adhesives. It suggests the proper conditions for the curing agent, the additional hexafunctional monomer, photo-initiator and the coating thickness.

2. Adhesion performance and curing behaviors of UV-curable acrylates with 3-MPTS for 3D multi-chip packaging process

As Si wafers, as used in the electronic industry, become thinner and thinner, it is important to investigate the conditions which are suitable for easily peelable acrylates. In the Si wafer process, the adhesion strength decreased after UV irradiation as a result of polymer network formation. The interpenetrating polymer network (IPN) structured acrylates were investigated with two different types UV irradiation, a steady UV irradiation and a pulsed UV irradiation of 100 mJ/cm². The binder contained 2-ethylhexyl acrylate (2-EHA), acrylic acid (AA) and 3-methacryloxypropyl trimethoxysilane (3-MPTS). The hexafunctional monomer, dipentaerythritol hexaacrylate (DPHA) and 3-MPTS were used as diluent monomers. The adhesion performance as related to the peel strength and the tack properties on the Si wafer substrates, was examined with increasing UV dose. The effect of UV-curing on the behavior and viscoelastic properties of the acrylates was investigated using fourier transform infrared – attenuated total reflectance spectroscopy (FTIR-ATR) and an advanced rheometric expansion system (ARES). It is also necessary to consider the contaminants on the Si wafer substrates left behind after releasing the adhesives, because of possible damage to the Si wafer and subsequent processes. Field emission-scanning electron microscopy (FE-SEM) and X-ray photoelectron spectroscopy (XPS) analysis revealed little residue

on the Si wafer after removing the adhesives and after more than the specific level of UV dose.

3. UV-curing and thermal stability of dual-curable urethane epoxy adhesives for temporary bonding and debonding in 3D multi-chip packaging process

Multi-chip package (MCP) refers to a packaging configuration, connected via wirebonds to a multilayer circuit board, and protected by either a molded encapsulant or a low-cost ceramic package. As it requires high processing temperature, the adhesives for MCP need to show proper adhesion and thermal stability at high temperature. Hence, it employed interpenetrating network structured (IPNs) polymer using UV-curing with an acrylate terminated UV-curable urethane binder, a dipentaerythritol hexaacrylate (DPHA), a glycidylmethacrylate (GMA) and a hydroxydimethyl acetophenone as a photo-initiator. UV-curing and thermal stability focused on different photo-initiator contents were investigated using photo-DSC, FTIR-ATR spectroscopy, gel content and TGA. The results show that different formulation with different content of a photo-initiator affects UV-curing and thermal stability.

4. Synthesis and properties of UV laser debondable fluorinated silicone-modified urethane acrylic adhesives for temporary bonding and debonding in 3D multi-chip packaging process

Using adhesives is the one of the possible solutions for thin wafer handling, and how to synthesize adhesives materials and investigate debonding behaviors for temporary bonding and debonding are an important research. UV laser irradiation is considered for debonding temporary adhesives in a 3D multi-chip package process. It was required bonding temperature at 200 ~ 220 °C for a conventional method, but bonding temperature at 80 ~ 150 °C was obtained for this method. Also, short debonding time less than 2 minutes was conducted in contrast to long debonding time of a conventional method which uses solvent to dissolve adhesives for more than 6 hours. For this, the adhesives were synthesized with BTHPEMA for UV absorbing material which reacted at certain wavelength, especially 40 % of absorbance at 355 nm in 0.4 phr of BTHPEMA content as measured by UV-visible spectroscopy. BTHPEMA plays an important role in both light to heat conversion (LTHC) reaction for UV laser debonding and UV curing which is conducted by a synthesized urethane acrylic binder and other curable acrylic monomers for bonding properties. In LTHC reaction, the additional thermal curing by an epoxy functionality of a glycidyl methacrylate and a carboxyl functionality of an acrylic acid was generated as measured by FTIR-ATR and gel fraction. As mentioned results and investigations, suitable UV laser debonding was presented by effective energy density of 355 nm UV laser at 5.65 ~ 6.72 J/cm².

References

Alexe, M., Gosele, U. (2004). *Wafer Bonding and Applications and Technology*. Springer-Verlag, Berlin, Germany.

Allcock, H. R., Lampe, F. W., Mark, J. E., Allcock, H. (1990). *Contemporary Polymer Chemistry*. Prentice Hall Englewood Cliffs, NJ

Anseth, K. S., Kline, L. M., Walker, T. A., Anderson, K. J., Bowman, C. N. (1995). Reaction kinetics and volume relaxation during polymerizations of multiethylene glycol dimethacrylates. *Macromolecules*. 28(7): 2491-2499.

Asahara, J., Takemura, A., Hori, N., Ono, H., Matsui, H. (2004). Crosslinked acrylic pressure sensitive adhesives. 3. Effect of adherend on film formation. *Polymer*. 45(14): 4917-4924.

Atai, M., Watts, D. C., Atai, Z. (2005). Shrinkage strain-rates of dental resin-monomer and composite systems. *Biomaterials*. 26(24): 5015-5020.

Athawale, V. D., Kolekar, S. L., Raut, S. S. (2003). Recent developments in polyurethanes and poly (acrylates) interpenetrating polymer networks. *Journal of Macromolecular Science, Part C: Polymer Reviews*. 43(1): 1-26.

Auchter, G., Aydin, O., Zettl, A., Satas, D. 1999. *Handbook of pressure sensitive adhesive technology*. Satas Associates, Warwick.

Audet, S. A., Edenfeld, K. M. (1997). Integrated sensor wafer-level packaging. Proceeding of Transducers, Chicago, USA.287-289.

Bai, D. (2009). Edge protection of temporarily bonded wafers during backgrinding. *ESC transactions*. 18(1): 757-762.

Banik, I., Bhowmick, A. K. (1999). Influence of electron beam irradiation on the mechanical properties and crosslinking of fluorocarbon elastomer. *Radiation Physics and Chemistry*. 54(2): 135-142.

Barrales - Rienda, J., Ramos, J. G., Chaves, M. S. (1979). Polymerization of N - (fluoro phenyl) maleimides. *Journal of Polymer Science: Polymer Chemistry Edition*. 17(1): 81-96.

Bilenberg, B., Nielsen, T., Clausen, B., Kristensen, A. (2004). PMMA to SU-8 bonding for polymer based lab-on-a-chip systems with integrated optics. *Journal of Micromechanics and Microengineering*. 14(6): 814.

Bou, M., Martin, J. M., Le Mogne, T., Vovelle, L. (1991). Chemistry of the interface between aluminium and polyethyleneterephthalate by XPS. *Applied Surface Science*. 47(2): 149-161.

Boudaden, J., Piekass, M. (2008). Carrier technology for wafer thinning_Be Flexible forum, Munich.

Brubaker, C., Wimplinger, M., Malzer, A., Lindner, P. (2005). Advanced in processing of compound semiconductor substrates. MANTECH.

Chattopadhyay, D., Panda, S. S., Raju, K. (2005). Thermal and mechanical properties of epoxy acrylate/methacrylates UV-cured coatings. *Progress in Organic Coatings*. 54(1): 10-19.

Chattopadhyay, D., Raju, K. (2007). Structural engineering of polyurethane coatings for high performance applications. *Progress in Polymer Science*.

32(3): 352-418.

Chattopadhyay, D., Webster, D. C. (2009). Thermal stability and flame retardancy of polyurethanes. *Progress in Polymer Science*. 34(10): 1068-1133.

Cheng, Y.-T., Lin, L., Najafi, K. (2000). Localized silicon fusion and eutectic bonding for MEMS fabrication and packaging. *Journal of Microelectromechanical Systems*. 9(1): 3-8.

Chibowski, E. J. (2005). Surface free energy and wettability of silyl layers on silicon determined from contact angle hysteresis. *Advances in Colloid and Interface Science*. 113(2-3): 121-131.

Chiu, Y. S., Liu, Y. L., Wei, W. L., Chen, W. Y. (2003). Using diethylphosphites as thermally latent curing agents for epoxy compounds. *Journal of Polymer Science Part A: Polymer Chemistry*. 41(3): 432-440.

Cho, S.-D., Lee, J.-Y., Hyun, J.-G., Paik, K.-W. (2004). Study on epoxy/BaTiO composite embedded capacitor films (ECFs) for organic substrate applications. *Materials Science and Engineering: B*. 110(3): 233-239.

Combe, S., Cullen, J., O'Keefe, M. (2006). Reversible wafer bonding: challenges in ramping up 150 mm GaAs wafer production to meet growing demand. MANTECH.

Czech, Z. (2004). Development in the area of UV-crosslinkable solvent-based pressure-sensitive adhesives with excellent shrinkage resistance. *European Polymer Journal*. 40(9): 2221-2227.

Czech, Z. (2007). New generation of crosslinking agents based on multifunctional methylaziridines. *International Journal of Adhesion and Adhesives*. 27(1): 49-58.

Decker, C., Nguyen Thi Viet, T. (2000). Photocrosslinking of functionalized rubbers IX. Thiol-ene polymerization of styrene-butadiene-block-copolymers. *Polymer*. 41(11): 3905-3912.

Decker, C., Zahouily, K., Decker, D., Nguyen, T., Viet, T. (2001). Performance analysis of acylphosphine oxides in photoinitiated polymerization. *Polymer*. 42(18): 7551-7560.

Delmdahl, R., Pätzelt, R., Brune, J. (2013). Large-area laser-lift-off processing in microelectronics. *Physics Procedia*. 41:241-248.

Do, H.-S., Park, J.-H., Kim, H.-J. (2008). UV-curing behavior and adhesion performance of polymeric photoinitiators blended with hydrogenated rosin epoxy methacrylate for UV-crosslinkable acrylic pressure sensitive adhesives. *European Polymer Journal*. 44(11): 3871-3882.

Do, H. S., Kim, D. J., Kim, H.-J., Lee, Y. K. (2003). The effect of temperature and photoinitiator concentration on conversion of photopolymerized multifunctional glycol dimethacrylate by photo-DSC. *Journal of Adhesion and Interface. Korea*. 4(3): 14-20.

Do, H. S., Kim, S. E., Kim, H.-J. (2005). *Preparation and Characterization of UV-crosslinkable Pressure-sensitive Adhesives*. Wiley-VCH, Weinheim, Germany.

Dubuisson, A., Ades, D., Fontanille, M. (1980). Homogeneous epoxy-acrylic interpenetrating polymer networks: preparation and thermal properties. *Polymer Bulletin*. 3: 391-398.

Ebe, K., Sasaki, T. (2003). Electron beam curing of aliphatic unsaturated polyesters. I. Mechanistic study on converting to pressure-sensitive adhesives. *Journal of Applied Polymer Science*. 88(7): 1854-1857.

Ebe, K., Seno, H., Horigome, K. (2003). UV-curable pressure-sensitive adhesives for fabricating semiconductors. I. Development of easily peelable dicing tapes. *Journal of Applied Polymer Science*. 90(2): 436-441.

Ellerstein, S. M., Lee, S. A., Palit, T. K. (1993). *Radiation curing in polymer science and technology, Vol.4. practical aspects and applications*. Elsevier Applied Science, London. UK.

Elzubair, A., Suarez, J. C. M., Bonelli, C. M. C., Mano, E. B. (2003). Gel fraction measurements in gamma-irradiated ultra high molecular weight polyethylene. *Polymer Testing*. 22(6): 647-649.

Fernandez-Bolanos, M., Ionescu, A. (2010). Heterogeneous integration for novel functionality. IEEE International 3D System Integration Conference (3DIC 2010).

Garrou, P. (2009). Temporary Bonding for 3DIC Thinning and Backside Processing. Perspectives from the Leading Edge.

Garrou, P., Bower, C., Ramm, P. (2008). *Handbook of 3D Integration*. Wiley-VCH, Weinheim.

Ge, Z., Zhang, X., Dai, J., Li, W., Luo, Y. (2009). Synthesis, characterization and properties of a novel fluorinated polyurethane. *European Polymer Journal*. 45(2): 530-536.

Ghosh, A., Banerjee, S., Komber, H., Schneider, K., Häußler, L., Voit, B. (2009). Synthesis and characterization of fluorinated poly (imide siloxane) block copolymers. *European Polymer Journal*. 45(5): 1561-1569.

Gragg, J. E., McCulley, W. E., Newton, W. B., Derrington, C. E. (1984). Compensation and calibration of a monolithic four terminal silicon pressure transducer. Proceeding of IEEE Solid States Sensor and Actuator Workshop, Hilton Head, SC.147.

Hermanowski, J. (2009). Thin wafer handling-study of temporary wafer bonding materials and processes. Electronic Components and Technology Conference.

Hong, B. T., Shin, K. S., Kim, D. S. (2005). Ultraviolet - curing behavior of an epoxy acrylate resin system. *Journal of Applied Polymer Science*. 98(3): 1180-1185.

Hosali, S. (2008). *Through Silicon Via Fabrication, Background and Handle Wafer Technologies, in Wafer Level 3-D ICs Process Technology*. Springer, New York.

Hua, F. J., Hu, C. P. (2000). Interpenetrating polymer networks of epoxy resin and urethane acrylate resin: 2. Morphology and mechanical property. *European Polymer Journal*. 36(1): 27-33.

Iyer, S. S., Auberton-Herve, A. J. (2002). *Silicon Wafer Bonding Technology for VLSI and MEMS*. INSPEC, London, UK.

Jin, S., Atrens, A. (1987). ESCA-studies of the structure and composition of the passive film formed on stainless steels by various immersion times in 0.1 M NaCl solution. *Applied Physics A*. 42(2): 149-165.

Joo, H.-S., Do, H.-S., Park, Y.-J., Kim, H.-J. (2006). Adhesion performance of UV-cured semi-IPN structure acrylic pressure sensitive adhesives. *Journal of Adhesion Science and Technology*. 20(14): 1573-1594.

Joo, H.-S., Park, Y.-J., Do, H.-S., Kim, H.-J., Song, S.-Y., Choi, K.-Y. (2007). The curing performance of UV-curable semi-interpenetrating polymer network structured acrylic pressure-sensitive adhesives. *Journal of Adhesion Science and Technology*. 21(7): 575-588.

Kang, D. H., Lee, B. C. (2007). Preparation and characteristics of silicone modified polyacrylic hybrid elastomer. *Polymer(Korea)*. 31:86-91.

Kayaman-Apohan, N., Demirci, R., Cakir, M., Gungor, A. (2005). UV-curable interpenetrating polymer networks based on acrylate/vinylether functionalized urethane oligomers. *Radiation Physics and Chemistry*. 73(5): 254-262.

Kessel, C. R. (2007). Wafer thinning with the 3M wafer support system. Proceedings of the International Wafer-Level Packaging Conference.

Khulbe, K. C., Matsuura, T. (2000). Characterization of synthetic membranes by Raman spectroscopy, electron spin resonance, and atomic force microscopy; a review. *Polymer*. 41(5): 1917-1935.

Kim, J. B., Chiao, M., Lin, L. (2002). Ultrasonic bonding of In/Au and Al/Al for hermetic sealing of MEMS packaging. Proceeding of MEMS, Las Vegas, NY, USA.

Kim, J. K., Kim, W. H., Lee, D. H. (2002). Adhesion properties of UV crosslinked polystyrene-block-polybutadiene-block-polystyrene copolymer and tackifier mixture. *Polymer*. 43(18): 5005-5010.

Kim, Y.-B., Park, S.-C., Kim, H.-K., Hong, J.-W. (2008). Dual-curable acrylic pressure-sensitive adhesives based on UV and thermal processes. *Macromolecular Research*. 16(2): 128-133.

Kim, Y.-C., Roh, J.-B., Lee, B.-J. (2002). Synthesis and Characterization of Liquid Crystalline Epoxy Acrylate. *Journal of Korean Industrial and Engineering Chemistry*. 13(6): 538-543.

Kloosterboer, J. (1988). *Network Formation by Chain Crosslinking Photopolymerization and Its Applications in Electronics. Electronic Applications*, Springer Berlin Heidelberg. 84: 1-61.

Krok, F., Szymońska, J., Tomasik, P., Szymoński, M. (2000). Non-contact AFM investigation of influence of freezing process on the surface structure of potato starch granule. *Applied Surface Science*. 157(4): 382-386.

Kwon, O. H. (2011). Eco-friendly semiconductor technologies for health living (plenary lecture). IEEE International Solid-State Circuits Conference (ISSCC).

Kwon, Y., Seok, J. (2005). An evaluation process of polymeric adhesive wafer bonding for vertical system integration. *Japanese Journal of Applied Physics*. 44(6R): 3893.

Lee, D. J., Choi, J. Y., H.D., K. (1999). Preparation and properties of UV-curable polyurethane acrylate (II)-effect of types and concentration of reactive diluents. *Journal of the Korean Fiber Society*. 36(11): 798-805.

Lee, S.-W., Lee, T.-H., Park, J.-W., Park, C.-H., Kim, H.-J., Kim, S.-M., Lee, S.-H., Song, J.-Y., Lee, J.-H. (2014). The effect of laser irradiation on peel strength of temporary adhesives for wafer bonding. *International Journal of Adhesion and Adhesives*. In Press.

Lee, S.-W., Lee, T.-H., Park, J.-W., Park, C.-H., Kim, H.-J., Song, J.-Y., Lee, J.-H. (2014). Curing behaviors of UV-curable temporary adhesives for a 3D multichip package process. *Journal of Electronic Materials*. 43(11): 4246-4254.

Lee, S.-W., Park, J.-W., Kim, H.-J., Kim, K.-M., Kim, H.-I., Ryu, J.-M. (2012). Adhesion performance and microscope morphology of UV-curable semi-interpenetrated dicing acrylic PSAs in Si-wafer manufacture process for MCP. *Journal of Adhesion Science and Technology*. 26: 317-329.

Lee, S.-W., Park, J.-W., Kwon, Y.-E., Kim, S., Kim, H.-J., Kim, E.-A., Woo, H.-S., Swiderska, J. (2012). Optical properties and UV-curing behaviors of optically clear semi-interpenetrated structured acrylic pressure sensitive adhesives. *International Journal of Adhesion and Adhesives*. 38:5-10.

Lee, S.-W., Park, J.-W., Park, C.-H., Lim, D.-H., Kim, H.-J., Song, J.-Y., Lee, J.-H. (2013). UV-curing and thermal stability of dual curable urethane epoxy adhesives for temporary bonding in 3D multi-chip package process. *International Journal of Adhesion and Adhesives*. 44:138-143.

Lim, D.-H., Do, H.-S., Kim, H.-J., Bang, J.-S., Yoon, G.-H. (2007). Preparation of SIS/SBS-based UV-cross-linkable pressure-sensitive adhesives using the thiol-ene reaction. *Journal of Adhesion Science and Technology*. 21(7): 589-603.

Lim, J., Kim, D., Hwang, J. (2003). Synthesis and properties of photocurable aliphatic epoxy acrylate (I). *Journal of Korean Industrial and Engineering Chemistry*. 14(6): 818-823.

Mahabiz, M. M., Cohn, M. B., Howe, R. T., Horowitz, R., Pisano, A. P. (1999). Batch micropackaging by compression-bonded wafer-wafer transfer. Proceeding of MEMS, Orlando, FL.

Massey, S., Roy, D., Adnot, A. (2003). Study of natural ageing of polypropylene by X-ray photoelectron spectroscopy. *Nuclear Instruments and Methods in Physics Research Section B: Beam Interactions with Materials and Atoms*. 208: 236-241.

Mathias, T. (2007). Ultrathin-wafer processing utilizing temporary bonding and debonding technology. Proceedings of International Wafer-Level Packaging Conference.

Matsumoto, A., Kimura, T. (1998). Synthesis of heat - and solvent - resistant polymers by radical polymerization of trifluoromethyl - substituted N - phenylmaleimides. *Journal of Applied Polymer Science*. 68(10): 1703-1708.

Mokhtar, S., Abd-Elaziz, S., Gomaa, F. (2010). Synthesis characterizations and properties of a new fluoro-maleimide polymer. *Journal of Fluorine Chemistry*. 131(5): 616-620.

Moore, J., Smith, A., Nguyen, D., Kulkarni, S. (2004). High temperature resistant adhesive for wafer thinning and backside processing. MANTECH.

Morrow, P. R., Kobrinsky, M. J., Ramanathan, S., Park, C. M., Harmes, M., Ramachandrarao, V., Park, H. M., Kloster, G., List, S., Kim, S. (2004). Wafer-level 3D Interconnects Via Cu Bonding. Materials research society. symposium of proceeding.

Nelson, E., Jacobs, J., Scranton, A. B., Anseth, K., Bowman, C. (1995). Photo-differential scanning calorimetry studies of cationic polymerizations of divinyl ethers. *Polymer*. 36(24): 4651-4656.

Niklaus, F., Stemme, G., Lu, J.-Q., Gutmann, R. (2006). Adhesive wafer bonding. *Journal of Applied Physics*. 99(3): 031101.

Oprea, S., Vlad, S., Stanciu, A., Macoveanu, M. (2000). Epoxy urethane acrylate. *European Polymer Journal*. 36(2): 373-378.

Ozawa, T., Ishiwata, S., Kano, Y., Kasemura, T. (2000). Acrylate Copolymer/Ultraviolet Curable Oligomer Blends as Pressure-sensitive

Adhesives. *The Journal of Adhesion*. 72(1): 1-16.

Dufour, P. (1993). *Radiation Curing in Polymer Science and Technology, Vol. 1. Fundamentals and Methods*. Elsevier Science Publishers, London.

Pargfrieder, S. (2009). 3D Integration by Through-Silicon-Via (TSV) Processing Enabled by Temporary Bonding and Debonding Technology. *Advanced Packaging*.

Park, Y.-J., Lim, D.-H., Kim, H.-J., Park, D.-S., Sung, I.-K. (2009). UV-and thermal-curing behaviors of dual-curable adhesives based on epoxy acrylate oligomers. *International Journal of Adhesion and Adhesives*. 29(7): 710-717.

Petersen, K., Barth, P. W., Poydock, J., Brown, J., Mallon, J., Bryzek, J. (1988). Silicon fusion bonding for pressure sensors. *Proceeding of IEEE Solid States Sensor and Actuator Workshop*, Hilton Head, SC.

Petrie, E. M. (2000). *Handbook of Adhesives and Sealants*. McGraw-Hill, New York, USA.

Pu, F., Williams, R., Markkula, T., Hunt, J. (2002). Effects of plasma treated PET and PTFE on expression of adhesion molecules by human endothelial cells in vitro. *Biomaterials*. 23(11): 2411-2428.

Puligadda, R. (2006). High-performance temporary adhesives for wafer bonding applications. *Materials research society. symposium of Proceeding*. 970.

Ramm, P., Lu, J. Q., Taklo, M. V. (2012). *Handbook of Wafer Bonding*. Wiley-VCH, Weinheim.

Ratnam, C. T., Nasir, M., Baharin, A., Zaman, K. (2001). Evidence of irradiation - induced crosslinking in miscible blends of poly (vinyl chloride)/epoxidized natural rubber in presence of trimethylolpropane triacrylate. *Journal of Applied Polymer Science*. 81(8): 1914-1925.

Rimmer, J. S., Missous, M., Peaker, A. R. (1991). A new, fast method for the computer simulation of CV profiles in multilayer structures. *Applied Surface Science*. 50(1-4): 149-153.

Sacher, E. (1994). Fluoropolymer metallization for microelectronic applications. *Progress in Surface Science*. 47(3): 273-300.

Saiki, N., Inaba, K., Kishimoto, K., Seno, H., Ebe, K. (2010). Study on Peeling Behavior in Pick-up Process of IC Chip with Adhesive Tapes. *Journal of Solid Mechanics and Materials Engineering*. 4(7): 1051-1060.

Scherzer, T. (2004). Photopolymerization of acrylates without photoinitiators with short-wavelength UV radiation: A study with real-time fourier transform infrared spectroscopy. *Journal of Polymer Science Part A: Polymer Chemistry*. 42(4): 894-901.

Schmidt, M. A. (1998). Wafer-to-wafer bonding for microstructure formation. *Proceeding of IEEE*. 86(8):1575-1585.

Severini, F., Gallo, R., Di Landro, L., Pegoraro, M., Brambilla, L., Tommasini, M., Castiglioni, C., Zerbi, G. (2001). Chemical and physical modifications of alternating ethylene–carbon monoxide copolymer by outdoor exposure. *Polymer*. 42(8): 3609-3625.

Song, Y.-W., Do, H.-S., Joo, H.-S., Lim, D.-H., Kim, S., Kim, H.-J. (2006). Effect of grafting of acrylic acid onto PET film surfaces by UV irradiation on the adhesion of PSAs. *Journal of Adhesion Science and Technology*. 20(12): 1357-1365.

Sosson, F., Chateauminois, A., Creton, C. (2005). Investigation of shear failure mechanisms of pressure-sensitive adhesives. *Journal of Polymer Science Part B: Polymer Physics*. 43(22): 3316-3330.

Sperling, L. H. (1977). Interpenetrating polymer networks and related materials. *Journal of Polymer Science: Macromolecular Reviews*. 12(1): 141-180.

Sukengwu, M. H. (2008). Temporary bonding of wafer to carrier for 3D-wafer level packaging. 10th Electronics Packaging Technology Conference.

Sun, S., Sun, P., Liu, D. (2005). The study of esterifying reaction between epoxy resins and carboxyl acrylic polymers in the presence of tertiary amine. *European Polymer Journal*. 41(5): 913-922.

Tan, S., Zhang, D., Zhou, E. (1996). Dynamic mechanical properties of interpenetrating polymer networks based on polyacrylates and epoxy. *Acta Polymerica*. 47(11-12): 507-510.

Tasic, S., Bozic, B., Dunjic, B. (2004). Synthesis of new hyperbranched urethane-acrylates and their evaluation in UV-curable coatings. *Progress in Organic Coatings*. 51(4): 320-327.

Tong, Q.-Y., Gosele, U. (1999). *Semiconductor Wafer Bonding: Science and Technology*. Wiley, New York, US.

Uchida, E., Uyama, Y., Iwata, H., Ikada, Y. (1990). XPS analysis of the poly(ethylene terephthalate) film grafted with acrylamide. *Journal of Polymer Science Part A: Polymer Chemistry*. 28(10): 2837-2844.

Udagawa, A., Yamamoto, Y., Inoue, Y., Chûjô, R. (1991). Dynamic mechanical properties of cycloaliphatic epoxy resins cured by ultra-violet-and heat-initiated cationic polymerizations. *Polymer*. 32(15): 2779-2784.

Uhl, F. M., Webster, D. C., Davuluri, S. P., Wong, S.-C. (2006). UV-curable epoxy acrylate-clay nanocomposites. *European Polymer Journal*. 42(10): 2596-2605.

Voronkov, M. G. e., Mileshekevich, V. P., ÎŪzhelevsk'iĭ, I. U. I. A. (1978). *The Siloxane Bond: Physical Properties and Chemical Transformations*. Consultants Bureau New York.

Wang, W. (2003). Synthesis and characterization of UV-curable polydimethylsiloxane epoxy acrylate. *European Polymer Journal*. 39(6): 1117-1123.

Wolf, J. M. (2008). 3D process integration-requirements and challenges. Materials research society. symposium of proceeding. 1112.

Wu, G., Zeng, S., Ou, E., Yu, P., Lu, Y., Xu, W. (2010). Photoinitiator grafted styrene–butadiene–styrene triblock copolymer. *Materials Science and Engineering: C*. 30(7): 1030-1037.

Yacobi, B., Martin, S., Davis, K., Hudson, A., Hubert, M. (2002). Adhesive bonding in microelectronics and photonics. *Journal of Applied Physics*. 91(10): 6227-6262.

Yang, S.-l., Wu, Z.-H., Yang, W., Yang, M.-B. (2008). Thermal and mechanical properties of chemical crosslinked polylactide (PLA). *Polymer Testing*. 27(8): 957-963.

Yin, T., Rong, M. Z., Zhang, M. Q., Yang, G. C. (2007). Self-healing epoxy composites–preparation and effect of the healant consisting of microencapsulated epoxy and latent curing agent. *Composites Science and Technology*. 67(2): 201-212.

Zhang, M. C., Kang, E. T., Neoh, K. G., Tan, K. L. (2001). Surface modification of aluminum foil and PTFE film by graft polymerization for adhesion enhancement. *Colloids and Surfaces A: Physicochemical and Engineering Aspects*. 176: 139-150.

Zhu, Q., Han, C. C. (2010). Study of telechelic polyurethane with perfluoropolyether tails. *Polymer*. 51(4): 877-882.

Zinck, C. (2010). 3D integration infrastructure and market status. Proceeding of the IEEE International 3D System Integration Conference (3DIC 2010), Munich.

Zosel, A. (1991). Effect of cross-linking on tack and peel strength of polymers.
The Journal of Adhesion. 34: 201-209.

초록

최근 스마트폰을 중심으로 한 모바일 기기는 고성능화와 동시에 경박단소가 요구되기에 TSV 3D 멀티칩 패키징 기술이 대두하게 되었다. 이 기술을 실현하기 위해서는 실리콘 웨이퍼를 가공하고 핸들링 할 수 있는 임시 고정 접착제가 필요하다. 하지만 기존 접착제를 사용하여 두께 50 μm 이하의 박형 실리콘 웨이퍼를 핸들링하는 것은 쉽지 않다. 그 이유는 첫 번째로 고순도를 유지하기 위해 본딩 공정과 디본딩 공정 사이에 200 $^{\circ}\text{C}$ 이상의 공정 온도가 요구되는데 사용되는 접착제의 열분해로 인한 저분자량 물질 발생과 이로 인한 박형 실리콘 웨이퍼의 오염이 발생되기 때문이다. 두 번째는 디본딩 시 강한 접착력으로 인해 박형 실리콘 웨이퍼의 크랙 또는 깨짐 등의 불량 발생하게 된다.

따라서 본 연구에서는 TSV 3D 멀티칩 패키징용 임시 고정 접착제를 본딩 관점과 이후 진행되는 디본딩 관점으로 나누어 각각의 요소 기술을 이용하여 접착제를 새롭게 합성하였고 물성 평가를 통해 경화 거동 및 디본딩 메커니즘을 규명하고자 하였다.

먼저 본딩 관점에서는 본딩 시, 기존의 용제형 접착제가 갖는 스

핀 코팅 후 접착제가 실리콘 웨이퍼 밖으로 흘러내리는 현상, 용제 휘발로 인해 웨이퍼 표면이 오염되고 코팅 두께가 불균일해지는 현상, 작업장의 오염 등의 문제점을 갖는다는 단점을 개선하고자 무용제형 우레탄 아크릴계 접착제를 설계 및 제조하였다. 우레탄 합성시 hard segment로써 아이소포론 다이이소시아네이트를 사용하였고, soft segment로는 기존의 탄화수소계 다이올이 아닌 실리콘계 다이올을 이용하여 고분자 구조의 내열성을 향상시키고자 하였다. 또한 기존의 광 경화 또는 열 경화형과 같은 단일 경화형 접착제가 아닌 광 경화 이후 열 경화를 추가적으로 도입하는 이중 경화형 접착제를 설계하여 내열성을 향상시키고자 하였다. 합성한 우레탄 올리고머의 한쪽 말단에 다관능성 아크릴계 모노머를 end-capping 하였고, 다른 말단에는 불소기를 함유한 모노머를 end-capping 하여 다관능성 아크릴계 모노머의 관능기 개수와 조사되는 자외선 에너지 밀도, 사용되는 광개시제의 함량에 따라 달라지는 경화 거동 및 열 안정성, 박리 강도를 측정하여 분석해보았다. 그 결과 아크릴계 모노머의 관능기 개수는 mono < di << tri, hexa 순으로 겔 분율법을 이용한 간접적인 경화율이 증가하는 것을 확인할 수 있었으며, 이는 광 경화 초기 반응에 있어서 반응 사이트의 증가 및 이로 인한 가교밀도의 증가로 해석할 수 있다. Tri-acrylate 이상에서는 겔 분율이 60%

로 더 이상 증가하지 않은 것을 확인할 수 있었는데 이는 미반응 올리고머의 라디칼 trap에 의해 반응 활성도가 떨어지는 것으로 해석할 수 있다. 조사되는 자외선 에너지 밀도는 400 mJ/cm^2 이상에서 겔 분율이 60%로 일정해지는 것을 확인할 수 있었다. 자외선 에너지 밀도 증가에 따른 박리력 감소를 위해 광 조사 시 주로 사용되는 steady irradiation법이 아닌 100 mJ/cm^2 씩 나누어 조사하는 pulsed irradiation법을 도입하여 고분자의 분자량 분포를 heterogeneous한 상태로 유도하고자 하였으며, steady irradiation법으로 한 경우 5.9의 PDI값을 나타낸 반면, pulsed irradiation법으로 한 경우 16.1의 높은 PDI값을 나타내었고 이러한 특성은 박리강도 측정 결과 pulsed irradiation법이 steady irradiation법보다 보다 낮은 강도 수치를 보여주는 것으로 확인되었으며, 본딩 뿐만 아니라 디본딩까지 고려한다면 pulsed irradiation법이 보다 적합한 광 조사 방법임을 알 수 있었다. 본 연구에서는 기존의 연구에서와는 달리 광 개시제의 함량에 달라지는 경화 거동을 평가하고 분석해보고자 하였다. 그 결과 바인더 대비 2 phr 이상의 광 개시제 투입 시 겔 분율이 더 이상 증가하지 않고 일정해지는 것을 알 수 있었는데 이는 과량의 광 개시제 투입 시 발생할 수 있는 미반응 개시제에 의한 부반응을 고려할 때 초기 투입량에 대한 최적의 배합비 조성이 중요하다는

것을 알려준다. 열 안정성 확보를 위하여 자외선 에너지 밀도와 광개시제의 함량을 달리하여 열중량 분석법을 이용하여 열 분해 거동을 살펴본 결과 250 °C 이상의 조건에서 열 안정성이 유지되는 것을 확인 할 수 있었는데, 이는 이중경화 메커니즘의 도입과 실리콘계, 에폭시계, 불소계 작용기를 모두 갖는 하이브리드 타입의 접착제 합성으로 내열성이 보다 향상된 것으로 해석할 수 있다.

한편, 본딩 이후 디본딩을 위하여 자외선 레이저를 이용한 edge zone debonding법을 제안하였다. 기존의 방식이 200 ~ 220 °C의 본딩 온도를 요구하는 반면, 본 연구를 통해 80 ~ 150 °C의 낮은 온도로 본딩을 진행할 수 있게 되었다. 또한 디본딩 시 용제의 침투에 의해 6시간 이상의 공정 시간이 소요되는 기존 방식에 비해 자외선 레이저를 이용하여 2분 이내에 디본딩이 이루어지도록 연구하였다. 이를 위해 접착제 제조 시 2-[3-(2-Benzotriazol-2-yl)-4-hydroxyphenyl]ethyl methacrylate (BTHPEMA)를 도입하였다. BTHPEMA는 디본딩 시 Light To Heat Conversion (LTHC) 역할을 함으로써 접착제의 열 경화에 의한 고분자 필름 형성으로 디본딩이 진행됨을 FTIR-ATR 분석과 겔 분율 측정을 통한 에폭시 작용기의 열 경화 메커니즘으로 규명하였다. 합성한 접착제의 자외선 레이저에 대한 흡수도를 UV-visible spectroscopy를 이용하여 파장에 따라

측정하였으며 그 결과, 355 nm 파장에서 BTHPEMA의 함량 증가에 따라 바인더 대비 투입량 0.4 phr에서 최대 60%의 흡수도를 나타내었으며 배합비를 달리함으로써 접착제의 자외선 레이저 흡수도를 다양하게 조절할 수 있었다. 또한 자외선 레이저 조사 시 5.65 ~ 6.72 J/cm² 영역의 유효에너지 밀도 조건에서 적합한 디본딩이 이루어지는 것을 분석 기기를 통해 확인할 수 있었다.

주요어 : 접착제, 이중경화, 3D 멀티칩 패키징, 임시 고정, 자외선 레이저 디본딩, 불소화 우레탄 아크릴 접착제

학번 : 2009-21204

